An overview of first-year sea ice ridges

Timco, Garry; Croasdale, K.; Wright, B.

Publisher's version / Version de l'éditeur:
https://doi.org/10.4224/12327286
PERD/CHC report, Technical Report (National Research Council of Canada. Canadian Hydraulics Centre); no. HYD-TR-047, 2000-08

CHC CANADIAN HYDRAULICS CENTRE

An Overview of First-Year Sea Ice Ridges

G.W. Timco[1], K. Croasdale[2] and B. Wright[3]
[1]Canadian Hydraulics Centre
Ottawa, Ont. K1A 0R6
[2]K. R. Croasdale and Associates
Calgary, Al.
[3]B. Wright & Associates,
Canmore, Al.

Technical Report
HYD-TR-047

PERD/CHC Report 5-112

August 2000

PERD

ABSTRACT

This report presents an overview of several aspects of the engineering properties of first-year sea ice ridges. The report focuses on first-year ridges in temperate climates, and is sub-divided into 4 main sections that deal with the following aspects of ridges:

- Morphology of ridges
- Physical and mechanical properties of ridges
- Measured ridge loads on offshore structures
- Methods for predicting ridge loads

TABLE OF CONTENTS

LIST OF FIGURES

LIST OF TABLES

An Overview of First-Year Sea Ice Ridges

1.0 INTRODUCTION

First-year ridges are common features in most sea ice environments, and as such, play an important role in a wide range of ice-related processes. From an engineering perspective, first-year ridges are often a key consideration. For example, in ice-covered waters like those found off the West Coast of Newfoundland, large first-year ridges control the design load levels for sea ice interactions with offshore structures. Ridges are also well known as a significant impediment to shipping in most ice-covered regions. In addition, first-year ridges can scour the seafloor in relatively shallow waters. This has significant implications on the design of pipelines and other subsea facilities.

Ridges form when level ice floes are level ice areas are compressed and sheared by environmental driving forces. Ridge-building processes (see Figure 1) are complex, but usually involve some rafting in combination with various bending, buckling or crushing failures. The resulting ridge feature contains a large number of ice pieces of varying sizes that are piled in a haphazard manner (Figure 2). Ridges are often characterised as linear features (Figure 3), but in fact they are sinuous and highly variable in form. The ice broken in the ridge building process creates ice rubble both above and below the waterline which is in hydrostatic equilibrium. Hence the rubble above the water line (the *sail*) has a volume of about one tenth of the rubble below the water line (the *keel*). The central portion of the ridge along the waterline is often re-frozen together, forming the *consolidated layer* of the ridge.

Ridges are classified according to the following features:

- **Age –** The age of the ice that comprises the ridge will influence its properties and strength. The ridges are categorised as *multi-year ridges* (i.e. ice that is more than two seasons old) and *first-year ridges*. The former are generally much larger and significantly stronger than the first-year ridges.
- **Formation Process –** Ridges are categorized as *compression (pressure) ridges* or *shear ridges*, depending upon the mode of formation.
- **Location –** First-year ridges are also subdivided according to their location – either as *Arctic ridges*, or *temperate ridges* (i.e. ridges in more temperate climates).

Offshore petroleum developments in Canada and many other regions of the world will have to deal with the interaction of ridges on any structure placed offshore. In Canada, multi-year ridges are the primary ice design features in the Beaufort Sea. Off the West Coast of Newfoundland, first-year ridges provide the highest sea ice load, and have the potential to scour the seafloor in the nearshore region.

Figure 1 Photograph showing the initial formation of a ridge during the collision of very thin ice floes (photo from M. Johnston).

Figure 2 Photograph showing the sail of a large ridge. Note the large ice pieces and the haphazard arrangement of the ice (photo from M. Metge).

Figure 3 Photograph showing the linear nature of ridges (photo from M. Metge)

Over the past few years, a great deal has been learned about the properties of first-year ridges, and the loads they may exert on offshore structures. This report presents an overview of this knowledge. The report focuses on first-year ridges in temperate climates, and is sub-divided into 4 main sections that deal with the following aspects of ridges:

- Morphology of ridges - *Chapter 2*
- Physical and mechanical properties of ridges - *Chapter 3*
- Measured ridge loads on offshore structures - *Chapter 4*
- Methods for predicting ridge loads - *Chapter 5*

It should be noted that this report is not meant to be a "state-of-the-art" review of the current knowledge base on first-year ridges. Instead, it is intended as an overview of the results of recent activities and gives insight into the morphology, properties and behaviour of first-year ridges when they interact with structures.

2.0 MORPHOLOGICAL FEATURES OF ICE RIDGES

2.1 Introduction

First-year ridges are complex features with widely varying sizes, shapes and properties. This has made their characterization difficult. Numerous studies have been undertaken in which the geometry and physical properties of ridges have been measured and, to lesser extent, their mechanical properties. From these studies, a considerable amount of information on the morphology of pressure ridges has emerged.

From an engineering perspective, there are a number of key factors that are important in characterising ridges. These are the **shape** and **size** of the ridge, the **strength** of the ridge and the number of ridges (**frequency)** in a given area. In this chapter, information on ridge shape, size and frequency are highlighted. The strength of ridges is discussed in Chapter 3.

2.2 Measurement Techniques and Definitions

Information on the size and shape of ridges, and statistics on their spatial distribution have been obtained in a number of different ways. The data collection methods used to obtain information on ridges can be subdivided into 2 basic categories - ***continuous scanning*** of the ice surface or underside, and ***discrete measurements*** of specific ridge features. Both data collection methods have different objectives.

- With continuous scanning, information can be obtained about the distribution of ridges both over large spatial fields including their heights (or depths), spacing and orientation. Stereo photography and laser profilometers are the most commonly used techniques to collect statistical information about ridge sails. Upward-looking sonars, which are fixed on the seafloor or mounted on submarines, have been used to record the under ice keel profiles ice as the ice moves past it. With these techniques, a large amount of information can be obtained with relatively little effort. However, only one side of the ice cover is profiled (either the top or bottom), and direct correlation of the top and underside surfaces is not possible. This restricts information on the sail/keel geometries of individual ridges. This technique does provide very useful information on the distribution of ridges over large areas, as discussed in Section 2.6.
- With a discrete measurement, which is of most interest here, information can be obtained on the overall size and shape of an individual ridge at one particular location, both above and below the waterline. In this case, holes are drilled through the ice, and the thickness is measured using either a tape measure or a sonar transducer probe that is lowered into the drill holes. This approach provides detailed quantitative information on both the sail and keel size and shape, but of a specific ridge, as well as its porosity. It does not supply any information on ridge spacing. Also, the discrete measurement technique is significantly more labour-intensive than continuous profiling. The results of individual profile measurements are discussed in the following sections.

Based on extensive field work that has been done over the past several decades, a ridge is usually idealized as being made up of a **sail**, a **consolidated (or refrozen) layer,** and a **keel** (see Figure 4).

- The **sail** of the ridge is readily observable and relatively easy to profile. It consists of a number of ice pieces piled on the surface of the ice. These ice blocks can be partially re-frozen together, or they can be relatively unconsolidated.
- The **consolidated layer** is created from refrozen rubble and/or rafted ice. For a given number of freezing degree-days it can be shown that the freeze front in ice rubble will advance faster than under level ice. Hence the refrozen layer thickness in a ridge will be thicker than the surrounding ice. This is generally confirmed by measurements, but these also show significant variability in refrozen layer thickness. In fact, in some areas where snow and sail rubble provides insulation, the refrozen layer can be quite thin or discontinuous. In sub-arctic regions where maximum level ice thickness is generally less than a metre, typical maximum refrozen layer thickness should be less than about 2.5m. However, if a feature has low porosity due to grounding, rafting or shearing processes, then the thickness can be greater, up to 5 m or more (Betetsky et al. 1996: Croasdale et al. 1990).
- The **keel** of the ridge is also comprised of a large number of ice blocks, but it is significantly larger than the sail. The keel is usually defined as one rubble region, with a haphazard arrangement of ice blocks. In temperate regions such as Northumberland Strait and West Newfoundland, typical maximum keel depths would be about 16 m, whereas in the Arctic, keels may be greater than 50 m. In cold sub arctic regions, keel depths to 25 m or more can occur. Since the keel is below the waterline and surrounded by sea water, the surface of the ice blocks are at the freezing point of the sea water. Although the keel is usually treated as a single layer, its strength properties often vary and are usually higher near the top. For this reason, some investigators assign another layer in the ridge idealization, which they define as a semi-consolidated region. This conceptualization may or may not be correct and is discussed in more detail later in this report.

2.3 Sail and Keel Relationships

Timco and Burden (1997) compiled the profiled shapes of 184 ridges from 22 different field studies, including 112 first-year ridges with 46 from the Arctic and 66 from more temperate regions, and 64 multi-year ridges from the Arctic. They did extensive comparisons of all of the geometric characteristics of these ridges and developed empirical algorithms to relate them. In many cases, a good correlation was found between different ridge characteristics, but in others, there was little or no correlation. A number of techniques were used to quantify the important relationships between the height (H), width (W) and cross-sectional area (A) of the ridges (see Figure 4). Usually, the best-fit relationship between 2 parameters was a complex relationship that had no apparent physical basis - it was simply the best curve-fit to a limited number of data points. Thus, Timco and Burden characterized the relationships using 2 types of curves - one, a simple *linear relationship* (forced through the origin), and two, the *best-fit power relationship*. In most cases, there was very little difference between the two approaches, with typical correlation (r^2) coefficients on the order of 0.7 to 0.9. This level of correlation is quite good, given the wide natural variability of the ridges. The detailed plots of the data are too voluminous to reprint here, and the original source should be referenced for full information.

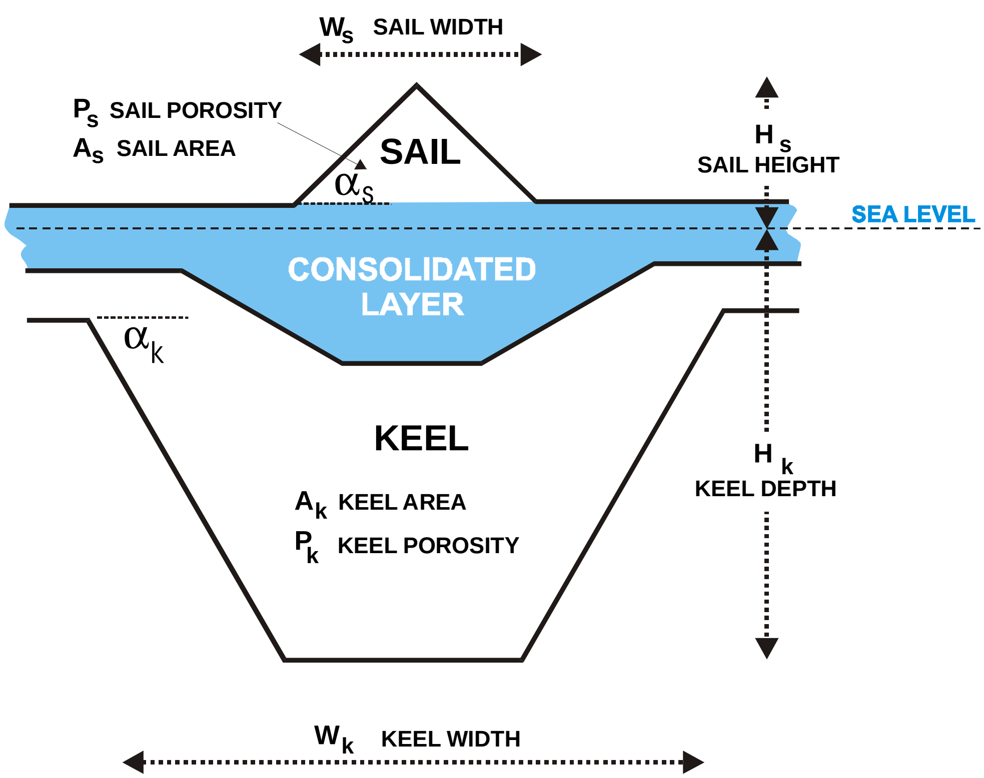

Figure 4 Illustration of an idealized first-year sea ice ridge.

Table 1 summarizes the best-fit linear and power relationships along with the information on the number of data points (n), and the statistical correlation (r^2) between the parameters. In addition, the value of the coefficients along with their standard error and 95% confidence limits are presented. The first four equations relate to first-year ridges. The last two equations (with the subscript m) relate to multi-year ridges and they are included for comparison.

Timco and Burden (1997) also analyzed the distribution of the measured sail and keel angles of the ridges. For this analysis, the reported angles for both the sail and keel of the different ridges were tabulated, and a statistical function was fit to the data. Unfortunately, in many cases, there was not sufficient data to be able to unambiguously define the best functional relationship. Therefore, the data was fit to either a simple normal or log-normal distribution, depending upon the general shape of the distribution.

Based on the average values, Timco and Burden (1997) produced a plot to show a representation of the geometries of an "average" first-year ridge (see Figure 5). It should be kept in mind that this ridge represents average values. There is wide variability in the properties of ridges and this variability must always be kept in mind when considering the interaction of ridges with offshore structures.

Table 2 lists the information on the mean and standard deviation for the normal distribution, and the Log(mean) and Log(standard deviation) for the Log-normal distribution. In addition, the goodness of fit for each distribution is listed as determined using a χ^2 test.

Table 1 Summary of Parametric Relationships for Ridges (after Timco and Burden 1997).

Equation	n	r^2	a					b				
			value	st. error	t-value	95% confidence		value	st. error	t-value	95% confidence	
$H_k = a\ H_s^b$	97	0.783	3.95	0.12	34.09	3.72	4.18	1.00	-	-	-	-
		0.793	4.60	0.31	15.07	4.00	5.21	0.88	0.05	18.17	0.79	0.98
$W_k = a\ H_k^b$	65	0.739	3.91	0.16	24.53	3.59	4.22	1.00	-	-	-	-
		0.746	5.67	1.13	5.02	3.41	7.92	0.87	0.07	12.05	0.72	1.01
$W_k = a\ H_s^b$	75	0.675	14.85	0.63	23.48	13.59	16.11	1.00	-	-	-	-
		0.713	20.75	1.98	10.51	16.81	24.69	0.78	0.06	12.34	0.65	0.90
$A_k = a\ A_s^b$	33	0.871	7.96	0.33	24.32	7.29	8.63	1.00	-	-	-	-
		0.896	17.46	4.28	4.08	8.73	26.19	0.82	0.06	14.43	0.70	0.94
$H_{k,m} = a\ H_{s,m}^b$	47	0.873	3.17	0.08	41.83	3.02	3.33	1.00	-	-	-	-
		0.878	3.66	0.30	12.37	3.06	4.26	0.91	0.05	19.23	0.82	1.01
$A_{k,m} = a\ A_{s,m}^b$	10	0.931	8.81	0.44	19.81	7.80	9.82	1.00	-	-	-	-
		0.921	8.82	4.42	1.99	-1.42	19.06	1.00	0.10	9.75	0.76	1.24

Based on the average values, Timco and Burden (1997) produced a plot to show a representation of the geometries of an "average" first-year ridge (see Figure 5). It should be kept in mind that this ridge represents average values. There is wide variability in the properties of ridges and this variability must always be kept in mind when considering the interaction of ridges with offshore structures.

Table 2 Summary of Distributions for First-year Ridges (after Timco and Burden 1997).

RELATIONSHIP	TYPE	n	MEAN	ST. DEV.	χ^2	p-value	DOF
keel/sail ratio - first-year ice	normal	97	4.46	1.85	36.11	0.01	13
	log-normal	97	1.41	0.41	10.05	0.69	13
sail angle - temperate	normal	40	20.68	11.45	16.80	0.21	13
	log-normal	40	2.87	0.61	16.80	0.21	13
sail angle -Beaufort	normal	40	32.90	9.16	13.60	0.40	13
	log-normal	40	3.45	0.29	14.40	0.35	13
keel angle - first-year ice	normal	70	26.56	13.39	30.11	0.00	13
	log-normal	70	3.17	0.47	16.40	0.23	13
kkel/sail ratio - Multi-year ice	normal	47	3.34	0.85	37.77	0.00	13
	log-normal	47	1.12	0.20	18.70	0.13	13
sail angle - multi-year ice	normal	73	19.50	8.50	11.38	0.58	13
	log-normal	73	2.81	0.68	47.33	0.00	13

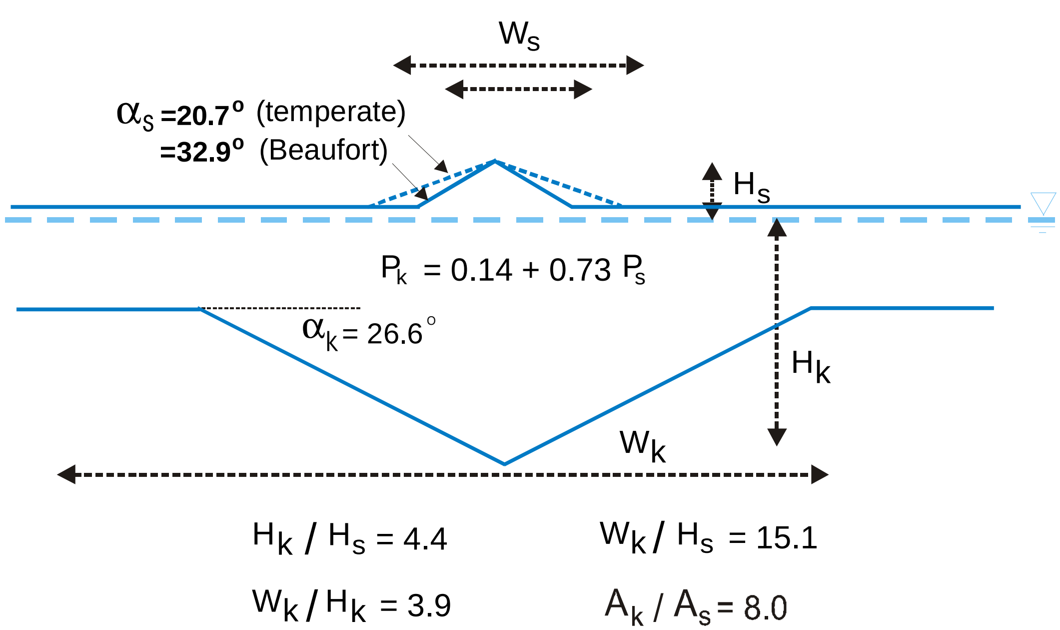

Figure 5 Illustration of an "average" first-year ridge based on the analysis of 112 ridges (after Timco and Burden 1997).

The data used by Timco and Burden (1997) did not include any information from the West Newfoundland region of Canada. Recently, Croasdale et al. (1999) carried out a field program in this region and profiled the ice features in a number of different areas. Sail heights were measured and keel depths were inferred from measurements of ice thickness in several places in individual ridges. It is of interest to compare these measurements to the summary of results for the temperate regions and the Arctic region.

Figure 6 shows the relationship between the sail height and the keel depth for ridges from the West Newfoundland, Arctic, temperate locations and the Sakhalin region. This latter region has become a region of high interest for oil and gas development. Ridge profiles have recently been measured and reported for this region by Beketsky et al. (1996, 1997a, 1997b) and Surkov (1997a, 1997b).

The linear relationship developed by Timco and Burden (1997)

$$H_k = 3.95\, H_s \qquad \textbf{2-1}$$

where H_k is the maximum keel depth and H_s is the maximum sail height is also indicated on Figure 6. There is good agreement amongst all regions, with an apparent larger scatter for the Sakhalin region. Note that first-year ridges with keels up 28 m and 20 m have been publicly reported for the Arctic and Sakhalin regions respectively.

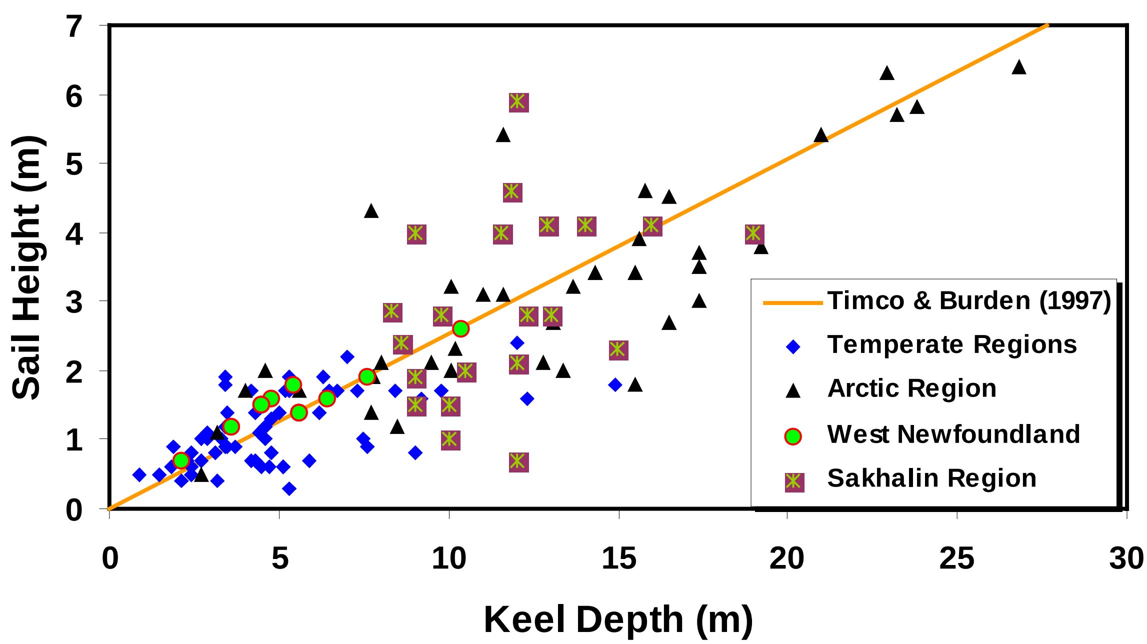

Figure 6 Sail height versus keel depth for profiled first-year ridges for different geographical regions. The line from Timco and Burden (1997) shows a keel-to-sail ratio of 3.95.

Figure 7 shows a plot of the keel depth (H_k) versus the keel width (W_k) based on ridges profiled in three different geographic regions. The linear equation developed by Timco and Burden (1997)

$$W_k = 3.91\,H_k \qquad \textbf{2-2}$$

is also included on the plot. Although there is considerable scatter, the general trends and agreement are the same for each region.

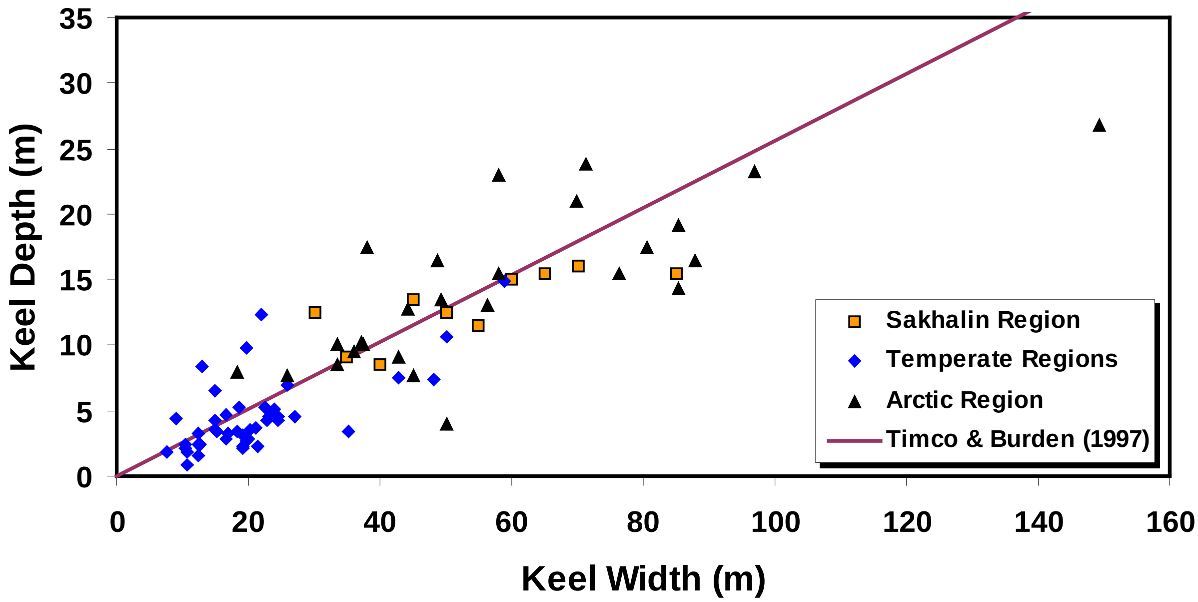

Figure 7 Keel depth versus keel width for profiled first-year ridges for 3 different geographical regions.

2.4 Consolidated Layer

Timco and Burden (1997) also compiled information on the thickness of the refrozen (consolidated) layer for a large number of different ridges from numerous field studies. Information on the variation of thickness of this layer is especially important in ice engineering applications, since the consolidated layer often exerts the highest forces on offshore structures during a ridge/structure interaction. Presentation of the information on the consolidated layer thickness was not straightforward, since there was a wide range of thickness for the ridges. To get some insight into the variability of the thickness of the consolidated layer, the maximum, minimum and average thickness values were determined for 25 different ridges. With this information, the ratio of the minimum-to-average thickness and the maximum-to-average thickness were determined for each ridge. The mean of the minimum-to-average thickness ratio was 0.51 with a standard deviation of 0.2. The mean of the maximum-to-average thickness ratio was 1.68 with a standard deviation of 0.37. These ratios show that there is a large amount of variability in the thickness of the consolidated layer in first-year ridges. Typical space scales for significant spatial variations in consolidated layer thickness are in the range of a few meters to several tens-of-meters.

2.5 Porosity

There have been a few direct measurements of the porosity of the sail and keel portions of ridges. Lapparanta and Kakala report on these properties for 6 ridges in the Baltic Sea. Beketsy et al. (1996) have reported on the porosity of 4 ridges in the Sakhalin region. The results of these measurements have been summarized in Table 3. It is interesting to note that the reported porosities are quite different for these 2 regions. In the Baltic, the average porosity of the sail (0.19) is lower than the average porosity of the keel (0.29). In the Sakhalin region, the average sail and keel porosities are 0.33 and 0.22 respectively. Porosity measurements in the Beaufort Sea show similar values.

Timco and Burden (1997) performed an analysis to determine the porosity of the sail and keel regions, based on an assumption of iso-static equilibrium for the ridge. The ridge profiles were digitized, and the sail, keel and snow areas were determined. Using this approach, the best-fit equation to describe the sail and keel porosity for first-year ridges was found to be

$$P_k = 0.14 \quad + \quad 0.73\,P_s \qquad \textbf{2-3}$$

where P_k is the porosity of the keel and P_s is the porosity of the sail (see Figure 4).

Table 3 Summary of Measured Porosities

	Lepparanta & Hakala (1992)							Beketsy et al. (1996)				
	1	2	3	4	5	6	Ave.	1	2	3	4	Ave.
Sail Porosity	0.31	0.14	0.17	0.19	0.23	0.09	0.19	0.43	0.30	0.26	0.31	0.33
Keel Porosity	0.30	0.23	0.28	0.32	0.33	0.28	0.29	0.23	0.15	0.28	0.20	0.22

There was little difference between the data for the Beaufort and temperate ridges, and the above equation is a reasonable representation for both regions. It should be noted that this equation predicts that the keel porosity is non-zero, even with zero sail porosity. Equation 2-3 can be used to estimate the porosity of the keel, if the sail porosity is measured.

If this equation is applied to the measured values for the Baltic and Sakhalin ridges discussed above, it would predict, for a sail porosity of 0.19, a keel porosity of 0.28. This is in good agreement with the measured porosity for the keel in the Baltic ridges of 0.29. On the other hand, using the equation and the measured sail porosity of 0.33 for the sail for Sakhalin ridges, it would predict a keel porosity of 0.38. This is significantly different than the reported keel porosity of 0.22. Since Equation 2-3 was derived assuming iso-static equilibrium, this would suggest that the Baltic ridges were in iso-static equilibrium whereas the Sakhalin ridges were not.

2.6 Ridge Frequency and Spacing

Information on ridge spacing and frequency has important implications for ship routing in ice-covered waters, as well as determining the number of ridges that will interact with an offshore structure throughout a winter season. The development of functional relationships to describe the characteristics of ridge frequency has great importance in probabilistic numerical models for calculating ice loads. A large number of investigations have been made to measure ridge spacing, primarily using laser profilers, upward-looking laser and stereo photographic methods. Analysis of this data has suggested a negative exponential distribution fits well for the distribution of keel spacing (Wadhams et al. 1985). More recently, however, Davis and Wadhams (1995) have suggested that a log-normal distribution better describes the ridge spacing relationship than a negative exponential distribution.

Information on ridge spacing is very site-specific. Therefore this topic will not be dealt with in detail here. However, interested readers are referred to the recent review article by Wadhams (1999) that discussed this topic in detail.

2.7 Ridge Building Processes

From an engineering perspective, the ridging process is extremely important. It has been recognized as a potential load-limiting mechanism for extreme ice interaction. In short, the load levels necessary to cause ridging can provide a limit for the maximum loads that exerted by the ice; that is, the ridging process provides an upper bound limit to load levels. Over the years, various approaches have been used to understand the ridge-building process including field measurements, physical model tests, analytical models and numerical models. Each approach is briefly discussed below.

Field Measurements – A number of different field studies have been carried out to investigate the internal pack ice stresses in ice fields. Comfort et al. (1994) have summarized the results of 3 field programs that were carried out in the Canadian Arctic to measure pack ice stresses. In these studies, sensors were installed in the centre of large multi-year ice floes, and finite element analysis (Frederking and Evgin 1990) was used to interpret the results. The analysis indicated that the stress at the edge of the floe, which was assumed to be comparable to the ridge-building forces, ranged from 24 to 1191 kN/m. Coon et al. (1989) and Tucker and Perovich (1992) measured ice stresses in drifting pack ice in the eastern Arctic and estimated ridge-building forces to be 37 kN/m and 100-200 kN/m respectively. Nikitin and Kolesov (1993) summarized the field programs and predicted ridge-building forces that ranged from 150 kN/m for 0.3 m thick ice to 1720 kN/m for 2.5 m thick ice. Richter-Menge and Elder (1998) monitored stress levels in multi-year floes for 6 months in the Alaskan Beaufort Sea. They estimated a ridge-building force on the order of 150 kN/m.

Physical Model Tests – A number of investigators have used physical modelling techniques to investigate ridge-building forces and the ridge-building process including Abdelnour and Croasdale (1986), Timco and Sayed (1986) and Lensu and Green (1995). In these studies, the ridge-building process was simulated by ice sheet failure against a rigid plate, or by having a ridge form through the compression of an ice sheet being pushed together. The tests indicated scaled ridge-building forces on the order of 500 kN/m (Abdelnour and Croasdale, 1986) and 100 kN/m to 1700 kN/m for ice thickness ranging from 0.2 m to 0.8 m (Timco and Sayed, 1986). More recently, Tuhkuri et al (1999) simulated the ridge-building process in a more natural manner by having the ridge building occur when 2 ice sheets were pushed together. They found that in order to do this, it was necessary to use ice sheets with non-uniform thickness. They noted that the process usually started by rafting followed by the initiation and formation of the sail and keel. The tests indicated that during the initial stages of ridge formation, the force-thickness relationship is linear. The tests also suggested that during the latter stages of ridging the force-thickness relationship is non-linear.

Analytical Models – Parmerter and Coon (1972) developed the first analytical model of the ridge-building process. They considered a process where 2 ice sheets move towards one another, closing a lead filled with broken ice. Ridge-building force predictions from this approach indicated forces on the order of 10 to 30 kN/m. Sayed and Frederking (1988) modelled a ridge as 2-dimensional wedges and assumed that a critical state of the wedge simulates a ridge forming. Their model predicts forces up to 250 kN/m for ridges with a sail height of 7 m.

Numerical Models – Recently, Hopkins (1994, 1998) and Hopkins et al (1999) have developed a discrete element model and applied it to investigate the ridge-building process. The model uses an intact ice sheet moving at a constant speed against a thick multi-year floe. The thin ice sheet breaks apart repeatedly in flexure and creates a rubble pile that forms a sail and keel (see Figure 8). Hopkins (1998) discusses the ridge-building process as a 4-part process:

1. The first stage begins when an intact ice sheet impacts against a thick floe and ends when the sail reaches its maximum height;
2. During the second stage, the ridge keel deepens and widens and ends when the keel reaches its maximum depth;
3. In the third stage, the keel continues to grow leeward and creates a rubble field of more-or-less uniform thickness. This stage ends when there is no more thin ice to feed the process.
4. In the fourth stage, the rubble field is compressed between converging floes.

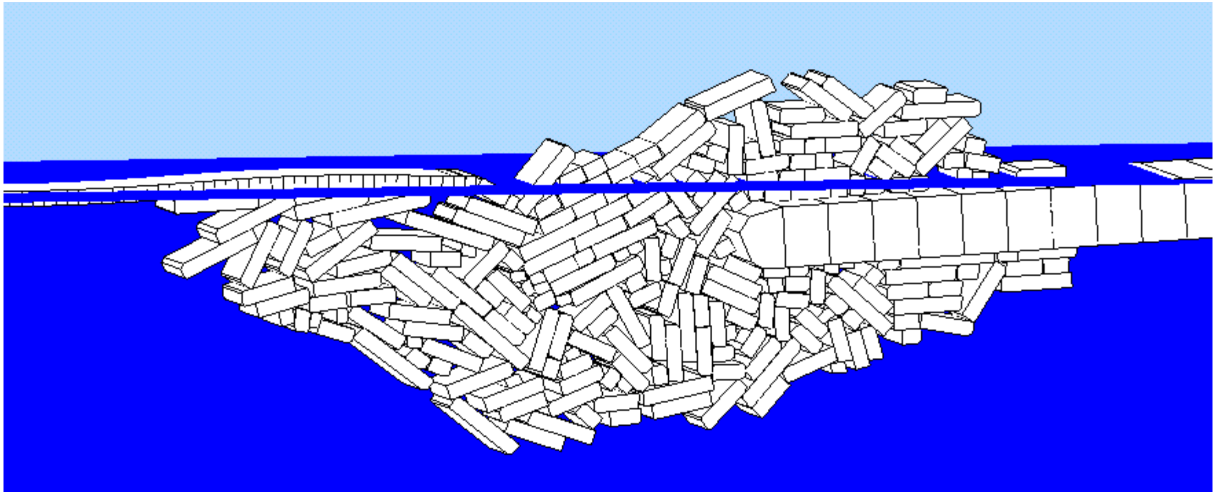

Figure 8 Snapshot from a simulation of the pressure ridging process (after Hopkins 1998).

2.8 References

Abdelnour, R. and Croasdale, K. 1986. Ice Forces Associated with Ridge Building: Model Tests and Results Compared with Theoretical Models. Proceedings IAHR86, Vol. 3, pp 227-245, Iowa City, Iowa, USA.

Beketsky, S.P., Astafiev, V.N., Truskov, P.A. 1996. Structure of Hummocks Offshore Northern Sakhalin. Proceedings of the 11th Okhotsk Sea and Sea Ice Symposium, pp.339-342, Hokkaido, Japan.

Beketsky, S.P., Astafiev, V.N., Bogdanchikov, S.M. 1997a. Technique of Determination of Design Parameters of Hummocks. Proceedings OMAE97 & POAC97, Vol. IV, pp. 239-244, Yokohama, Japan.

Beketsky, S.P., Astafiev, V.N., Truskov, P.A. 1997b. Design Parameters for Hummocks and Grounded Hummocks in the Sea of Okhotsk. Proceedings ISOPE97, Vol. II, pp. 487-493, Honolulu, USA.

Coon, M. et al. 1989. Observations of Ice Floe Stress in the Eastern Arctic. Proceedings POAC89, Vol. 1, pp 44-53, Lulea, Sweden.

Comfort, G., Dinnovitzer, A. and Gong, Y. 1994. Limit-force Ice Loads and their Significance to Offshore Structures in the Beaufort Sea. Fleet Technology Report 4346-C, Kanata, Ont., Canada.

Croasdale, K. et al. 1999. Field Study of Ice Characteristics off the West Cost of Newfoundland. Report to the National Research Council of Canada, Report PERD/CHC 2-70.

Davis, N.R. and Wadhams, P. 1995. A Statistical Analysis of Arctic Pressure Ridge Morphology. Journal of Geophysical Research 100, pp 10915-10925.

Frederking, R. and Evgin, E. 1990. Analysis of Stress Distribution in an Ice Floe. Proceedings ISOPE90, Vol. 4, pp 83-87.

Hopkins, M.A., Tuhkuri, J. and Lensu, M. 1999. Rafting and pressure ridging of thin ice sheets, Journal Geophysical Research 104, C6, 13605-13613.

Hopkins, M.A. 1998. On the four stages of pressure ridging, Journal Geophysical Research 103, C10, 21883-21891.

Hopkins, M.A. 1994. On the ridging of intact lead ice, Journal Geophysical Research 99, 16351-16360.

Lensu, M. and Green, J. 1995. Ice Tank Tests on Pressure Ridge Formation. Helsinki University of Technology Report M-202, Helsinki, Finland.

Leppäranta, M. and Hakala, R. 1991. The Structure and Strength of First Year Ice Ridges in the Baltic Sea. Cold Regions Science and Technology, 20: 291-311

Nikitin, V.A. and Kolesov, S.A. 1993. Stress and Forces under Ice Compacting. Int. J. Offshore Polar Eng. 3(2), pp 139-142.

Parmerter, R. and Coon, M. 1972. Model of Pressure Ridge Formation in Sea Ice. Journal Geophysical Research 77, No. 33, pp 6565-6575.

Richter-Menge, J. and Elder, B.C. 1998. Characteristics of Pack Ice Stress in the Alaskan Beaufort Sea. Journal Geophysical Research 103, No. C10, pp 21,817-21,829.

Sayed, M. and Frederking, R. 1988. Model of Ice Rubble Pile-up. J. Engineering Mechanics, Vol. 114, pp 149-160.

Surkov, G.A. 1997a. Consolidated Layer of Hummocks on the north Sakhalin Offshore, Proceedings of the 12th Okhotsk Sea and Sea Ice Symposium, pp. 53-58, Hokkaido, Japan.

Surkov, G.A. 1997b. Parameters of Ice Ridges of the Okhotsk Sea, Proceedings ISOPE97, Vol. II, pp.461-465. Vol. I, pp.68-69, Honolulu, USA.

Timco, G.W. and Sayed, M. 1986. Model Tests of the Ridge-Building Process, Proceedings IAHR86, Vol. 1, pp 591-602, Iowa City, Iowa, USA.

Tucker, T. and Perovich, D. 1992. Stress Measurements in Drifting Pack Ice. Cold Regions Science & Technology 20, pp 119-139.

Tukuri, J. Lensu, M. and Saarinen, S. 1999. Laboratory and Field Studies on the Mechanics of Ice Ridge Formation. Proceedings POAC99, Vol 3, pp 1118-1129, Helsinki, Finland.

Wadhams, P., McLaren, A.S. and Weintraub, R. 1985. Ice Thickness Distribution in Davis Strait in February from Submarine Sonar Profiles. Journal of Geophysical Research, 90(C1), pp 1069-1077.

Wadhams, P. 1999. Characteristics of Ice Cover Morphology. *in* Local Ice Cover Deformation and Mesoscale Ice Dynamics, Helsinki University of Technology Report M-243, Helsinki, Finland.

3.0 MECHANICAL AND PHYSICAL PROPERTIES

3.1 Introduction

Ice load models require the input of the appropriate ice and structure parameters including ice strength and certain physical properties such as density and friction. These parameters are reasonably well understood for level ice but less so for ridge ice (even though the ice blocks which form ridges are created by fracturing of the level ice).

As discussed in Chapter 5, the load due to the action of a first-year ridge on a structure is usually calculated as being made up of two components. These are the load due to failure of the consolidated layer and the load due to failure of the ice rubble keel.

Depending on the shape of the structure and continuity of the layer, the consolidated layer will fail in either in-plane “crushing” or out-of-plane "bending". For these failure modes it will be either, the crushing strength or the flexural strength of the consolidated layer, which will influence the loads. So these parameters are of interest.

Failure of the ridge keel will be controlled by the strength of the keel rubble, which is often idealized as a Mohr-Coulomb material having both frictional and cohesive properties. In keel rubble failure and clearing processes, the density difference between the ice rubble and the surrounding water also influences the loads.

During the past decade, research activity on the loads which first year ridges can impose on structures has increased due to developments in sub-Arctic regions such as the Confederation Bridge and offshore Russia (e.g. see Croasdale, 1999). These activities have led to increased effort in establishing the mechanical properties of first year ridges, which had largely been ignored in earlier Arctic research due to the dominance of multi-year features on design criteria.

As will now be reviewed, many of the properties of first-year ridges and rubble features are dependent on various processes occurring after ridge formation.

3.2 The Influence of Ridge Formation and Aging Processes on Properties

Immediately on formation, a ridge starts to undergo thermal and mechanical changes. The most obvious initial process is a thermal redistribution. Ridges are formed from level ice, which during the winter will have an average temperature several degrees below the freezing point. When ice blocks formed from this level ice are plunged into the ridge keel, the ice block temperature increases to that of the surrounding water. This releases negative sensible heat which creates additional freezing of the trapped water within the keel and reduces the effective ridge porosity. As shown by Kry (1977), depending on block temperature and initial porosity, the resulting porosity can be significantly affected, typically from say 0.35 to say 0.25.

This level of porosity change is plausible, however its manifestation is uncertain. For example, the additional ice created might be assumed to form at points of contact between ice blocks. This would lead to the creation of cohesive strength of the ice rubble. On the other hand, the additional ice created might exist in the form of frazil ice, which during the "churning process" of ridge creation, migrates to the upper part of the ridge keel. This would then lead to lower porosity in upper zones of the ridge, which would initially be in the form of slush ice. The presence of this slush ice would have a significant effect on subsequent diagenetic processes, which are both thermal and mechanical. These are discussed by Bruneau (1996).

The first and obvious aging process is caused by continued heat loss from the newly formed ice rubble, which creates the consolidated layer. As can be appreciated, the freeze front penetrates a material, which locally has considerable variability in factors controlling freeze front penetration. These include, gross porosity (the spaces between the ice blocks), the presence of slush ice between the blocks, orientation and size of the ice blocks, the presence of an overlying layer of level ice (or more layers if the ice is rafted), the location and size of the ridge sail, and snow cover.

Many investigators have developed freeze front penetration models to predict the consolidated layer thickness (e.g. Croasdale & Allyn, 1990: Lapparanta and Hakala, 1992; Cammaert and others, 1993). All use essentially the same 2D approach, based on Stefan's model and the results are highly dependent, not only on the freezing degree days, but also on the parameters noted above. This dependency may explain apparent anomalies in consolidated layer thicknesses between regions (Frederking and others, 1999). However, using plausible inputs, the models predict a thickness for the consolidated layer which is about 2 - 3 times the level ice in the region. A value which is supported by many measurements.

Even so, because of the uncertainties surrounding the influencing parameters, measurements of consolidated layer thickness are highly desirable. However, many such measurements are needed to ensure proper sampling of local variability within ridges. As well, it is known that measurements can be subject to errors. Rapid techniques such as hand operated thermal drills (which are favoured in order to obtain a large number of data) are the most susceptible to error. A concern is that tightly packed slush ice may be interpreted as frozen material by the drill operator. To address these concerns systematic comparisons of methods are recommended including comparisons with borehole jack profiles which give the strength variability within the layer.

As an example, Figure 9 shows a thermal drill profile taken in a ridge off the West Coast of Newfoundland in a recent project (Croasdale & Associates, 1999). On the basis of this profile alone, it would be concluded that the consolidated layer was between 3 and 5 m thick. However, the borehole jack profiles (Figure 10) indicate a thickness of 1.75 to 2 m, which is more in keeping with the freezing degree-days for the region.

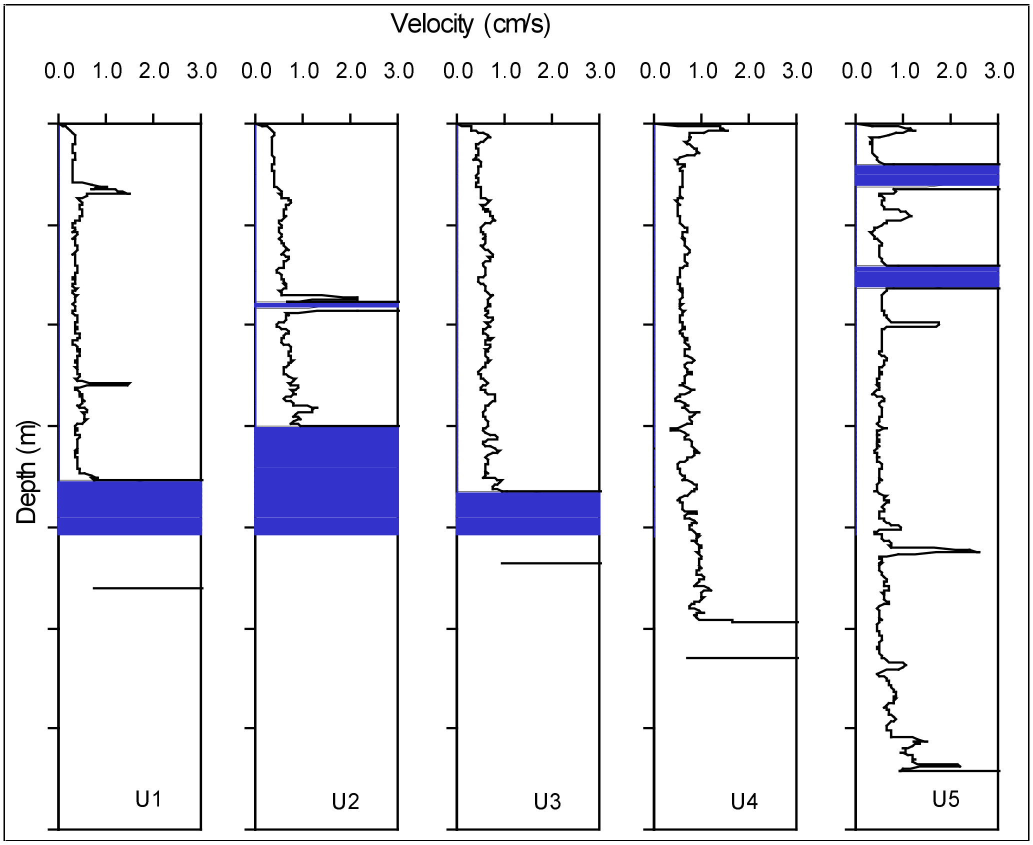

Figure 9 Thermal drill profile from West Coast Newfoundland (Site 12).

Except for the initial heat redistribution within the keel of a ridge, thermal processes should play no part in keel strengths throughout the winter because the keel is in thermal equilibrium with the sea water. Exceptions to this might occur nearshore if freshwater inflows occur. Also during breakup, when sea water temperatures start to increase, then keel strengths may start to be affected.

This raises the issue of how strengths can vary within the keel, which is at a uniform temperature. The answer may be in mechanical aging processes resulting from pressure consolidation and sintering. As reviewed by Bruneau (1996), Faraday in 1859 and Thomson in 1857 first assessed these processes of pressure bonding. Specific experiments were performed by Schaefer and Ettema (1986). They concluded that normal pressure between blocks increases cohesion, as does duration of the applied pressure. This process may be further complicated by ice creep which can potentially occur at the contact points between blocks. All these mechanical processes are enhanced by the increasing normal pressures between ice blocks which occurs in the upper layers of the ridge due to buoyancy forces (which increase with ridge depth).

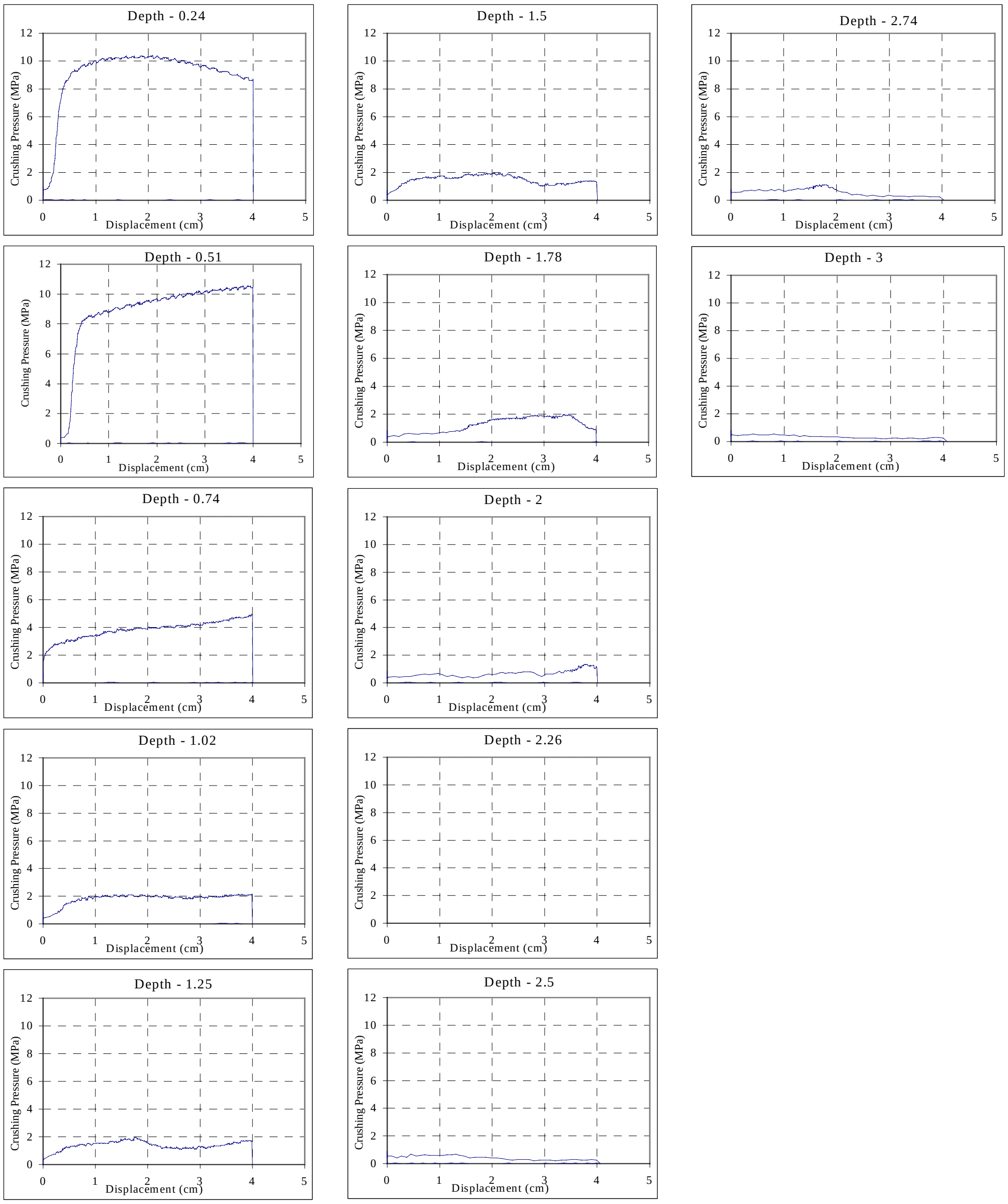

Site 12 - Hole 1

Figure 10 Typical bore hole jack profiles at various depths: West Coast Newfoundland (Site 12).

3.3 Consolidated Layer Properties - general

Recent fieldwork already described involved removal of full thickness blocks from the consolidated layer. Inspection of these blocks clearly shows the nature of the consolidated layer macrostructure. A photograph of a block taken from a consolidated layer of a ridge off Sakhalin Island is shown in Figure 11.

Figure 11 Photo showing thickness and fabric of a consolidated layer sampled off Sakhalin Island, Russia (Smirnov and others, 1999).

On the flanks of ridges there is usually a layer at the top, which was the full thickness level ice at the time of ridge formation. This may actually consist of two or more layers if rafting has occurred. These layers can be expected to have the same crystal structure as the original sea ice (probably columnar). Below this top layer, the ice below consists of a refrozen conglomerate (see Figure 12). The ice blocks forming the keel rubble are randomly oriented. Between these blocks the sea water refreezes. If there was considerable slush or frazil ice created at the time of ridge formation, then these spaces are likely to be refrozen as granular ice. It is not clear what role, salinity redistribution plays in the process of refreezing of the consolidated layer. On inspection of blocks cut from the consolidated layer occasionally, a cavity is observed. These may have been pockets of high salinity slush which have not refrozen. However, they do not appear to be very common and are not thought likely to significantly weaken the consolidated layer.

Figure 12 Section through a consolidated layer showing conglomerate ice

The temperature profiles through the consolidated layer will depend on the prevailing atmospheric conditions, as well as insulating layers such as snow or sail rubble. In the depth of the winter we can expect linear temperature profiles as seen in level sea ice, with a surface temperature well below zero. Without this, no heat loss can occur and the consolidated layer would not increase in thickness with time.

In the spring however, as air temperatures rise above freezing and solar radiation inputs heat, the temperature profile becomes less uniform until the whole ice thickness approaches the melting temperature. Recent measurements taken off the West Coast of Newfoundland exhibit this characteristic as shown in Figure 13.

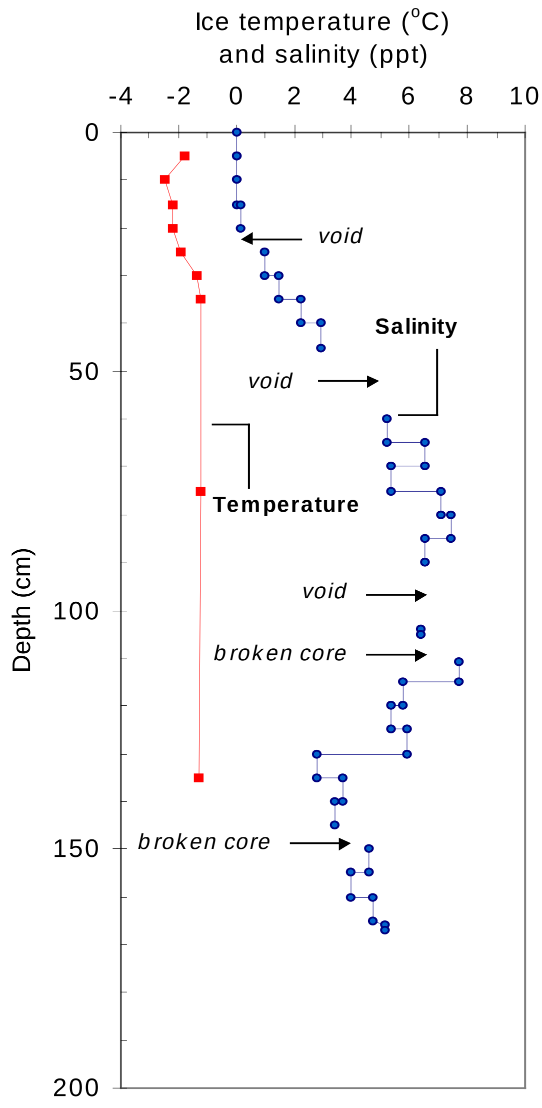

Figure 13 Temperature and salinity profiles through the consolidated layer in the spring (West Coast Newfoundland)

Also shown in the Figure 13 are typical salinity profiles. These tend to be non-uniform because of the random nature of the ice conglomerate. However, there is a general pattern of lower salinity in the top of the consolidated layer - which is often also seen in level sea ice and is due to brine drainage.

Once established, the consolidated layer is usually idealized as a layer of level ice with an assigned thickness based on an averaging assessment across the width of interest. Timco and Cornett (1997) have assessed the issue of whether the minimum thickness rather than average, controls the failure. Based on model tests, the work showed that for ice failing against an inclined structure, the maximum ice thickness controls the breaking component, whereas the average thickness controls the clearing of the ice. It is usual practice, however, to include the effect of averaging of the thickness across the structure width.

Another vital issue is how the strength of the consolidated layer compares with level sea ice for which most strength data exists. Clearly, much of the consolidated layer consists of a conglomerate with highly random crystal orientation. In general, conglomerate ice should be inherently tougher than columnar ice because the propagation of cracks will be inhibited. However, depending on the loading orientation it may be weaker than columnar ice in small-scale tests. In addition, there is the issue of porosity, which is largely dependent on salinity and temperature, although air entrapment may play a role. There may be some rationale to expect salinity to be higher in the consolidated layer compared to level ice at the same location and time of year. This would be due to more rapid freeze front penetration and the shorter length of time for brine drainage to occur.

Some strength comparisons of level ice with consolidated layer ice have been made using the borehole jack (Masterson, 1992). Some of this data supports a lower strength for the consolidated layer, however, as will be discussed later, other data does not. In any case, we must note that small-scale strength variation is often not manifested in similar variations in large-scale ice crushing pressures and loads on structures.

3.4 Crushing Strength of the Consolidated Layer

3.4.1 Small-Scale Crushing Strengths

Most data for the crushing strengths of sea ice (and freshwater ice) is obtained from small-scale uni-axial compression tests. This is also the strength, which is used in the indentation equation for ice loads (as reviewed in Chapter 5).

The crushing strength for level sea ice form a large data set, which exhibits considerable variability. A large part of the variability is due to the range of test procedures and test apparatus used. However, for tests using consistent methods, the strength has been shown to be dependent on parameters such as temperature, salinity, strain rate, ice fabric and direction of loading in relation to the ice fabric. (e.g. Michel, 1978; Lainey and Tinawi, 1984; Richter-Menge, 1986; Timco and Frederking, 1990; Truskov et al. 1992). Timco and Frederking (1990) have developed equations that relate the uni-axial compressive strength of sea ice explicitly to grain type, loading direction, loading strain rate and total porosity (i.e. brine + air), and implicitly to ice salinity, temperature and density. The compressive strength (σ_c) is given by (for granular ice)

$$\sigma_{c,g} = 49\,\dot{\varepsilon}^{\,0.22}\left[1-\left(\frac{\upsilon_T^{'}}{0.28}\right)^{0.5}\right] \qquad \textbf{3-1}$$

and, for columnar S2 ice loaded horizontally,

$$\sigma_{c,ch} = 37\,\dot{\varepsilon}^{\,0.22}\left[1-\left(\frac{\upsilon_T^{'}}{0.27}\right)^{0.5}\right] \qquad \textbf{3-2}$$

and, for columnar S2 ice loaded vertically,

$$\sigma_{c,cv} = 160\,\dot{\varepsilon}^{\,0.22}\left[1-\left(\frac{\upsilon_T^{'}}{0.20}\right)^{0.5}\right] \qquad \textbf{3-3}$$

where υ'_T is expressed as the total porosity fraction. The strain rate range for these equations is from 10^{-7} s^{-1} to 10^{-4} s^{-1}. Above this strain rate, premature (brittle) failure of the ice can occur in some, but not all instances. For higher strain rates (10^{-3} to $2x10^{-2}$ s^{-1}), Truskov et al (1992) have proposed

$$\sigma_c = -7.42 + 1.404\,T + 0.1458\,S + 11.5745\,\rho - 0.847\frac{S}{|T|} \qquad \textbf{3-4}$$

There is no indication of the loading direction or grain structure for the ice to develop this equation.

Little data, however, exists on small-scale uni-axial compression tests conducted on ice taken from the consolidated layer of ridges, especially in the context of consistent methods and wide ranges of influencing parameters. Therefore it is not possible to say, based on this approach and available data, whether consolidated layer ice is weaker or stronger than level sea ice. However, the equations described above should also be applicable to define the strength of ice from the consolidated layer.

One approach to determine the crushing strength of the consolidated layer in comparison with level ice is to use the in-situ borehole jack test already referred to. Blanchet (1998) shows a comparison of borehole jack data taken in level ice and consolidated layer ice. He shows that the consolidated layer ice is on average about 20 to 25% weaker. However, other data sets do not show such an obvious trend.

For example, Yashima and Tabuchi (1999) report on borehole jack tests conducted off Sakhalin in 1980. The average maximum borehole jack strength in the consolidated layer was 17.95 MPa whereas in the adjacent level ice, the average maximum was 16.99 MPa. Clearly, in this case one cannot attribute any lower strength to the consolidated layer. More recent tests off Sakhalin also did not indicate any strength reduction for the consolidated layer, based on borehole jack tests. (Smirnov and others, 1998, 1999).

In 1999, a field study of ridges off the West Coast of Newfoundland was conducted (Croasdale and others, 1999). As part of this program, borehole jack tests were performed. Unfortunately, the air and ice temperatures during this work were higher than normal and strength values were also lower. In consolidated layers, average maximum peak borehole jack strengths were 10.1 MPa, and in level sea ice, the average peak was 10.5 MPa. In both cases, the ice temperature was near melting and salinities were low. There were also too few data points to be confident that there were any real differences between the borehole jack strengths obtained in the consolidated layer compared to adjacent level ice.

In summary, based on the weight of the above evidence, it is apparent that there is no clear justification for lowering the crushing strength of the consolidated layer when compared to level sea ice.

3.4.2 Large-Scale Crushing Pressures

In estimating global ice loads on vertical structures, it is current practice to assign a global crushing pressure which is multiplied by the structure width and ice thickness to obtain the ice load. Global crushing pressures are usually based on the empirical treatment of measured data. Empirical treatments usually relate crushing pressure to either contact area, aspect ratio, width or thickness (or combinations of these). The topic of global ice loads due to the consolidated layer is covered in more detail in Chapter 5. However, it is appropriate to consider here whether we should factor these empirical treatments which are based on level sea ice.

In considering how to treat the global crushing strength of the refrozen layers of ridges, several investigators have proposed a reduction in global crushing pressure based on bore hole jack tests (e.g. Blanchet, 1998). However, as discussed above, the weight of evidence is that strengths are not lower in the consolidated layer. Therefore it is difficult to suggest that global ice pressures should be lower than those used for level ice.

On the other hand, there is much evidence from the Molikpaq, which suggests that the consolidated layer never failed in pure crushing but rather failed out of plane in a rubbling/mixed mode failure. Whether this will always be the case with ridges (or was an artefact of the Molikpaq lower sloping faces) is uncertain. This issue will be discussed further in Chapter 5.

3.4.3 Flexural Strength of Refrozen Layer

For loads on sloping structures due to the consolidated layer, the most important strength parameter is the flexural strength of the ice though its full thickness. Much work has been done on this topic for sea ice (Weeks and Assur, 1967; Vaudrey, 1977; Nadreau and Michel, 1984; Blanchet et al., 1997) but not for refrozen rubble. Early work testing full thickness, level ice beams was conducted by Vaudrey, (1977). Recently, Timco and O'Brien (1993) compiled virtually all published sea ice flexural strength data in a summary report.

Vaudrey's (1977) correlation with brine volume is given by:

$$\sigma_f = 0.960 - 1.920(\upsilon_b)^{0.5} \qquad \textbf{3-5}$$

where σ_f is the flexural strength in kPa and υ_b is the brine volume. Timco and O'Brien's (1994) relationship, which is based on approximately 1000 beam tests on sea ice, is given by

$$\sigma_f = 1.76 e^{-5.88\sqrt{\upsilon_b}} \qquad \textbf{3-6}$$

where the flexural strength in both cases is given in MPa. In both cases, the flexural strength has been related to the brine volume, υ_b, which is usually calculated from the Frankenstein and Garner (1967) equation

$$\upsilon_b = S\left(\frac{49.185}{|T|} + 0.532\right) \qquad \textbf{3-7}$$

where υ_b is the brine volume of the ice in parts per thousand (ppt), S is the ice salinity in ppt and T is the ice temperature in °C. This equation is a good approximation of the brine volume for temperatures –0.5 °C > T > -22.9 °C.

For the recent work on the design of the Confederation Bridge, the values calculated from Vaudrey's relationship was reduced by 85% to recognize scale effects and possible effects of the different ice fabric of the refrozen layer compared to sea ice. It has also been argued that when flexural failure of an ice sheet occurs against a structure it will be non-simultaneous, and this will also result in a reduction in the effective ice strength. Comparisons with the ice loads measured on the Kemi 1 lightpier in the Baltic, support such a reduction. (Cammaert et al., 1996). Comparison of Vaudrey's reduced values with the data reviewed by Timco & O'Brien shows good agreement over brine volumes of relevance to sea ice (Metge et al., 1996).

There has been recent work in which some flexural strength tests were conducted on *in-situ* cantilever beams cut in the consolidated layer of ridges (Croasdale and others, 1997; Smirnov and others, 1999). One issue that these tests revealed is that of the effects of the underlying ice rubble. It appears that an additional force is required to overcome underlying cohesion before the beam can be broken in flexure. The significance of this effect depends on the magnitude of the cohesive bond - see the results in 3.5.5.2.

3.5 Strength of Ice Rubble in the Ridge Keel

3.5.1 Background

As already discussed, the ice rubble in ridge keels is subject to a series of thermal and mechanical processes which can lead to interblock strength variability. This is expected to be a function of internal stress, temperatures prevailing at ridge formation, age of the ridge and possible other factors such as salinity.

The strength of ice rubble is often treated using soil mechanics concepts as derived for granular materials which leads to a strength description based on friction angle and cohesion. The Mohr-Coloumb relation is frequently used to describe the ice rubble properties, where the normal stress (σ_N) is related to the shear stress (τ) by

$$\tau = c + \sigma_N \tan(\phi) \qquad \mathbf{3\text{-}8}$$

where c is the apparent cohesion and ϕ is the angle of internal friction.

There have been extensive small-scale experiments performed on the strength properties of ice rubble. Bruneau (1997) reviewed the literature and his review is summarized in Table 4. Of the 19 investigations, only two were field based, the rest were relatively small-scale. Results for friction angle were approximately in the range 8 - 70°, and cohesion varied from 0 to about 20 kPa (but some investigators suggested cohesion is proportional to block size and would be higher in full scale).

The idealization of ice rubble as a Mohr-Coulomb material is understandable because ice rubble has the appearance of a granular material and certain aspects of its behaviour seem to be compatible with these concepts, e.g. angle of repose. On the other hand, ice rubble has characteristics that are different. For example, the thermal processes and sintering described earlier can lead to the development of cohesive bonds which, as discussed, will likely be a function of temperatures, geometry, salinity, time and stress history. These complexities are reviewed by Weaver (Croasdale & Associates, 1995) and summarized in the following extracted discussion:

> "The strength of ice rubble may be described in terms of the Mohr Coulomb model. Initial yield strengths are controlled by cohesion, and can be highly variable depending on structure and ambient temperature and salinity conditions during formation and aging. Cohesive strengths of 25 to 100 kPa may be expected under typical marine conditions. The design engineer should consider the problems that involve long failure planes (in developing load algoritms). Due to the progressive nature of rubble failure, cohesion may only govern along a small fraction of the failure plane. The shear stresses along the remainder of the failure plane may be controlled by the post yield friction behaviour of reworked ice rubble, and may also be quite variable. A typical friction angle would be in the range, 30° to 45° and perhaps higher, and is approximately linear over the range of stresses of interest to

engineers. Clearly, it is an over simplification to assign fixed cohesion and friction angle values for failure of all types of ice rubble, over high and low strain rates and for different stress histories."

It should be noted that several other experts do not agree with the range of cohesive strengths given above, they would predict lower values (typically up to 5 to 10 kPa). For example, in the design of the bridge to Prince Edward Island, the Developer assigned properties for the keel strengths as follows: cohesion - uniform distribution from 0 to 5 kPa: friction angle - uniform distribution from 10° to 50° (these values are used in the context of a probabilistic method). The Independent Engineer (in reviewing the loads) assumed that the cohesion bonds would be failed progressively and that peak loads would be controlled by friction only (Brown et al., 1995).

The design work for the Confederation Bridge, as well as increasing interest in offshore Russia, stimulated extensive efforts in recent years to obtain authentic values for the strength of saline ice rubble, these are now described.

3.5.2 Recent Laboratory Tests

For the design of the Confederation Bridge and ongoing ridge research (Croasdale, 1999), a series of bi-axial tests were conducted on saline ice blocks. The tests were performed by the National Research Council, Ottawa, using a 1m x 1m x 0.5m test device as shown in Figure 14 (Timco et al., 1992). The intent of the tests was to get the best possible data on the strength of saline ice rubble, especially within the envelope of conditions of temperature, salinity, pre-stress, stress state and confinement, which would be relevant to a typical design ridge. A key condition was to conduct most of the tests with submerged ice rubble rather than dry (although some dry tests were performed in order to compare with previous tests using the equipment).

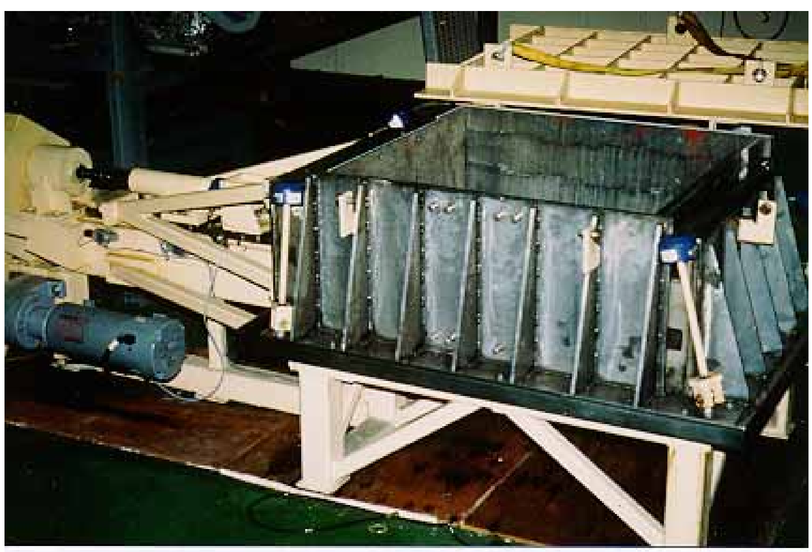

Figure 14 Photograph of the NRC bi-axial compression chamber.

Table 4 Summary of Strength Properties of Ice Rubble (after Bruneau 1997)

Author(s)	Ice Properties	Test type	Maximum confine. pressure kPa	Temp	Porosity %	Maximum Layer Depth mm	Speed mm/s	Friction angle deg	Cohesion Pa	Notes
Cheng and	Fresh ice: 2 types	Direct vert. 2-sided	0.087	Submerged	-na-	90-275	0.25-6	0-80+	0-3350	Wide range of tests
Tatinclaux	38x32x8 mm blocks, and	244-609 x 450 mm		0 C				(42-50 from		Merino (1974) records similar results
(1977)	crushed ice.	Rotary vane shear						Mellor 1980)		with same apparatus (cit. Cheng
		approx. 250 mm dia.								and Tatinclaux)
Keinonan	Saline parent sheet = 20 mm	Direct horiz. shear	1.47	Submerged	32-37	300	"Slow" by	47	11.3	
and Nyman	Flex. strength scaled 1:10 - 1:50	300 mm square box		0 C			hand			
(1978)	Blocks: h x 2.5h x 3.2h									
	Max block = 8h									
	Many small pieces by test end									
	Model ice elas. higher than natural									
Prodanovic	Uniaxial freezing saline water	Direct vert. shear	2.7	Submerged	38	304	Rate varied	47	250	Parent sheet h=19 mm
(1979)	Strength scaled 1:50 , thick = 19 mm	300x457 mm box		0 C		304	0.1-8	53	560	Parent sheet h=38 mm
	and 38 mm, max. block size = 8h									
	Flexural str. = 18 kPa, E=5.9 MPa									
	Compressive str. = 25.5 KPa									
Weiss et al	Saline parent sheet = 80 - 200 mm	Direct vert. shear	31	Submerged	19-50	1000	4	13	1700	Parent sheet h=80 mm
(1981)	Flexural strength = 30-80 kPa	1 m x1.5 m		-2.5 to -5 C		1000	25	11	1200	Parent sheet h=80 mm
	Strength scale approximately 1:10					1000	3	26	2300	Parent sheet h=150 mm
	Max block size: 4h					1000	24	25	1400	Parent sheet h=150 mm
	water S = 50-60 ppt, ice S = 10-18 ppt					1000	5	34	4100	Parent sheet h=200 mm
						1000	25	34	3400	Parent sheet h=200 mm
Hellmann	Three types:	Direct vert. shear	4.2	Submerged	-na-	700	10.9	54	580	Ice chips
(1984)	Fresh ice chips: 10-20 mm	'cross-shaped'		0 C		700	1.6	61	420	Ice chips
	Fresh ice cylinders: 30-50 mm	2 sides at 0.7x0.7 m				700	10.7	44	280	Cylinders
	Urea doped columnar: individual grains	1 m^2 total				700	10.7	64	0	Doped
Fransson&	Three ice types:	Direct horiz. shear	3	Submerged	20	500	10	34	550	Parent sheet h=39, length=110 mm
Sandkvist	Fresh: h = 39, Lx = 110, flex. = 1000KPa	500 mm square		ice = 0 C		500	10	14	450	Parent sheet h=46, length =8 mm
(1985)	Fresh: h = 46mm, Lx = 8 mm, flex. = 780 kPa			water = 2 C		500	10	13	240	Approx results from saline.
	Saline: 6 ppt ,h = 52 mm, Lx = 4 mm									Parent sheet h=52, length =4 mm
	flexural strength = 38 kPa									
Urroz and	Three sizes fresh ice and 1 plastic:	Simple shear	0.48	Floating	36-41	76-229	2	36.6	0	small (blocks)
Ettema	small: 18x18x18 mm	Rubble is vertically		layer, 0 C		76-229	2	51.6	0	med (blocks)
(1987)	medium: 38x32x16 mm	unconstrained				133-200	2	30.5	0	large (blocks)
	large: 95x95x38 mm	530x609 mm				152-229	2	51	0	large (blocks)
	polyethylene: 38x31x9.5 mm					152-76	2	35	0	plastic (blocks)
Sayed	Fresh ice: 30 mm cubes	Biaxial plane strain	Confining	-10 C	Initial 40-46	-na-	0.032-0.85	27-45	10000 -	
(1987)	Not submerged	Isotherm. cold, dry	press. = 35		Final 30-40				20000	
		500x300x300 mm	max. = 130							
Wong et al.	Crushed fresh ice cubes	Direct horiz. shear	(Very high)	-2 C	Initial 41-51	200	Very slow	No peak		Gale et al. (1986) similar testing
(1987)	Max size = 4.75 and 9.5 mm (3 mm av.)	300 mm square	140	Brine &			0.0098-0.046	- monotonic		arbitrary max selected for phi-c
	Uniformity coefficient 2.8 - 4.0			Dry				increase		but tests similar to these
Case (1991)	EGADS (doped fresh) ice sheet	Direct vert. shear	2.41	Submerged	34-37	450	1	48.9	523	7.5 hrs warmup
	30 mm thick, brocken into blocks	600x450 mm box		0 C		450	1	37.6	597	8.5 hrs warmup
	3.2h average length, 8h maximum size					450	1	34.8	674	10 hrs warmup
						450	1	27.2	824	11 hrs warm up
Lepparanta	Unknown ice type (scale =1:13)	Direct horiz. shear	1.5	Submerged	20	400	-na-	8.4	800-2400	Punch and direct shear results
and Hakala	15 mm thick parent sheet	800x500 mm box		0 C						Reported results unclear
(1992)		Punch tests 150 mm								
Eranti et al.	Fine grained model ice (FG,FGX)	Shear box	-na-	-na-	-na-	-na-	-na-	34	350	Average for loading rate
(1992)	Scale 1:40 to 1:50, E = 20-30 MPa							30	2000	Amount of slush and deter-
										ioration of rubble tested
Sayed et al.	EGADS (doped fresh) ice sheet	Biaxial plain-strain	100	Air = -2 C	24-34	500	0.27-5	47.7	0	Strain ratio:-.23 first 10 kPa only
(1992)	30-40 mm thick, brocken into blocks	1 m x 1 m x 0.5 m		Wat. = -0.3 C	for wet tests			59.7	0	Strain ratio:-.51 first 10 kPa only
	max. size = 20-25 cm, min. size = 5 cm	vert. shear zone						48.4	400	Strain ratio:-.23 first 10 kPa only
	Submerged tests reported here							30.6	333	Strain ratio:0.0 first 10 kPa only
Loset and	Freshwater ice blocks ranging from	Biaxial plain-strain	90+	Dry = -2				dry 37-65	- na -	Tested different size
Sayed (1993)	25 mm to 130 mm	1 m x 1 m x 0.5 m		Wet ice = -2	Initial 36-39			wet higher		distributions and varied
	dry and wet tested	vert shear zone		Water = 0		500	3.34-5.3	than dry		strain ratios
Lehmus and	Fresh water ice sheet sawn into	Direct horiz. shear	1.6	Submerged	28-42	800	20 & 10	- na -	- na -	Consolodation time and temp.
Karna (1995)	parallelepipeds approx. 40x150 mm	800x960 mm square		-10 C						varied at constant pressure
	largest = 300 mm	below refrozen layer		for varying						
				durations						
Cornett and	Saline ice parent sheet = 0.5% salt by wt.	Biaxial plain-strain	60	Dry -na-	- na -	500	4.0-5.3	45-70	- na -	Friction angle decreases with
Timco (1996)	h = 10 cm, pieces broken	1 m x 1 m x 0.5 m		Ice = -10 C				Saline		confining pressure
	by hammer to <10cm in length -	vert. shear zone		Water = 1 C				higher than		
	varying in size, angular in shape							fresh		
FULL SCALE										
Lavender	Apparent cohesion from large-scale	Analyzed from data						Not publ.	0-3800	
(1973)	river ice jams									
Lepparanta	Baltic first-year ridge keels	Punch shear	12 kPa	Submerged	23-33	3300-11700	Very slow		1700-4000+	Total shear strength reported
and Hakala		through keels	(11.7 m				<1 mm/min		3400	Median for keel depth =3.9 m
(1992)			keel depth)							
SOLID ICE										
Roggensack	Solid columnar freshwater ice	Large shear box	1.49	-2.5 C	0	-na-	0.06-0.12	22.8	500000	Peak strength
(1975)								25.2	750000	Ultimate strength
Zanegin et al.	In situ sea ice	Direct shear box	3 MPa	0 to -20 C	0	-na-	10^-3 to			
(1995)							10^-1 /s	up to 56	0.3 - 1.2MPa	Range of results given

Thirty-eight tests were performed. The details of the tests and the results are contained in the Project Report (Cornett and Timco, 1995). Some specific results are also discussed in Timco and Cornett (1999). Some of the salient features of the results were as follows:

- The friction angle mobilized by bulk ice rubble depended upon the characteristics of the ice rubble, the stress state of the rubble, and the nature of the imposed deformation;
- The tests showed very repeatable rubble properties for the same test conditions;
- The strain ratio had a significant influence on the stiffness and strength. The mobilized friction angle is lower for rubble that undergoes greater mechanical consolidation;
- Wet (submerged) rubble is substantially weaker than similar rubble that is not submerged (i.e. dry). Submergence reduces both the initial yield strength and the strength under deformation, and reduces the mobilized friction angle by about 30%. The submerged conditions are appropriate for the keel, where as the dry conditions are appropriate for the sail portions of a ridge.
- Measured friction angles ranged from 75° to 30°, depending upon the test conditions and stress state.
- Curing under a pre-stress dramatically increases the initial yield strength of the ice rubble, but has little influence on the friction angle mobilized by the material after the yield.

The results of these systematic tests clearly showed that the mechanical properties of the ice rubble in a ridge cannot be properly characterized by a single value of friction angle and an assumed cohesion intercept. There are 3 factors that complicate this characterization for a ridge:

1. The character of the ice rubble within a ridge varies from place to place (i.e. dry rubble in the sail, wet rubble in the keel, different block sizes, etc.);
2. The magnitude and character of the static stresses vary throughout the ridge;
3. When a ridge interacts with a structure, the rubble in the keel and sail experience a wide range of deformations.

3.5.3 In-Situ *Test Methods for Ice Rubble Strength*

In situ measurements are considered important because it seems apparent that the strength of ice rubble is influenced by the processes within a ridge which in themselves are not well understood. These range from the temperature and salinity of the ice at formation, to aging processes with time that in turn may be influenced by internal stress levels as well as thermal and salinity gradients. Therefore, artificially created ice rubble can never hope to be representative of real ice rubble, and even real ice rubble properties might change if samples are recovered for testing. Thus the best approach to the measurement and understanding of full scale ice rubble is to obtain the properties *in situ* on actual ridges.

In 1996 a study examined over 30 different *in situ* test methods in terms of their suitability (Croasdale & Assoc., 1996). The most promising methods were carefully tested at model scale, in an ice basin, as part of an extensive program on ice loads due to pressure ridges.

Methods of analysis of the tests were developed in terms of rubble shear strength, and preliminary designs for their full scale mobilization developed (see Bruneau et al., 1999). The two methods were the "direct shear test" and the "punch shear test" and these will now be described in detail below, along with a description of the “pull-up test”.

3.5.3.1 The Direct Shear Test

The direct shear test arrangement is shown in Figure 15 and the photographs in Figure 16. The test involves trenching through the refrozen layer of a ridge to isolate a rectangular slab. The load required to displace the slab horizontally is then measured and the corresponding displacement is recorded.

In the shear test, the failure plane occurs at, or near, the bottom of the consolidated layer, in a way that mimics the “shear plug” failure mode of a ridge keel. The shear strength just below the consolidated layer is one of the key properties needed to calculate ridge loads on structures (see Chapter 5).

This test technique has been successfully used to date in 4 separate field projects, 2 in Canada and 2 in Russia (Croasdale & Associates, 1997a, 1997b, 1998a, 1998b). The test equipment consists of a 25 tonne hydraulic ram with a 0.6 m stroke, a compression load cell, and universal joints connecting each end of the ram to the two aluminium reaction panels. String potentiometers record the displacement of the ice slab. Power is supplied to the ram through a hydraulic power pack driven by a gasoline engine.

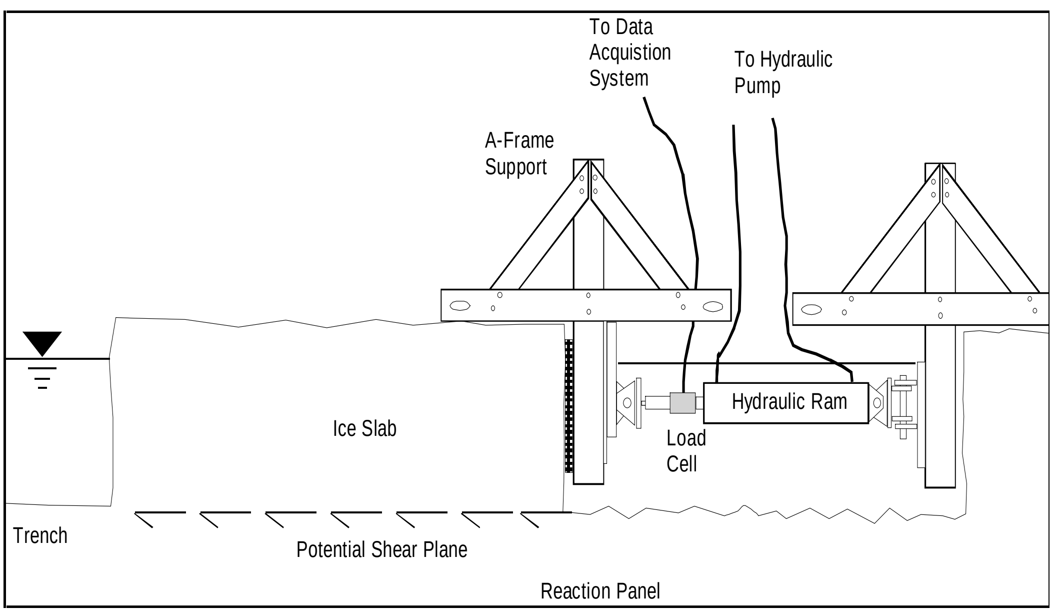

Figure 15 Configuration of the Direct Shear test

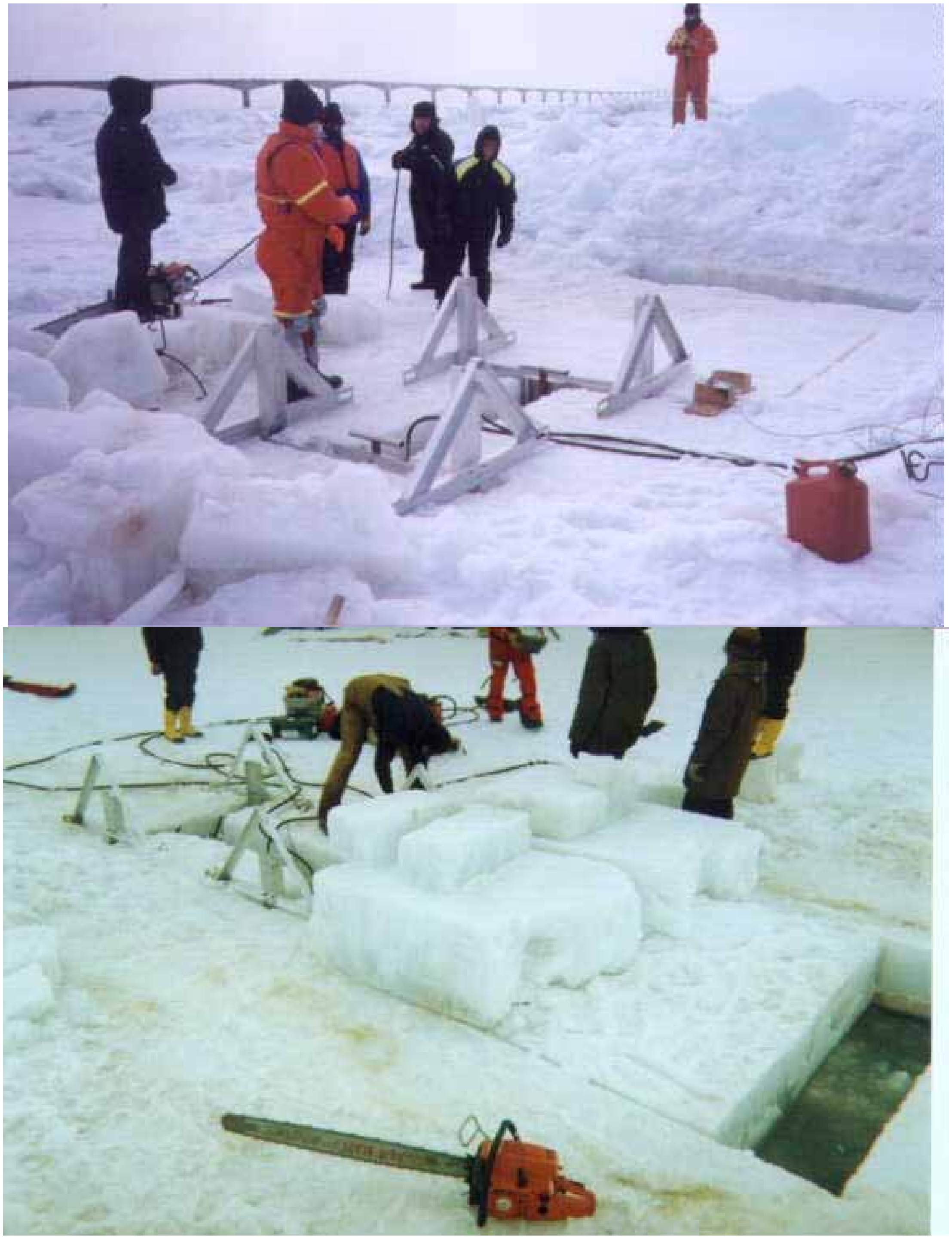

Figure 16 Photographs of the Direct Shear test

Site preparation requires that a number of cuts be made through the consolidated layer and some blocks removed to allow the apparatus to be lowered in place and to create room for the ice slab to be horizontally displaced. A plan view of the cut pattern and trenches required for the direct shear test is shown in Figure 17 (see also the photographs in Figure 16). Ideally, a site is chosen on the shoulder of a ridge so that the upper surface is relatively smooth but is underlain by keel rubble. For tests conducted in the sail region of a ridge, the sail blocks are removed and the ice surface made as flat as possible to facilitate easy cutting with the chain saws. Cutting is performed with chain saws. In Canada, the main cuts around the slab, and the slot behind the slab were made with a saw with a 59" (1.51m) double bar, mounted on a sled. The double bar created a slot approximately 2.5cm wide that helped minimize friction and binding as the slab was being displaced. The sled provided a stable platform and greatly reduced the effort required to operate the saw, and greatly increased the safety of the operation. For the tests in Russia, a much larger saw was developed with a 3.2m long blade, see Figure 18 (Smirnov and others, 1999).

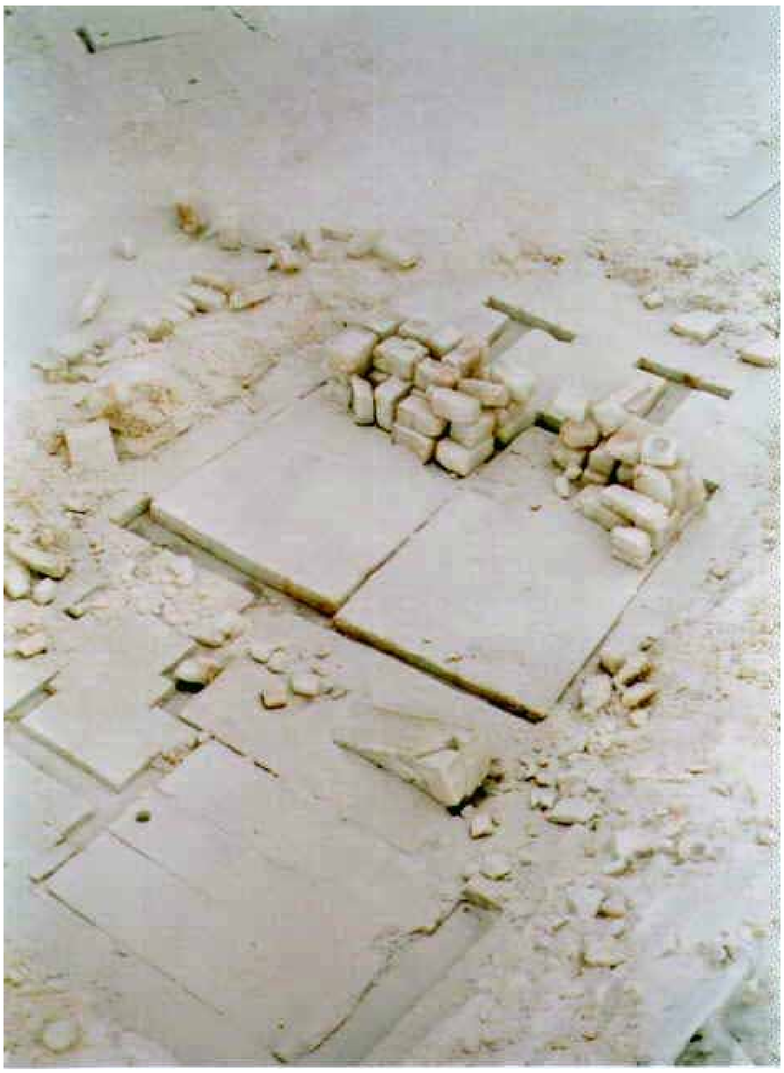

Figure 17 Pattern of ice slots cut into consolidated layer to perform direct shear test

Figure 18 Large saw developed for cutting through consolidated layer offshore Sakhalin

The slab was tapered slightly from front (where the load was applied) to back, to further reduce friction and binding problems. The trench behind the slab was made by cutting the ice into smaller pieces and removing them using either an A-frame with a block and tackle, or ice tongs. An “I” shaped slot in front of the slab was also required for the panels and ram. This was cut using the same methods.

The tests were recorded on video and extensive measurements of block displacement and qualitative descriptions were recorded. In some tests, small diameter styrofoam rods were placed vertically in drilled holes through the slab into the ice rubble. These gave an indication of the level of the shear plane that was usually directly at the base of the consolidated layer.

In some tests a surcharge was applied using the ice blocks removed from the slots in the refrozen layer.

Typical load and displacement records for the direct shear test are shown in Figure 19. The initial peak load is indicative of a cohesive bond that has to be overcome before the slab can be moved.

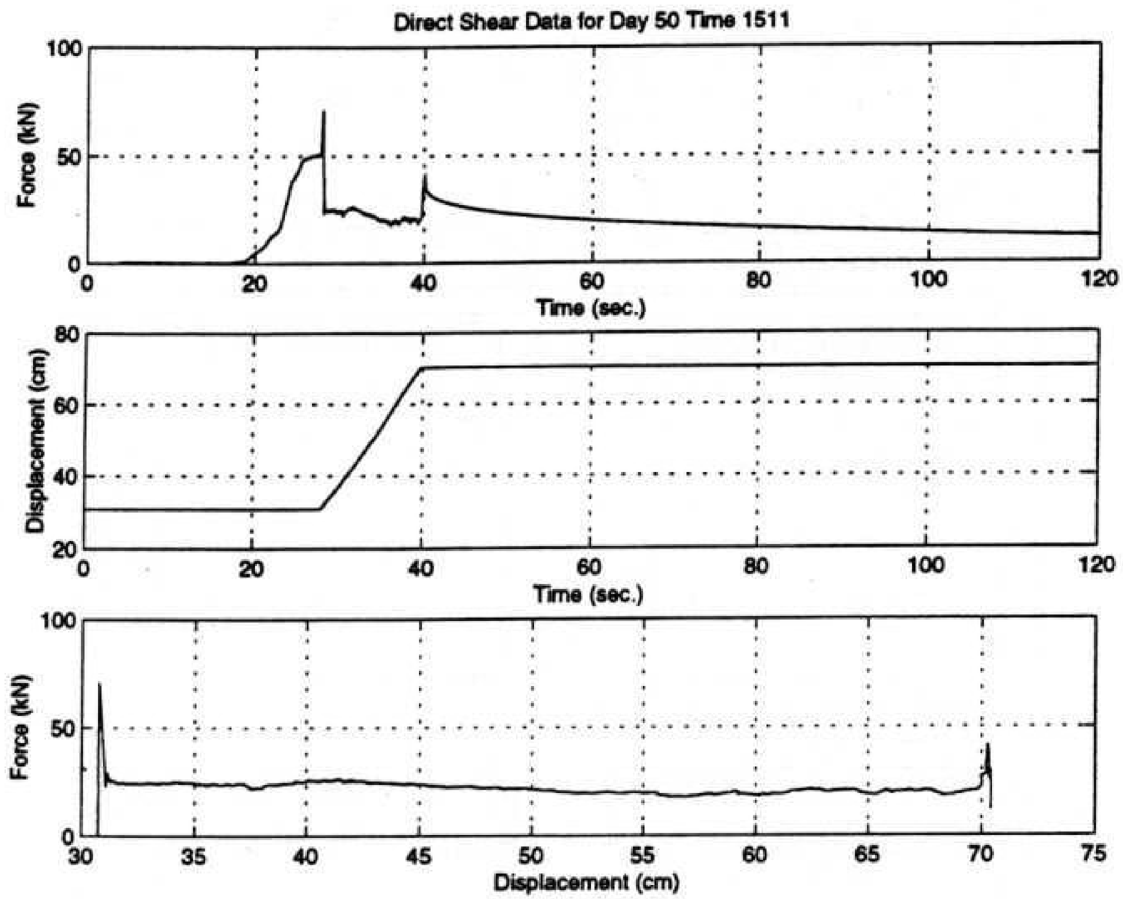

Figure 19 Typical load trace from direct shear test

3.5.3.2 The Punch Shear Test

As depicted in Figure 20, in the punch shear test, a plug of the consolidated layer layer is cut through to the underlying rubble. A load is then applied to fail a plug of the keel downwards. This technique was first tried in the Baltic by Lepparanta and Hakala (1992), with mixed success (due to insufficient load capacity). In 1996, extensive testing of the technique was performed in conjunction with the model tests conducted as part of the Ridge Load JIP (K.R. Croasdale & Associates Ltd., 1996b). In total, over 100 tests were performed in model ice rubble. Initially, evaluation tests were performed to assess the effects of platen speed, platen (plug) diameter, ridge depth and state of the rubble (new or aged). Then, before each ridge test against a model structure, several punch shear tests were performed on the ridge. The purpose being to obtain *in situ* shear strength for the ridge to help in interpretation of the measured ridge load against the structure.

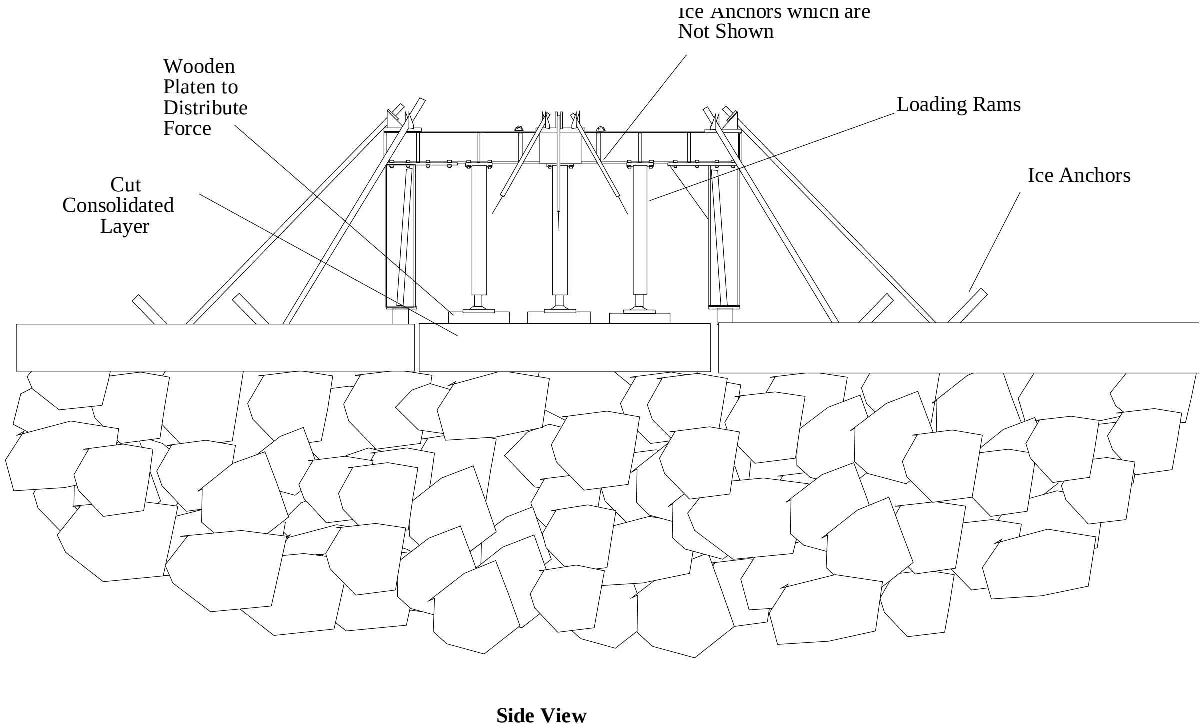

Figure 20 Configuration of punch shear test as used in Russia in 1997.

A scheme for interpretation of the punch shear test in terms of the friction angle and cohesion properties of the rubble was also developed, based on theories for a horizontal anchor plate in soil.

The main advantage of the punch shear test is that the failure surfaces traverse the full depth of the ridge as in the passive failure mode of a ridge keel. Therefore, large-scale average values of keel shear strength are obtained.

Following this successful use in model tests, a full-scale test device was tested in Northumberland Strait in 1997. In these tests the apparatus consisted of a 30 tonne (0.3 MN) hydraulic ram mounted on an aluminium frame secured to the ice via four ice anchors (see Figure 20 and the photos in Figure 21)

Following the use of the punch shear tests in Canada in 1997, larger equipment was developed for the subsequent year and for use in Russia. The equipment used in Russia in 1997 and 1998 is shown in Figure 22. By 1998, the equipment used in Russia was built to have a load capacity of 2 MN and designed to load a 3m by 3m block cut through the consolidated layer.

A typical load trace is shown in Figure 23. In this case, the first peak corresponds to the breaking of the bonds locally under the block, while the second peak corresponds to a global plug failure of the keel. It should also be noted that in many of the later tests, toggles and strings inserted into small holes drilled through the keel confirmed global plug failures with very little compression strain within the keel material.

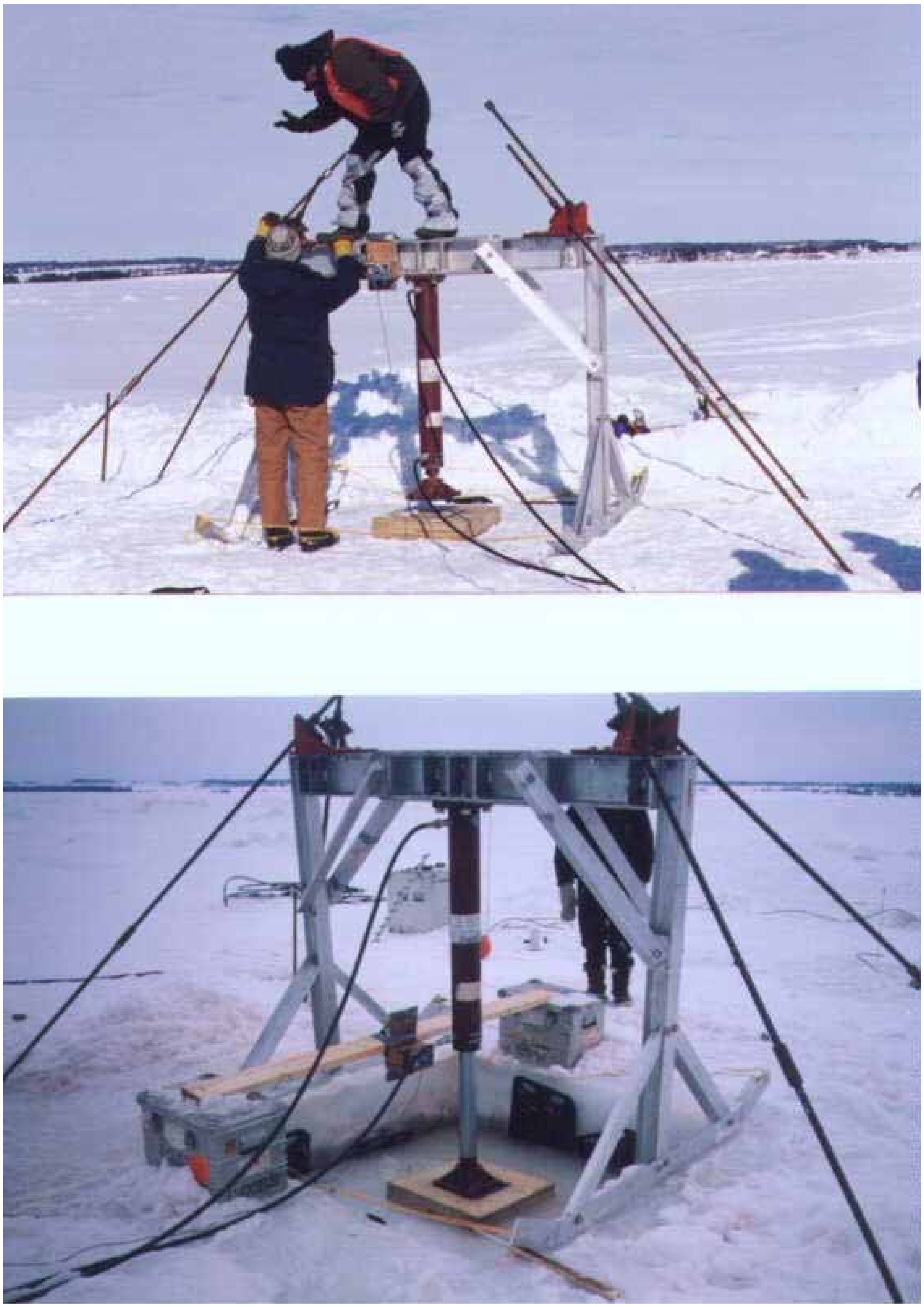

Figure 21 Photographs of the Punch Shear test in Canada, 1997

Figure 22 Equipment used for punch shear test in Russia, 1998.

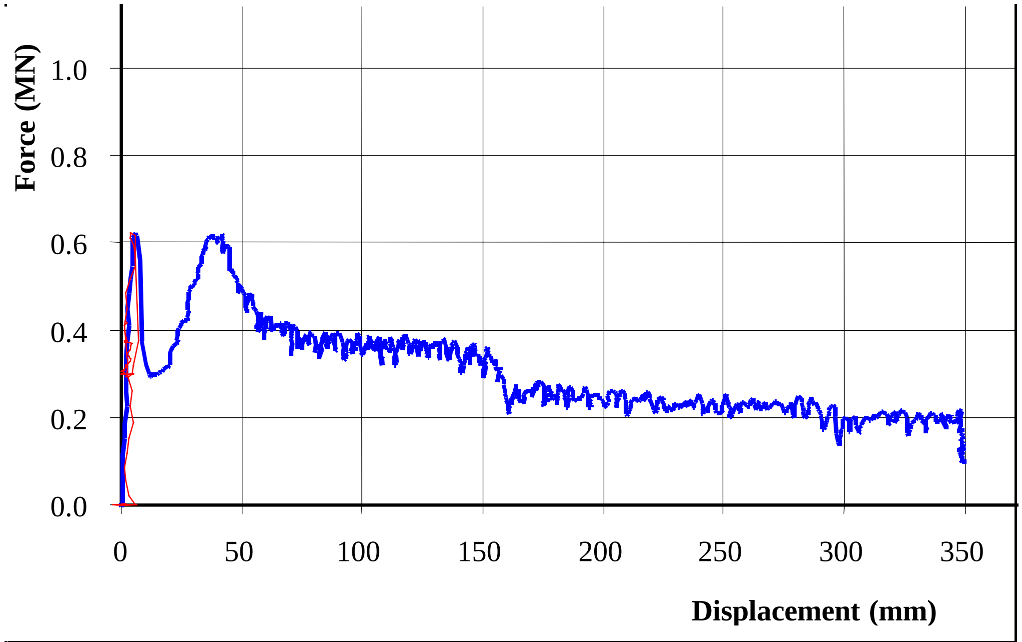

Figure 23 Typical load trace from a punch shear test (Smirnov and others, 1999).

3.5.3.3 The Pull up Test

The objective of the pull up tests was to investigate the presence and nature of any bond which might exist between the consolidated layer and the underlying ice rubble. The idea arose when it was known that blocks would have to be cut and lifted from the refrozen layer in order to perform the direct shear tests. It was also recognized that if there were no cohesive bond below the refrozen layer, then the load trace in lifting the block would reflect the loss of buoyant support as it was raised and should be at a constant gradient. On the other hand, any bond present would manifest itself as an increase in load superimposed on the buoyant gradient. Once the bond had been broken the load would revert to the buoyant gradient. The presence of a tensile bond would indicate the presence of cohesion.

A typical configuration of equipment to perform pull-up tests is shown in Figure 24.

A typical load trace obtained during a pull up test is shown in Figure 25. The initial load required to break the tensile cohesion is clearly shown and gives a strong indication of the cohesive nature of ice rubble (at least that immediately underlying the consolidated layer).

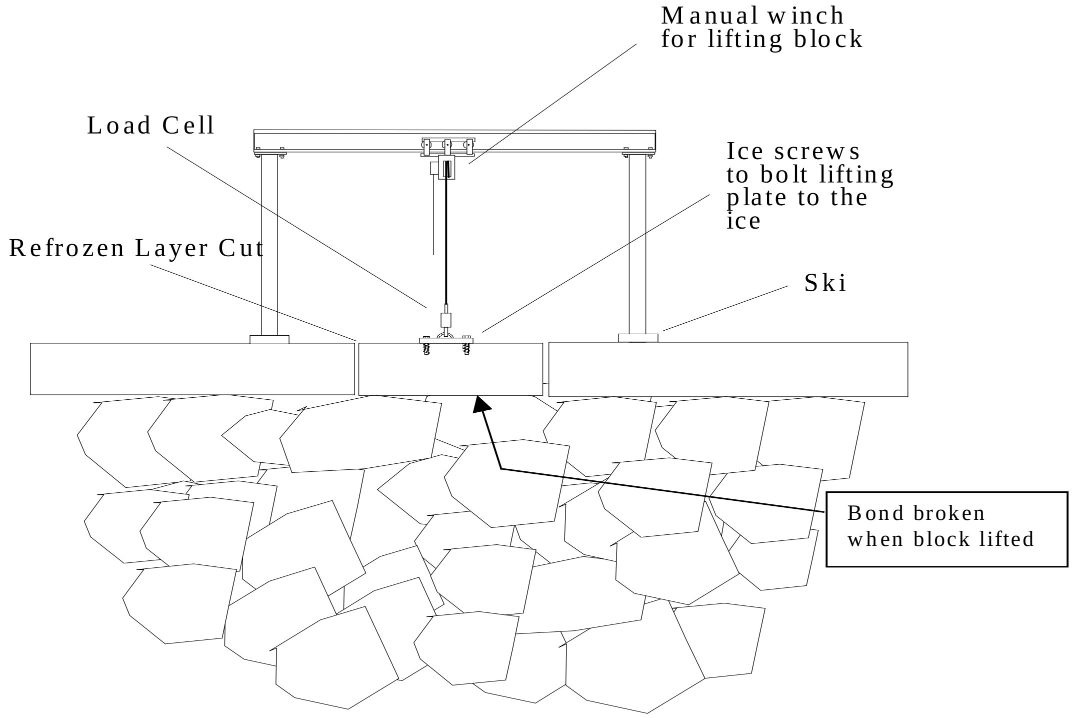

Figure 24 Typical configuration of the pull up test.

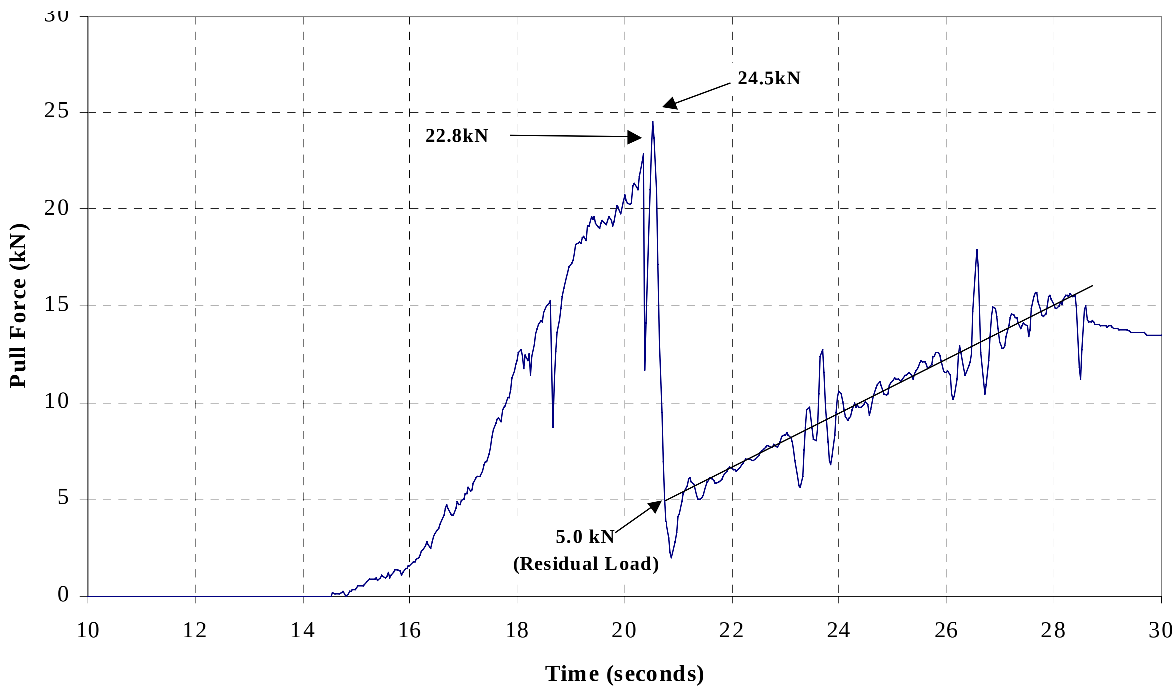

Figure 25 Typical load trace from a pull up test. Note the peak at 22 s corresponding to breaking the cohesive bond.

3.5.4 Overall Scope of In-situ Tests

The number of in-situ tests performed, using the equipment described in this report, at various locations is given in Table 5.

Table 5 Number and locations of in-situ ridge strength tests

Test location	Date	Direct shear tests	Punch shear tests	Pull up tests	Flexural tests	Comments
Northumberland Strait, Canada	Feb 18 - March 20, 1997	11	9	8	3	Proprietary until December 2000
N.E. Coast Sakhalin Island, Russia	April 14 - 23, 1997	1	5	7	0	Proprietary to Exxon Neftegas
Northumberland Strait, Canada	Feb 17 - 24, 1998	5	5	9	0	Proprietary until December 2001
Confederation Bridge	March 7 - 8, 1998	2	4	0	0	Proprietary until December 2002
N.E. Coast Sakhalin Island, Russia	March 23 - April 6, 1998	3	6	17	2	Proprietary to Exxon Neftegas

All the test results are still proprietary to the sponsors. However, the sponsors of the first test series (Exxon Production Research, and Program on Energy Research & Development) conducted in Canada in 1997 have kindly agreed to allow some of the data to be included in this report. These results now follow.

3.5.5 Overview of Northumberland Strait Results, 1997

3.5.5.1 Keel Strengths

About 30 successful tests were carried out during a two-phase field program. The first phase of the field program was carried out from February 18 to March 4, 1997. This was judged successful and the sponsors supported a second phase which was conducted from March 14 to 20, 1997.

A total of 11 direct shear tests were performed. The direct shear test measures the shear strength mobilized when a block cut from the refrozen layer of the ridge is pushed horizontally across the top of the keel rubble. This test is a measure of the strength of the interface between the keel rubble and the bottom of the refrozen layer. The maximum shear strength measured was 22.6 kPa and the average was 14.1 kPa.

A total of 9 punch shear tests were performed. In the punch shear test a block is cut through the refrozen layer and pushed down into the keel creating a plug failure of the keel material. The punch shear strength is a measure of the average strength through the keel thickness. In these tests the maximum value measured was 12.8 kPa and the average of all the tests was 8.5 kPa. But note that these values include three tests where there was insufficient load to fail the keel and therefore the test strengths represent lower bounds.

It should also be noted that in both tests, the shear strength can be interpreted as either pure cohesion or pure friction or a combination of the two. If in the direct shear tests, the strengths are interpreted as a friction angle, then the maximum obtained was 83° and the average was 74°. In the punch shear tests the maximum was 69° and the average was 57°.

Another test indicating the strength of the bond between the refrozen layer and the keel rubble is the pull up test. In this test, a block is cut through the refrozen layer and lifted upwards. The tensile bond strength is measured. Eight of these tests were performed. The highest strength obtained was 26 kPa and the average 17 kPa. Because these tests show a clear indication of cohesion, further interpretation of the tests is based on a cohesive material.

Figure 26 shows the total results from the three types of tests on a common plot as a function of keel depth. This is not to infer that each test should give the same strength for a given ridge. On the contrary, as already discussed, the direct shear measures the shear strength immediately under the refrozen layer (where it may be the highest). Whereas, the punch shear gives the average shear strength through keel, and the pull up test measures tensile cohesion. Nevertheless, the plots do show that there is a trend of increased cohesive strength with ridge thickness. Other observations in relation to the results are given below.

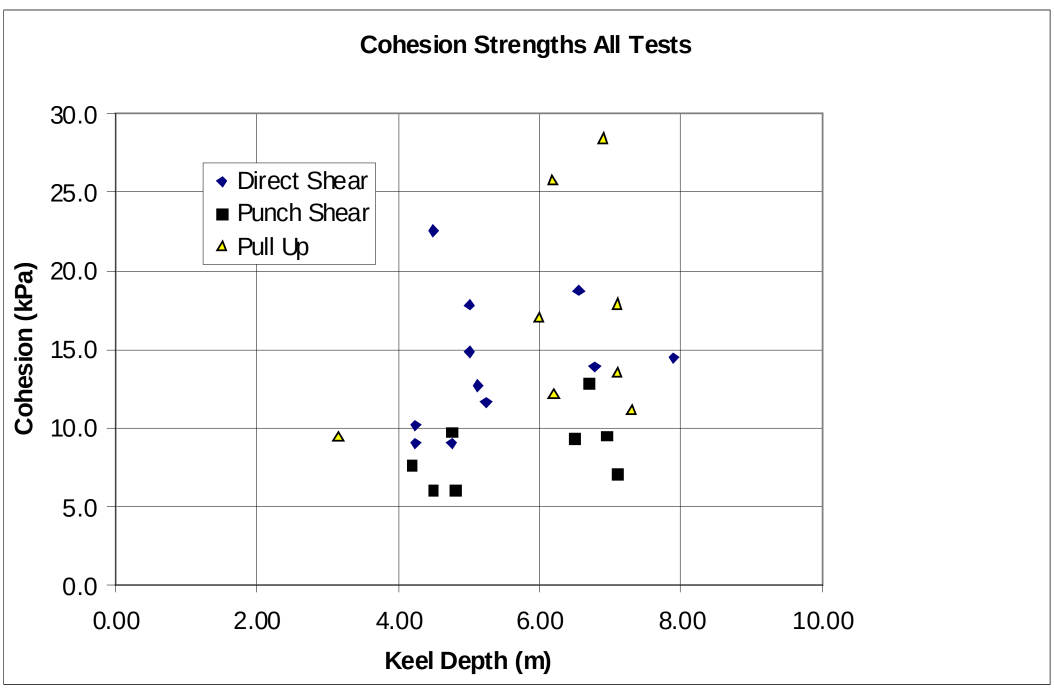

Figure 26 Results from all test types - Canada 1997.

The average punch shear cohesive strength is about 1/2 of the average direct shear test strength (8.5 : 14.4). This suggests that the shear strength varies from near zero at the bottom of the keel to its maximum value just below the refrozen layer. Ignoring for a moment the presence of added weight to some of the direct shear tests, this ratio is also consistent with the linear normal stress dependency (Mohr-Coulomb like) theory for ice rubble shear strength. The results show without a doubt that the shear strength of ice rubble is normal stress dependent. However, allocating the shear resistance into meaningful friction and cohesion values as a traditional Mohr Coulomb material may be incorrect.

The average pull up strength value of 17.1 kPa may be high as the two tests which resulted in the highest force may not have had a fully cut consolidated layer. Without these two tests the remaining pull-up tests averaged 13.7 kPa, which is within 5% of the direct shear values. If it was correct to discard the higher pull up values, then for the rubble material *in-situ* there does not appear to be any differentiation between cohesive tensile strength and shear strength. However, if the higher pulls up values are included, then the tensile strength is higher than the shear strength, which would be the case for a Tresca type material.

It is of interest to examine the trends in the data with keel depth. As already suggested, not all tests are directly comparable, so we first plot punch shear only. This data gives the average cohesion strength through the keel depth. Figure 27 shows the results, including a best-fit linear trend given as:

$$\mathbf{c = 0.88\ H + 3.52} \qquad \mathbf{3\text{-}9}$$

Here, c is the cohesion in kPa and H is the total keel depth in metres from the ice line.

The standard deviation of the cohesion strength data is 2.29 kPa. Extrapolation to a 16 m deep keel yields an average strength of 17.6 kPa.

If it is assumed that the keel cohesion strength varies linearly from zero at the keel bottom to a maximum under the refrozen layer, then it should be possible to combine half the direct shear and punch shear data in a common plot. This is done in Figure 28. This data also shows a dependence of cohesion on keel depth given as:

$$\mathbf{c = 0.68\ H + 3.91} \qquad \mathbf{3\text{-}10}$$

The standard deviation of the cohesion strengths is 2.27 kPa. In this case, extrapolation to a 16 m keel gives an average strength of 14.8 kPa.

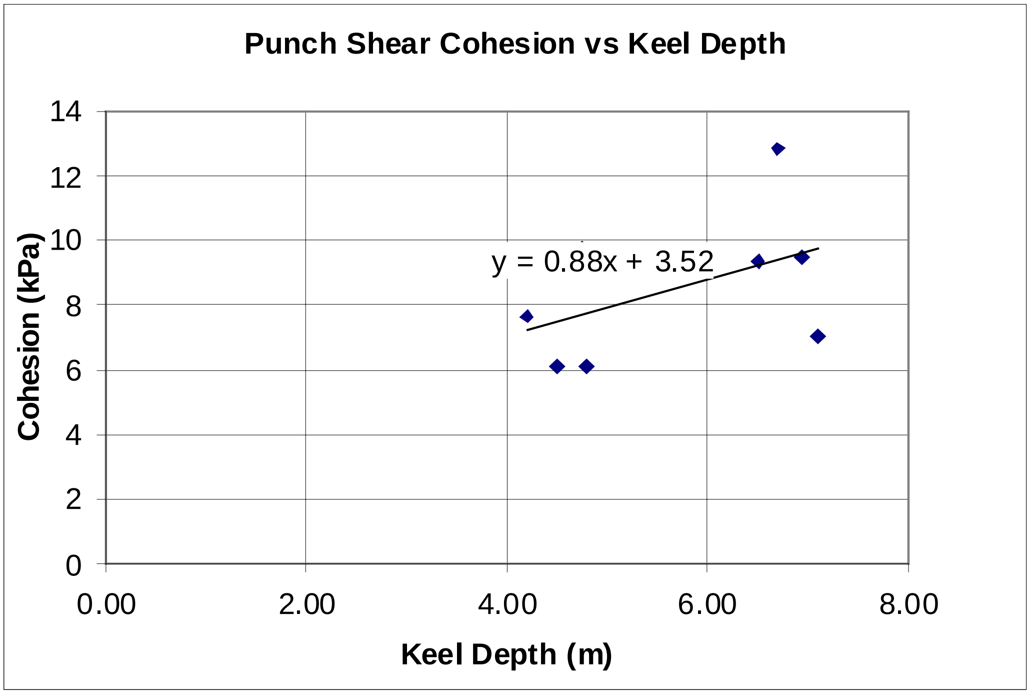

Figure 27 Punch shear test results - Canada 1997.

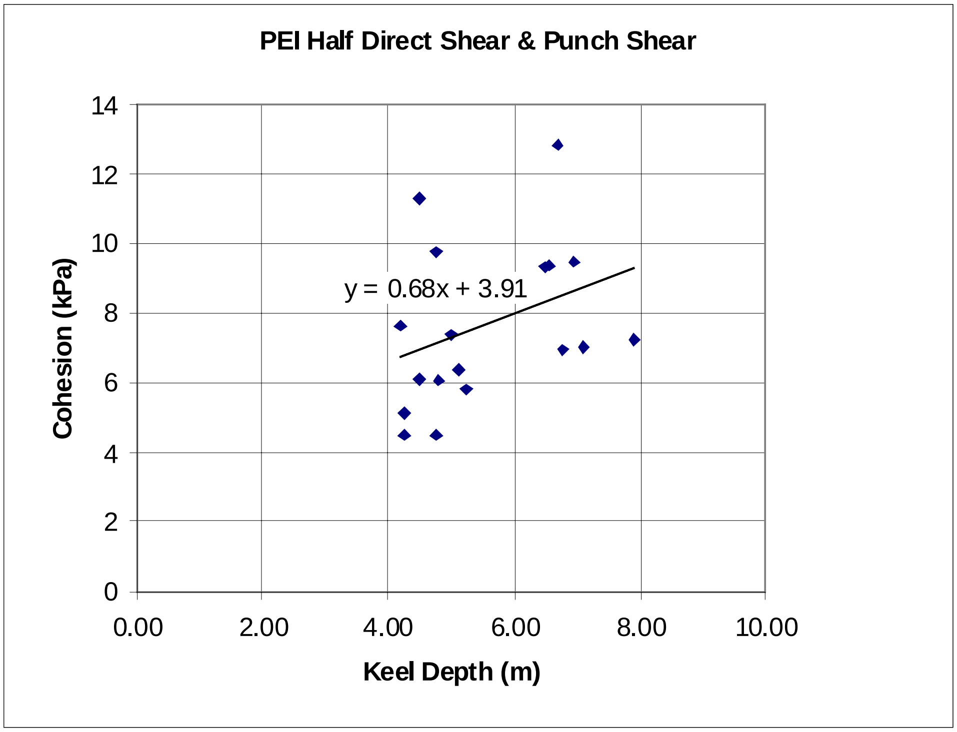

Figure 28 Punch shear cohesion and half direct shear versus keel depth, Canada 1997.

The punch test results in this field program may be compared to those from Lepparanta and Hakala (1992). In that field program 6 ridges were punch tested - for four of those tests (one being a mistrial and another did not fail the ridge) ridge thickness was between 3.6 and 3.8m and the measured shear strength (based on vertical shear planes etc.) ranged from 1.7 to 3.4 kPa. The punch tests in this field program resulted in higher strength values, around 6 kPa for those tests on ridges under 5 m in thickness. There may be a few explanations for these differences. The shear rate (less than 1 mm/minute average) in the Baltic field program was very much slower than that in the PEI field program (in some cases more than 1cm/second). The slow rate would likely to have permitted creep to play a role in strength reduction. Also block size and flexural strength were different in the Baltic program. These factors and the variation in testing procedures may account for the differences.

Bruneau (1997) conducted a detailed regression analysis of several ice rubble shear strength laboratory test results. Simplified formulas for shear strength and cohesion were determined as:

$$\tau = 3.52\,(\sigma_N)^{0.852} \tag{3-11}$$

$$c = 17\,L_I \tag{3-12}$$

where L_i is the average block thickness. When normal stresses from the direct shear tests are used in the first formula the resulting computed shear strength is 9.4 kPa on average, significantly less than the average 14.4 kPa measured. For an average block thickness L_i of around 0.4 to 0.5 m for the PEI field program, the computed cohesive shear strength would be around 7 kPa. This value is less than that measured in many of the full-scale tests (although close to the average of the punch shear and half the direct shear of about 7.7 kPa).

Based on these comparisons, the use of small-scale lab data is not recommended for design. Also, the direct scaling of model tests has to be done with extreme caution.

3.5.5.2 Flexural Strengths

Three flexural strength tests were performed during the 1997 program. All three were positioned within the refrozen layer of ridged ice and were thus supported by rubble underneath. There are no references in the literature to *in-situ* flexural tests of the refrozen layer and so these experiments were the first of their kind. Of the three tests, two were conducted on "direct shear" slabs that had been sheared a few days before (and the underlying bond broken). The third was performed in undisturbed ice nearby. The two different support conditions were expected to provide insight into the affects of keel bonding on refrozen layer flexural strength. The upward breaking cantilever beam method was selected in advance.

The simple cantilever bending equation was used to estimate the effective flexural strength as follows:

$$\sigma_f = 6FL/BH_b^2 \qquad \text{3-13}$$

where F is the uplift force, L is the cantilever beam length, B is the beam width and H_b is the beam thickness.

The force traces for the three flexural strength tests are remarkably similar. The load climbs rapidly to the breaking point of the beam, then it falls rapidly to a residual level, which corresponds to the slab weight.

To obtain peak breaking forces the residual loads were removed from the peak recorded force. The residual loads were close to 2 kN for all three tests and showed similarity in form as well as magnitude. The third flexural test on undisturbed ice was performed next to a pull-up test site for which the uplift tensile cohesion is known. Flexural strength was computed with and without this cohesion component (based on subtracting the opposing root moment created by the additional force necessary to first break this tensile cohesion).

The equation used for the corrected flexural strength is:

$$\sigma_f = 6FL/BH_b^2 - 3cL^2/2H_b^2 \qquad \text{3-14}$$

Where c is the tensile cohesion between the beam and the underlying rubble.

The flexural strength computed from test 3 without correction is 712 kPa and with correction it is 605 kPa.

The average flexural strength from the field trials was 570 kPa without correction to the third (keel-bonded) test. With the correction, this number becomes 530 kPa. The test conditions and results for the flexural tests are given in Table 6. It is of some interest to compare these results with known strength tests recorded and analyzed in the literature.

Several of the equations described in Section 3.4.3 have been used to compute the flexural strength of each test beam, based on measurements of temperature and salinity averaged through the thickness. Table 6 also shows these calculated flexural strengths using the Vaudrey (1977) and Timco and O'Brien (1994) equations.

Table 6 Test Conditions and Results - Flexural Test Northumberland Strait 1997

Test No.	Apparent measured flexural strength	Underlying cohesion	Corrected flexural strength	Average temperature	Averag e salinity	Computed strength (Vaudrey)	Computed strength (Timco & O'Brien)
	KPa	kPa	kPa	°C	ppt	kPa	kPa
FS1	526	0	526	-2.46	5.42	326	250
FS2	469	0	469	-2.52	4.36	422	310
FS3	712	9.5	605	-1.76	3.32	385	290

Inspection of Table 6 indicates that the measured flexural strengths are substantially higher than those computed using standard algorithms. Also, the highest value occurred when the underlying bond between refrozen layer and keel rubble had not been previously sheared.

The implication of this phenomenon on ice forces is unclear. It can be argued that the underlying cohesion will increase the force necessary to fail the consolidated layer in flexure. If the algorithm used assumes a floating condition for the consolidated layer, then the ice force may be underestimated. However, this may not be the case if the flexural strengths used are based on tests conducted on actual consolidated layers with underlying rubble and no correction is made for the rubble cohesion.

On the basis of these somewhat limited tests, there does not appear to be sufficient justification for reducing the flexural strength of the consolidated layer of ridges below the generally accepted values for level sea ice (which some investigators suggest).

3.5.6 Ice Density Measurements

Ice density is important in predicting ridge failure loads and ice strength. Recently, Timco and Frederking (1996) reviewed the sea ice literature on reported densities and found a wide range with reported values from 0.72 Mg/m^3 to 0.94 Mg/m^3. This variation is mainly due to the nature of sea ice, the location of the sample in the original ice sheet, the test technique and improper handling of the ice after it had been removed form the ice sheet. The findings suggested that although there can be a wide variation in the density for ice above the waterline, below the waterline the density is more consistent with a range of 0.90 to 0.94 Mg/m^3.

The density can be most accurately measured by using the submergence technique (as opposed to determining the density based upon sample dimensions and weight alone). However, submerged density measurements are not easy to perform. Details of the method as used in the recent ridge field program off the West Coast of Newfoundland (Croasdale and Associates, 1999) are described below:

> "The density measurement apparatus was set up (in the hurry tent if wind was a problem). The equipment consisted of an electronic scale, a graduated beaker, and calipers for measurement of dimensions. The beaker was half filled with sea water from the core hole. The scale was leveled, then the weight of beaker and water was measured. A sample was prepared by coring or cutting ice from the keel (approx. 0.5 litre in size). The sample was then placed in the water, and the weight of water + ice was measured. The block was then submerged using a thin metal rod. The total vertical force on the scale was measured. The water level with the sample submerged was recorded. The sample was then taken out and the new water level was recorded (as a double check, water level was measured both by reading the graduations and by independently measuring the height of water above the bottom of the beaker with a ruler).

Outside dimensions of the sample were recorded to provide a measure of the bulk volume. Four lengths and four diameters were recorded, to within better than a millimeter (apart from irregular samples for which the dimensions were estimated). The weight of the sample (drained) was again recorded. Water density in the beaker was recorded every 30 minutes, using a hygrometer. It did not vary significantly."

Typical results from one of the test sites are described below.

"Densities at Site 3 were measured on three different days. On March 11, 36 density measurements were done on two cores extracted from Station S3L1-70. The density measurements were done on "drained" samples (i.e. samples that had been out of the water for several minutes) which had been used for temperature measurements. Results of these measurements are shown in Figure 29 and Table 7. It is interesting to note that for the core at station S3L1-70 there is a clear drop in bulk buoyancy at the –1.17m level. This level also corresponds to the bottom of the consolidated layer (based on auger and borehole jack tests). At station S3L1-65, the drop in buoyancy is at the -0.85m level, which also corresponds to the bottom of the consolidated layer based on auger data at that station (0.9m).

Table 7 Drained Densities at Site 3

sample #	depth (m)	W0 Weight (g)	W1 Weight (g)	W2 Weight (g)	V1 Volume (cm3)	V2 Volume (cm3)	dw Hygro meter	B2 Buoyancy Force (g)	V3, Bulk volume (cm3)	V, Sample Volume (cm3)	Bulk Density (g/cm3)	Submerged Density (g/cm3)	Bulk Buoyancy (g/cm3)
		Water only	Water + ice	Block under water	Block under water	No ice	Water density	W2-W1	from Length & Diameter	V1-V2	(W1-W0)/V3	dw-B2/V	B2/V3
core at Station S3L1-70													
2	-0.42	1568	2077	2170	1590	930	1.025	93	693	660	0.734	0.884	0.134
3	-0.55	1622	2192	2300	1725	1030	1.025	108	670	695	0.851	0.870	0.161
4	-0.67	1597	2118	2214	1670	1030	1.026	96	592	640	0.880	0.876	0.162
5	-0.89	1585	2100	2202	1625	1000	1.026	102	598	625	0.862	0.863	0.171
6	-1.01	1579	2187	2292	1720	995	1.026	105	705	725	0.863	0.881	0.149
7	-1.17	1569	2008	2080	1517	970	1.026	72	567	547	0.774	0.894	0.127
8	-1.35	1759	2350	2438	1870	1180	1.026	88	782	690	0.755	0.898	0.112
9	-1.5	1754	2123	2174	1600	1380	1.026	51		220		0.794	
10	-1.85	1749	2333	2410	1835	1180	1.026	77	683	655	0.855	0.908	0.113
11	-2	1746	2392	2477	1900	1370	1.026	85	721	530	0.896	0.866	0.118
12	-2.42	1735	2076	2116	1555	1170	1.026	40	412	385	0.828	0.922	0.097
13	-2.5	1721	2346	2451	1890	1140	1.026	105	730	750	0.856	0.886	0.144
14	-2.7	1695	2193	2294	1700	1120	1.026	101		580		0.852	
15	-2.97	1686	2178	2250	1680	1090	1.026	72	563	590	0.874	0.904	0.128
16	-3.36	1654	1841	1869	1300	1080	1.026	28		220		0.899	
17	-3.64	1650	2194	2280	1715	1060	1.026	86	716	655	0.760	0.895	0.120
										avg.	**0.830**	**0.881**	**0.134**
										stdev	**0.054**	**0.030**	**0.022**
core at station S3L1-65													
1	-0.05	1626	2215	2338	1775	1050	1.026	123	704	725	0.837	0.856	0.175
2	-0.25	1612	2209	2328	1775	1030	1.025	119	714	745	0.836	0.865	0.167
3	-0.45	1598	2182	2298	1730	1010	1.025	116	690	720	0.846	0.864	0.168
4	-0.65	1591	2225	2350	1790	1010	1.025	125	757	780	0.838	0.865	0.165
5	-0.85	1594	2156	2230	1675	1000	1.025	74	683	675	0.822	0.915	0.108
6	-1.05	1562	2186	2251	1700	1000	1.024	65	687	700	0.908	0.931	0.095
7	-1.25	1691	2189	2245	1690	1125	1.023	56	561	565	0.887	0.924	0.100
8	-1.45	1687	2277	2342	1790	1120	1.022	65	682	670	0.865	0.925	0.095
9	-1.65	1768	2219	2280	1710	1200	1.022	61	542	510	0.832	0.902	0.113
10	-1.85	1742	2336	2403	1845	1180	1.022	67	678	665	0.876	0.921	0.099
11	-2.05	1734	2338	2407	1850	1175	1.022	69	689	675	0.877	0.920	0.100

12	-2.25	1727	2357	2434	1875	1170	1.022	77	722	705	0.872	0.913	0.107
13	-2.45	1719	2414	2497	1940	1160	1.022	83	788	780	0.882	0.916	0.105
14	-2.65	1709	2373	2441	1890	1150	1.022	68	732	740	0.907	0.930	0.093
15	-2.85	1705	2309	2377	1815	1140	1.022	68	680	675	0.888	0.921	0.100
16	-3.05	1696	2317	2390	1830	1130	1.022	73	709	700	0.876	0.918	0.103
17	-3.25	1745	2348	2428	1870	1175	1.022	80	695	695	0.868	0.907	0.115
18	-3.45	1741	2281	2356	1790	1170	1.022	75		620		0.901	
19	-3.65	1733	2352	2452	1880	1125	1.022	100	775	755	0.799	0.890	0.129
										avg.	**0.862**	**0.904**	**0.119**
										stdev	**0.030**	**0.024**	**0.029**

On March 14 and 15, 27 density measurements were done on "undrained" samples, taking care to do the measurements without lifting the sample out of the water, or doing it very quickly (less than 1 second) when necessary. Results are shown in Table 8. Note that as expected, the drained densities are lower (by 3%) than the undrained densities. There is also a fairly clear tendency for the specific buoyancy of the ice samples to decrease with depth as shown in Figure 30. This could also be interpreted as a relatively high buoyancy near the surface and a lower (but fairly constant) buoyancy below.

Table 8 Undrained Densities at Site 3

Sample #	**Depth m**	**W0 Weight of water (g)**	**W1 Weight of water +ice block (g)**	**W2 Weight (block under water) (g)**	**V1 volume (block under water) (cm3)**	**V2 volume (no ice) (cm3)**	**weight block (+bag)**	**dw Hygro meter water density**	**B2 Buoyancy Force (g)**	**V Volume of ice sample (cm3)**	**W Weight of ice sample (g)**	**Ice sample density (g/cm3)**	**Ice sample density (g/cm3)**	**Ice sample buoyancy (g/cm3)**
									W2-W1	**V1-V2**	**W1-W0**	**W/V**	**dw-B2/V**	**B2/V**
Core at SW corner of block 1														
1	0.395	1734	2335		1870	1165	601	1.023		705	601	0.852		
2	0.445	1846	2354		1865	1270	512	1.023		595	508	0.854		
3	0.52	1894	2281	2348	1770	1305	397	1.023	67	465	387	0.832	0.879	0.144
4	0.62	1882	2446	2545	1980	1315	570	1.023	99	665	564	0.848	0.874	0.149
5	0.72	1500	2161	2264	1685	920	662	1.023	103	765	661	0.864	0.888	0.135
6	0.82	1496	2090	2162	1580	920	600	1.023	72	660	594	0.900	0.914	0.109
7	0.895				1985	1105	891	1.023		880				
8	0.945	1481	2434	2560	1970	905	954	1.023	126	1065	953	0.895	0.905	0.118
9	0.995	1909	2548	2603	2025	1400	565	1.023	55	625	639	1.022	0.935	0.088
10	1.045	1886	2502	2561	1980	1305	621		59	675	616	0.913	0.936	0.087
											avg.	**0.887**	**0.904**	**0.119**
											stdev	**0.058**	**0.025**	**0.025**
Core at SE corner of block 1														
1	-1.72	2013	2471	2527	1900	1405	467	1.023	56	495	458	0.925	0.910	0.113
2		1847	2394	2458	1820	1230	553	1.023	64	590	547	0.927	0.915	0.108
3		1891	2298	2337	1720	1290	419	1.023	39	430	407	0.947	0.932	0.091
4		1859	2500	2625	1960	1240	643	1.023	125	720	641	0.890	0.849	0.174
5		2003	2476	2525	1940	1400	485	1.023	49	540	473	0.876	0.932	0.091
6	-1.92	1953	2477	2524	1915	1340	534	1.023	47	575	524	0.911	0.941	0.082
7		1955	2114	2127	1510	1345	167	1.023	13	165	159	0.964	0.944	0.079
8	-2.26	1719	2095	2131	1510	1105	382	1.023	36	405	376	0.928	0.934	0.089
9	-2.39	1724	1843	1855	1240	1105	124	1.024	12	135	119	0.881	0.934	0.089
10	1.84	1805	2214	2280	1640	1190	420	1.024	66	450	409	0.909	0.877	0.147
11		1808	2392	2450	1840	1210	591	1.024	58	630	584	0.927	0.932	0.092
12	2.8	1824	2398	2452	1875	1220	583	1.024	54	655	574	0.876	0.942	0.082
13		1846	2416	2491	1880	1245	578	1.024	75	635	570	0.898	0.906	0.118
14		2019	2376	2407	1800	1415	369	1.024	31	385	357	0.927	0.943	0.081
Igor1		1744	1897	1923	1305	1125	161	1.024	26	180	153	0.850	0.880	0.144
Igor 2		1759	1918	1943	1340	1150	167		25	190	159	0.837	0.892	0.132
											avg.	**0.905**	**0.917**	**0.107**
											stdev	**0.039**	**0.027**	**0.027**

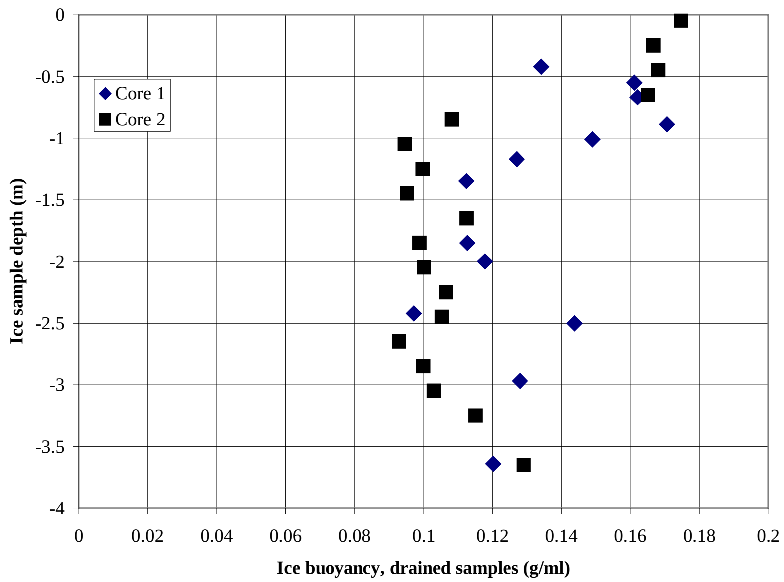

Figure 29 Specific Buoyancy, Drained Samples, Site 3, Cores 1 & 2

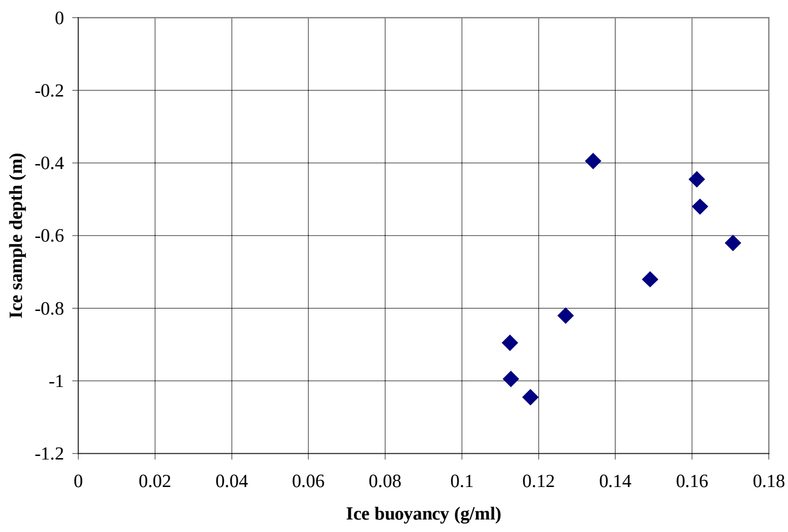

Figure 30 Specific Buoyancy, Undrained Samples, Site 3, Core 3

3.6 References

Blanchet D. and DeFranco S.J., 1996. Global First-year Ice Loads: Scale Effect & Non-simultaneous Failure, IAHR Ice Symp., Vol. 1, pp 203-213, Beijing, China.

Blanchet, D., Abdelnour, R. and Comfort, G. 1997. Mechanical properties of first year sea ice at Tarsiut island. ASCE Journal of Cold Regions Eng. 11 (1): 59-83.

Blanchet, D. 1998. Ice Loads from First Year Ice Ridges and Rubble Fields. Canadian Journal of Civil Engineering. 25: 206 – 219 (1998).

Brown, T. G., Cheung, M.S., Croasdale, K. R., and Wright, B. D, 1995. Advice on Design Ice Loads for The Northumberland Strait Bridge Piers. Report to Public Works and Government Services Canada, Charlottetown, PEI, 124p.

Bruneau, S. E., McKenna, R. F., Croasdale, K. R. and Crocker G. C. 1996. In-situ direct shear of ice rubble in first year ridge keels. Proceedings of 49th Canadian Geotechnical Conference. St. John's September 1996.

Bruneau, S. 1997. Development of a First-Year Ridge Keel Load Model, PhD thesis, Memorial University of Newfoundland, St. John's, Nfld., Canada.

Bruneau S. E., Crocker G. B., Croasdale K. R., McKenna R. F., Metge. M., Ritch, R. and Weaver, J. S. 1998. Development of techniques for measuring in situ ice rubble shear strength. Proc. 14th Intl. Symposium on Ice, Vol. 2, pp 1001-1007, Potsdam, N.Y., USA.

Cammaert, A. B. and Muggeridge, D. A. 1988. Ice Interaction with Offshore Structures. Van Nostrund Reinhold, New York.

Cornett, A.M. and Timco, G.W. 1996. Mechanical Properties of Dry Saline Ice Rubble. Proceedings of the 6th ISOPE Conference, Vol. II, pp 297-303 , Los Angeles, Cal., USA.

Cornett, A.M. and Timco, G.W. 1995. Laboratory Tests on the Mechanical Properties of Saline Ice Rubble. NRC Controlled Report HYD-CTR-002, Ottawa, Ont. Canada.

Croasdale, K. R., Allyn, N. and Marcellus, R. W. 1990. Thermal response of ice rubble: Predictions and observations. Proc. IAHR Ice Symposium, Vol. 1, pp 153-167, Espoo, Finland.

Croasdale & Associates Ltd., 1995. Ice Load Models for First Year Pressure Ridges and Rubble Fields – Phase 1 Report. Joint Industry Government Project, Partly sponsored by the National Energy Board (PERD) and Public Works Canada.

Croasdale & Associates Ltd. 1996. Ice Load Models for First Year Pressure Ridges and Rubble Fields. A Joint Industry Project supported by Mobil and Exxon.

Croasdale & Associates Ltd. 1996. In situ strength measurements of first year pressure ridges and rubble fields. A study for the National Energy Board, supported by PERD.

Croasdale & Associates Ltd. 1997. In Situ Ridge Strength Measurements – 1997. A study sponsored by NRC (PERD) and Exxon Production Research Co. (Proprietary until December 2000).

Croasdale & Associates Ltd. 1998. In situ Ridge Strength Measurements - 1998. A study sponsored by NRC (PERD) and Exxon Production Research Co. (Proprietary until December 2001).

Croasdale & Associates, Arctic & Antarctic Research Institute. 1998. Measurement of Large Scale Ice Ridge Strengths off the North East Coast of Sakhalin Island, 1998. A proprietary study for Exxon Neftegas and partners.

Croasdale & Associates Ltd. 1999. Field Study of Ice Characteristics off the West Coast of Newfoundland. Report to National Research Council, Ottawa, and Exxon Production Research Co. PERD/CHC Report 2-70 and 2-71 (Proprietary)

Croasdale, K. R. 1999. A study of ice loads due to ridge keels. Proc. 4th Intl. Conf. on Development of Russian Offshore (RAO), St. Petersburg, 1999.

Frankenstein, G. E. and Garner, R. 1967. Equations for Determining the Brine Volume of Sea Ice between -0.5 and -22.9 Degrees C . Journal of Glaciology. Vol 6, No. 48.

Frederking, R., Timco, G. W., Kamesaki, K. and Tada, H. 1999. Review of first year ridge geometries and properties in the Sakhalin region. Proc. Intl. Workshop on Rational Evaluation of Ice Forces on Structures, pp 21-33, Mombetsu, Japan.

Kry, P. R., 1977. Ice fields in the vicinity of artificial islands. Proc. 4th Intl. POAC '77 Conf., Vol 1, pp 200-211, St. John's, Nfld., Canada.

Lepparanta, M. and Hakala, R. 1992. The Structure and Strength of First Year Ice Ridges in the Baltic Sea. Cold Regions Science and Technology, Vol. 20, pp. 295-311.

Masterson, D. and W. Graham, 1992. Development of the Original Ice Borehole Jack. Proc. IAHR Symposium on Ice, Vol. 2, pp 748-759, Banff, Alberta, Canada.

Michel, B. Ice Mechanics. University Laval Press, Quebec, Canada.

McKenna R.F., Bruneau S.E.,Williams F.M., 1996. In-Situ Shear Strength Measurements of Model Ice Rubble Using a Punch Technique. Proc. 49th Canadian Geotechnical Conference, St John’s, Newfoundland.

Nadreau, J. P. and Michel, B. 1984. Ice Properties in Relation to Ice Forces. Proc. 2nd IAHR State of Art Report on Ice Forces. Vol. 4, IAHR Symposium, Hamburg, 1984.

Richter-Menge, J. A. 1986. Comparison of the compressive behaviour of naturally and laboratory grown saline ice. Proc. 2nd workshop on ice penetration technology. Special CRREL Report 86-30.

Sayed, M., Timco, G.W. and Sun, L. 1992. Testing Model Ice Rubble under Proportional Strains. Proceedings of the Offshore Mechanics and Arctic Engineering Symposium (OMAE 1992), Vol. IV Arctic/Polar Technology, pp.335-341, Calgary, Al., Canada.

Smirnov,V., Sheikin, I.B., Shushlebin, A., Kharitonov, V., Croasdale, K. R., Metge, M., Ritch, R., Polomoshnov, A., Surkov, G., Wang, A., Beketsky, S., and Weaver, J.S., 1999. Large Scale Strength Measurements of Ice Ridges: Sakhalin, 1998. RAO Conference, St. Petersburg, 1999.

Timco, G. W., Funke E.R., Sayed M. and Laurich P.H., 1992. A Laboratory Apparatus to Measure the Behaviour of Ice Rubble. Proc. OMAE 1992, Vol. IV, PP 369 – 375, Calgary, Al, Canada.

Timco, G.W. and Frederking, R.M.W. 1990. Compressive Strength of Sea Ice Sheets. Cold Regions Science and Technology, Vol. 17, pp 227-240.

Timco, G.W. and Cornett, A.M. 1997. The Influence of Variable-Thickness Ice on the Loads Exerted on Sloping Structures. Cold Regions Science and Technology 26, pp 39-53.

Timco, G.W. and O'Brien, S. 1994. Flexural Strength Equation for Sea Ice. Cold Regions Science and Technology, 22, pp 285-298.

Lainey, L. and Tinawi, R. 1984. The mechanical properties of sea ice: A compilation of available data. Can. Journal of Civil Eng. 11(4): pp 884-923.

Vaudrey, K. D. 1977. Ice Engineering - Study of related properties of floating ice sheets and summary of elastic and viscoelastic analyses. Naval Civil Eng. Lab. TR-860. Port Hueneme, CA, USA.

Weeks, W. and Assur, A. 1967. The Mechanical properties of Sea Ice. Us Army CRREL Monograph II-C3, Hanover, NH, USA.

Yashima, N. and Tabuchi, H. 1999. Field survey of pressure ridges in offshore Sakhalin. Proc. Intl. Workshop on Rational Evaluation of Ice Forces on Structures, pp 11-20, Mombetsu, Japan.

4.0 RIDGE INTERACTIONS WITH OFFSHORE STRUCTURES

4.1 Introduction

In this section of the report, some of the full-scale data that has been obtained about first year ridge interactions with offshore structures is reviewed. Clearly, this type of information is of fundamental importance, since it forms a "real basis" for understanding the nature of ridge interactions, and the associated ice load levels. Full scale ridge interaction data is also valuable and in fact, a logical prerequisite, in the development and verification of different methods for reliably estimating ice load levels from various ridge features.

Over the years, there have been a number of different structures placed in ice infested areas that contain first year ridges. Although all of these structures have provided "opportunities" to obtain full scale information about first year ridge interactions and loads, few have been specifically monitored for this purpose, for a variety of reasons. As a result, the amount of full-scale data that is currently available about ridge interactions is surprisingly limited.

The types of structures that have been exposed to ridge interactions can be subdivided into two basic categories. These are:

Wide structures

- this category refers to offshore structures with waterline widths in the order of 100m, primarily those used for oil exploration in the Beaufort Sea
- these structures include artificial islands, shallow caissons (Esso's CRI and the Tarsiut caissons) and deeper caisson structures (Canmar's SSDC, the CIDS, and the Molikpaq which is now being used as a production platform off Sakhalin Island)

Narrow structures

- this category refers to nearshore structures with waterline widths in the order of 10m, primarily those used to support various facilities in coastal areas
- these include lighthouses (eg: in the Baltic Sea), bridge piers (eg: the Confederation Bridge), and the oil production platforms in Cook Inlet

Of all these structures, the Molikpaq and Confederation Bridge have provided most of the quantitative information that is now available about ridge interactions and loads. Both structures have been well instrumented and monitored, and have also been exposed to a large number of direct interactions with first year ridges. In all likelihood, these two structures will continue to be the main sources of new data on ridge interactions and loads, at least over the next few years.

The Molikpaq data that was obtained during its Beaufort Sea deployments is now publicly available and accordingly, is dealt with in the highest level of detail in this report. This data is considered representative of ridge interactions with wide offshore structures and is very instructive. A few comments about the first year ridge interactions that the Molikpaq is now experiencing at its new deployment location off Sakhalin Island are also provided, although this new Molikpaq data remains proprietary. For completeness, some of the more qualitative observations that can be gleaned from experiences with other wide Beaufort Sea structures are also highlighted, where they are considered to be relevant.

With regard to narrow structures, the information that is now being acquired about first year ridge interactions with instrumented piers on the Confederation Bridge is the best full scale data source. Unfortunately, this information is proprietary and cannot be discussed in any detail in this report. However, some of the more qualitative observations that have been released about ridge interactions with the Confederation Bridge piers are briefly reviewed, and a few insights from other narrow structures (Baltic lighthouses and the Cook Inlet platforms) are given.

Here, it is worthwhile noting that considerably more experience has been gained with ships moving through first year ridges, than with ridges moving against fixed structures. Since this type of "vessel information" is not directly relevant to the question of ridge interactions with fixed offshore structures, it is not addressed in this report, other than through some very rough and qualitative comparisons.

4.2 Wide Structures

4.2.1 Molikpaq Observations from the Beaufort Sea

As noted earlier, the data that was obtained during the Molikpaq's Beaufort Sea operations provides the best source of full scale information about first year ridge interactions with wide offshore structures. During the 1980s, the Molikpaq was deployed at four different locations in the Beaufort, where it encountered a wide range of ice conditions, including both first and multi-year ice. The Molikpaq's first three deployment locations were in the Beaufort Sea's transition zone, which experiences moving pack ice throughout the winter, while the fourth was closer to shore, in the "near stationary" landfast ice zone.

The first two locations where the Molikpaq was used were both in about 30m of water (the Tarsuit P-45 and Amauligak I-65 wellsites, drilled in 1984/85 and 1985/86 respectively).At these locations, the Molikpaq was placed on deep submerged berms with a set down depth of ~ 20m. Because of this deployment configuration, there was no permanent accumulation of grounded ice rubble around the Molikpaq at either location, and the caisson was directly exposed to moving pack ice throughout the winter (Figure 31). Since the pack was in near continuous motion, a significant range of ice conditions moved past the Molikpaq over the course of these two winter seasons, including a large number of first year ridges.

Figure 31 The Molikpaq at the Amauligak I-65 drilling location. During the winters of 1984/85 and 1985/86, the caisson was directly exposed to moving pack ice conditions, because grounded ice rubble did not form around it.

At its last two Beaufort deployment locations (the Amauligak F-24 and Isserk I-15 wellsites drilled in 1987/88 and 1989/90 respectively), the Molikpaq was set down with shallower drafts (10 to 15m). These deployment configurations tended to impede ice clearance and resulted in the formation of grounded ice rubble fields around the Molikpaq at both sites. These grounded rubble fields, which formed during freeze-up and persisted until late break-up, precluded direct ice interactions with the structure (including first year ridges). Because of this, the first-year ridge interaction observations that were acquired at the Molikpaq's 1984/85 and 1985/86 deployment locations are of primary interest, since they involve "direct ice action" against the structure.

4.2.1.1 Background

The Molikpaq and many of its "in-ice" operating experiences have been described in various reports and papers (eg: Wright et al, 1986, Gulf Canada, 1986, Gulf Canada, 1988, Rogers et al, 1998), and will not be repeated here. However, a few points about the structure and its instrumentation system are given as follows, before discussing the first year ridge interaction information that has been obtained from it.

The Structure

- the Molikpaq is a gravity based structure that consists of an octagonal steel caisson annulus, with dredged sand placed in its central core (Figure 32)
- the caisson has outside dimensions of 111 m at its base and 86 m at its deck, and an overall height of 33.5 m (including its 4.5 m ice deflector)
- when deployed at a set down draft of ~20 m (as it was in 1984/85 and 1985/86), the caisson has a waterline diameter of 90 m, and an above water freeboard of 13.5 m
- at this 20m set down draft, the "long sides" of the octagonal caisson are 60 m in length at the waterline, while the "shorter sides" are 22 m long
- with this deployment draft, the caisson's walls are "near vertical" (8°) through the waterline, and 23° off vertical from 3.5 m to 15 m below mean sea level, flaring out at an angle of about 40° thereafter
- in 1984/85 and 1985/86, the Molikpaq was placed on fairly small subsea berms, with relatively narrow "benchtops" that extended about 15 m out from the caisson's toe, and had side slopes of roughly 1 in 7

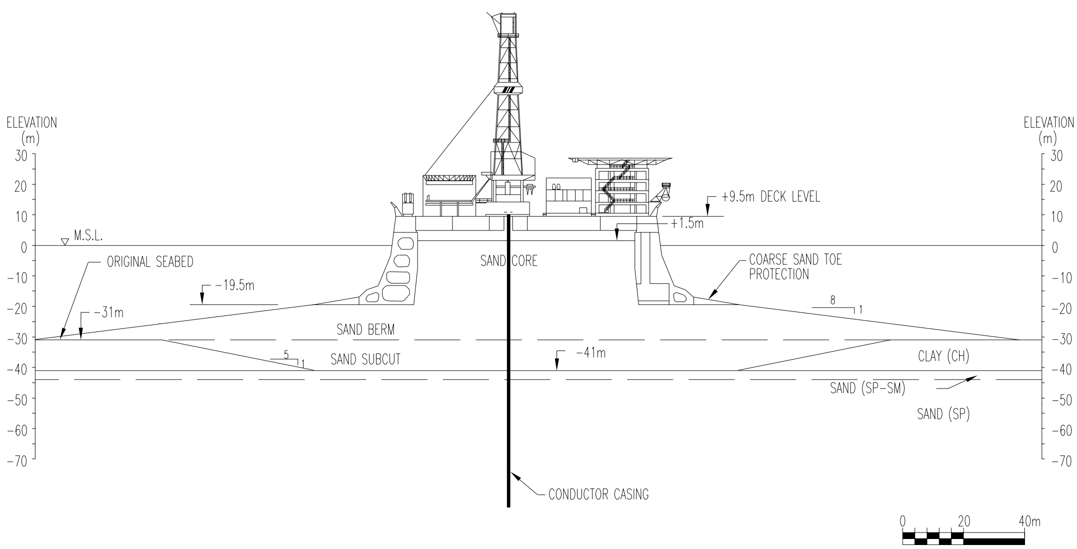

Figure 32 A schematic illustration of the Molikpaq's deployment configuration

In terms of the first year ridge interactions that the Molikpaq experienced in 1984/85 and 1985/86, this deployment configuration suggests:

- the consolidated layer of the ridges moved against a near vertical face
- the keel portion of most ridges moved against a 23° face
- only the largest ridge keels interacted with the more sloped, deeper section of the Molikpaq's base

Instrumentation & Monitoring

During all of its deployments, the Molikpaq has been very well instrumented, with various sensors installed on the caisson and in its sand core, berm and foundation soils, to measure ice loads and a variety platform responses

During these deployments, direct observations of ice conditions around the structure were also acquired by onboard monitoring personnel, and by video coverage of ice interactions with the Molikpaq

In terms of investigating first year ridge interaction and loads, the most important components of the Molikpaq's instrumentation and monitoring systems are those which provided information on ice loads, the ice conditions that caused these loads, and the associated ice failure behaviours

Ice loads on the Molikpaq were measured by three separate systems (Figure 33), which include clusters of Medof panels on the caisson's N, NE, and E faces (these measure ice loads directly), strain gauges on the caisson's main bulkheads, and extensometers that sense the caisson's overall deformations (the strain gauges and extensometers measure caisson responses, from which ice loads can be inferred)

An extensive amount of work has been carried out with the data from these ice load measurement systems (eg: Gulf Canada, 1988, Wright, 1998, Frederking et al, 1999), and a good level of confidence has been developed in the ice load estimates that have been obtained from them.

Figure 34 gives one example of the ice load estimates from the Medof panel and extensometer measurement systems during a first year ridge interaction, showing the compatibility of the ice load estimates, which are felt to be accurate to about 30%

The ice loads that were obtained from the Medof panel data have been used as the primary information source for ridge load estimation, although extensometer, strain gauge and other response data has also been reviewed for each interaction event

Data from the Molikpaq's instrumentation was recorded in three different ways, with the data acquisition system providing

- a number of 1 Hz fast files that provided ice load time series over periods of about one hour
- a number of 50 Hz burst files that provided ice load time series over periods of several minutes
- day files that provided statistics on mean, minimum and maximum values over five minute intervals

The ice loading information from fast files that were acquired during periods when first year ridges moved against the Molikpaq is of most importance for the purposes of this study

In terms of ice monitoring, ice conditions at the Molikpaq were documented by environmental observers who reported ice concentrations, ice types and thicknesses, ridge frequencies and heights, and drift speeds and directions on an hourly basis, and periodically made notes about the types of ice/structure interactions that were seen

Three time lapse video cameras were also located on the Molikpaq (two mounted on the northeast flare boom giving fixed coverage of the east and north caisson faces, and one on the derrick top), which provided a means of continuously documenting ice/structure interactions along the Molikpaq's walls, particularly on its north and east faces

Good video coverage of the ice interaction zone is the most important data source for much of the ridge assessment work that has been carried out, since this information provides a basis for identifying specific ridge interactions, estimating ridge sizes, evaluating ridge failure modes and, when fast files are available, their correlation with concurrently measured ice load levels

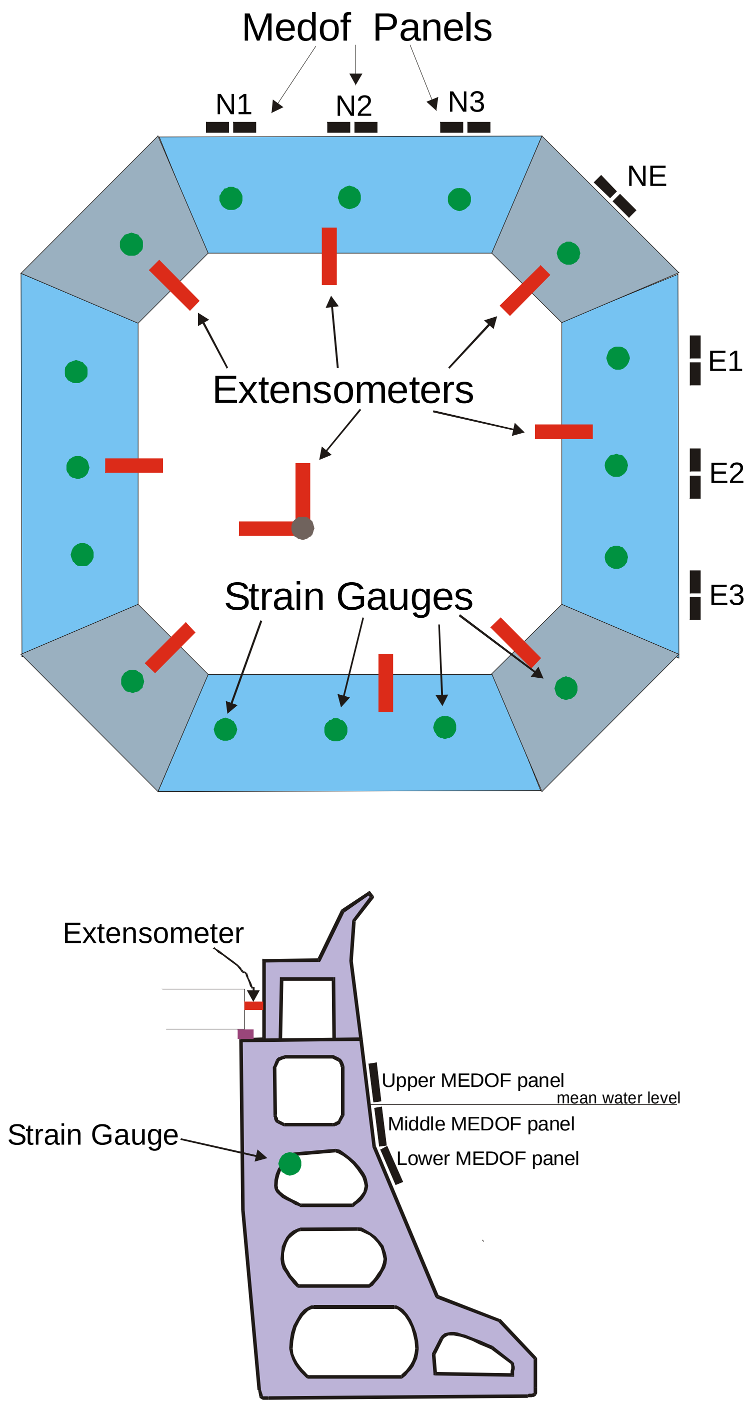

Figure 33 Ice load measurement systems on the Molikpaq included clusters of Medof panels, strain gauges and extensometers.

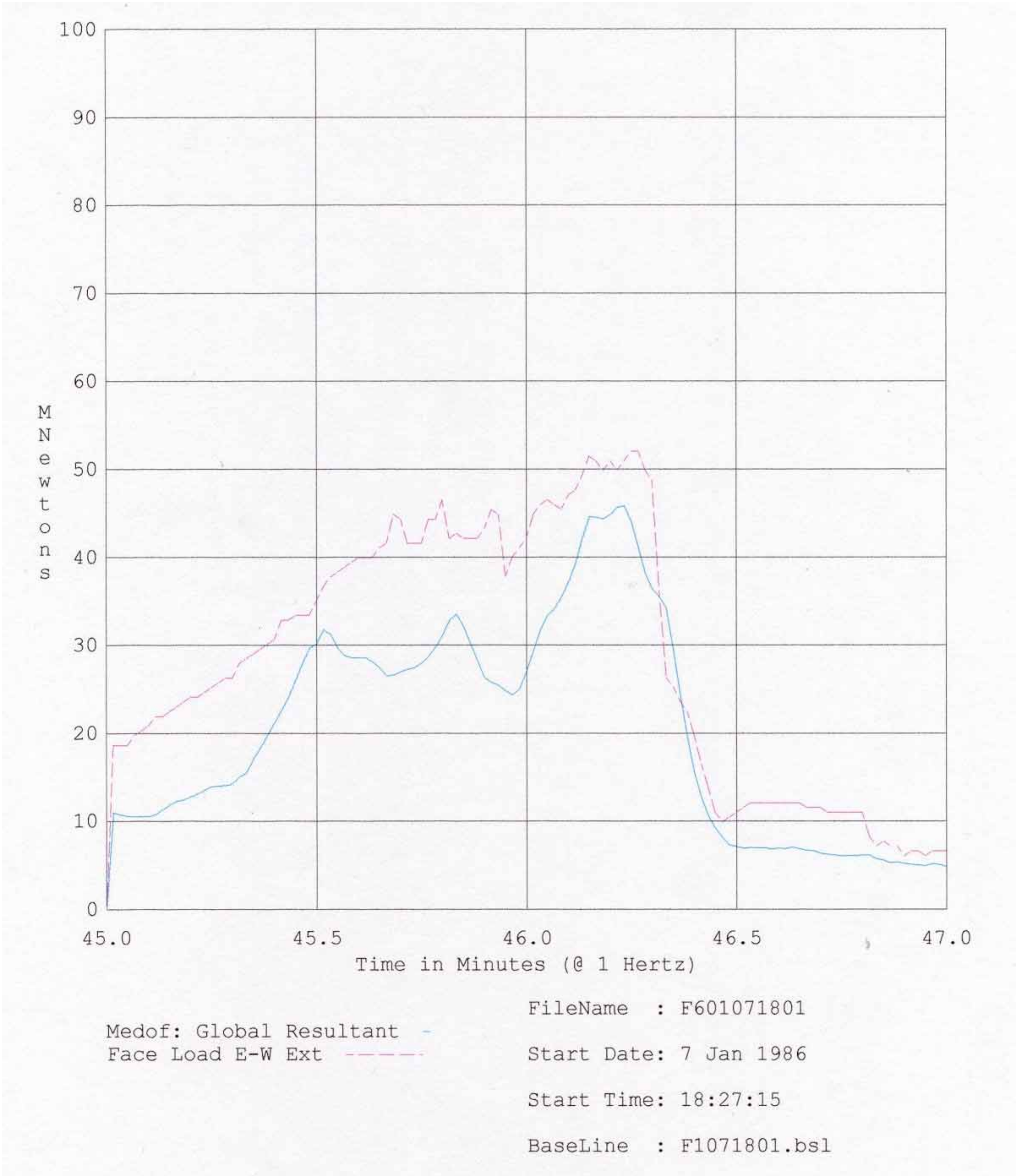

Figure 34 Global ice load estimates that were obtained from the Medof panel and extensometer "fast file" data during a first year ridge interaction event on January 7, 1986.

Figure 35 shows a typical example of a frame that was obtained from time lapse video coverage along the caisson's east face, which contains a polar bear as an indication of scale

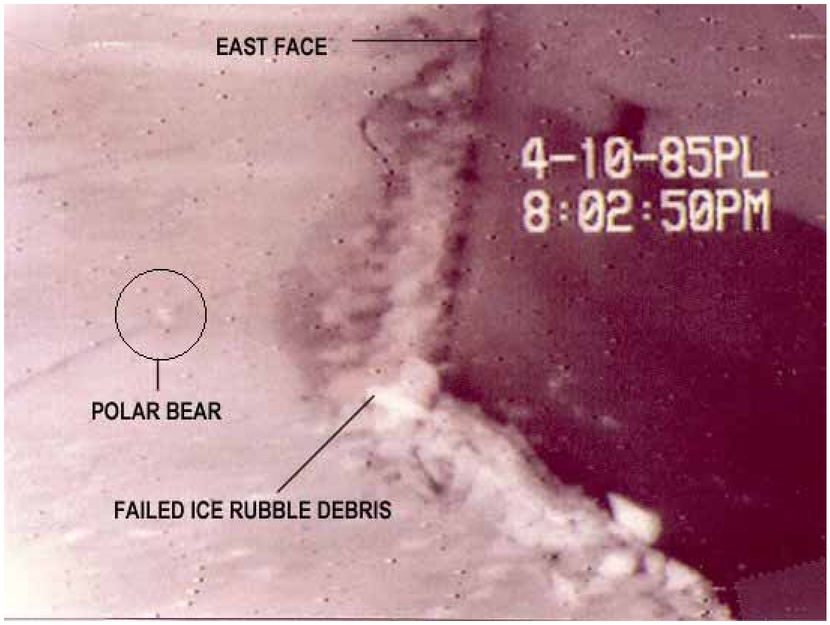

Figure 35 An example of the type of video coverage that was obtained at the Molikpaq, in this case along its east face. Note the polar bear on the level ice, which provides an indication of scale.

In terms of the first year ridge interaction data that was acquired from the Molikpaq in 1984/85 and 1985/86, the following points should be noted:

- the videos provides an excellent means of identifying ridge interactions and surface failure modes, but ridge height estimates from them are only rough
- the videos do not allow observation of failures in the submerged keel rubble portion of ridges, so that little can be inferred in this regard
- the Medof panel data, which has been used as the primary data source for ice load estimates, provides relatively good load measurement coverage (about 12% of the loaded width) through the consolidated layer portion of first year ridges, and also in the uppermost parts of their keel rubble (i.e: good coverage to depths of about 3m below sea level)
- however, for all but the smallest ridges, there is very limited measurement coverage in most of the keel rubble portion of ridges, since there are only three deep Medof panels installed on the caisson’s E, NE and N faces (i.e: from about 3m to 6m below sea level)
- although the Medof panels may “miss” some keel rubble load contributions, the consistency of the load estimates obtained from them when compared to ice load inferences from the extensometers and strain gauges (which sense responses to ice loads over greater depths) suggests that the Medof load estimates are quite reasonable

Evaluation Work

The data that was acquired during the Molikpaq's Beaufort Sea deployments has been the subject of extensive analyses regarding ice loads and pressures in level first and multi-year ice, and in relation to ice-induced dynamics (Wright et al, 1986; Jefferies & Wright, 1988; Wright and Timco, 1994). However, this data was not evaluated from the standpoint of first year ridge interactions and loads until quite recently. Over the past few years, several studies have been carried out to specifically address the question of first year ridge interactions with the Molikpaq, as interest in this topic area has increased. Information from these studies (Croasdale et al, 1995, Wright, 1997, Timco & Wright, 1998), together with some new analysis, has been used as a basis for the discussion given here.

The methodology that was used to investigate the Molikpaq data from a ridge interaction perspective is described elsewhere (see Croasdale et al., 1995) and will not be repeated in this summary. However, the assessment approach that was employed and some of its general implications are briefly highlighted as follows.

- an initial review of the 1985/86 and 1984/85 Molikpaq video data was carried out which provided a good feel for the level of ridge interaction information that was well documented
- this review indicated that there were a substantial numbers of documented first year ridge interactions, spanning a considerable range of ridge sizes, parent ice sheet thicknesses, and ice drift speeds
- the ridge sizes involved in these interactions were typically quite small, although some moderately sized and larger ridges did fail at or near the Molikpaq
- the ridge failure mechanisms that were seen were quite complex and appeared to depend on a number of factors, including the time varying boundary conditions at the caisson face
- the next step was to assess whether or not there was good ice load time series data available for some of the time periods that contained well documented first year ridge interaction events
- here, the main priority was to find 1 Hz fast files that were concurrent with some of the more useful video records, since these fast files typically covered time periods of about an hour, and were more compatible with the time scales of ridge interaction events than either the burst or day file records
- this review indicated that there was some fast file data spanning time periods that contained well documented first year ridge interactions, with an example of one of these "case histories" shown in Figure 36.

This type of fast file information provided a comparative context for the measured ridge loads, because the load levels that were associated with failures of the parent ice cover (in which the ridges were embedded) were also contained in the record

The fast files and concurrent video coverage of ridge interactions indicated that there were generally load peaks associated with the ridge interactions experienced by the Molikpaq

These load peaks could be up to several times as large as the mean loads associated with failure of the parent ice cover, but varied with ridge size and failure behaviour, and in terms of relative magnitudes, were quite sensitive to the failure behaviour of the level ice cover

The load levels caused by most ridge interactions did not appear to be particularly high, at least in relation to some of the higher ice loading events that were caused by ice crushing failures across the caisson faces, although large ridges tended to result in larger load levels than the norm

4.2.1.2 Ridge Failure Behaviours

Data Base

As noted earlier, good video coverage of the ice/structure interaction zone was the most important source of information for identifying first year ridge interaction events and their failure behaviours. In 1985/86, more than 6000 hours of reasonably good video coverage were available while in 1984/85, several thousand hours of coverage had been acquired. Eight of the better video coverage periods were selected as a representative sample for assessment, with the objective of gaining some insight into the nature of the ridge interaction process. This sample spanned a reasonable range of parent ice sheet thicknesses, ridge sizes and ice drift speeds. It is important to note that the video data that was screened and selected represents a relatively large portion of the 1985/86 and 1984/85 Molikpaq information base reasonably expected to have value in the context of well documented ridge interactions. Of the thousands of hours of ice/structure interaction video records acquired over the course of the first two Molikpaq deployments, roughly 33% of the 1985/86 data was viewed and assessed, together with about 15% of the 1984/85 information.

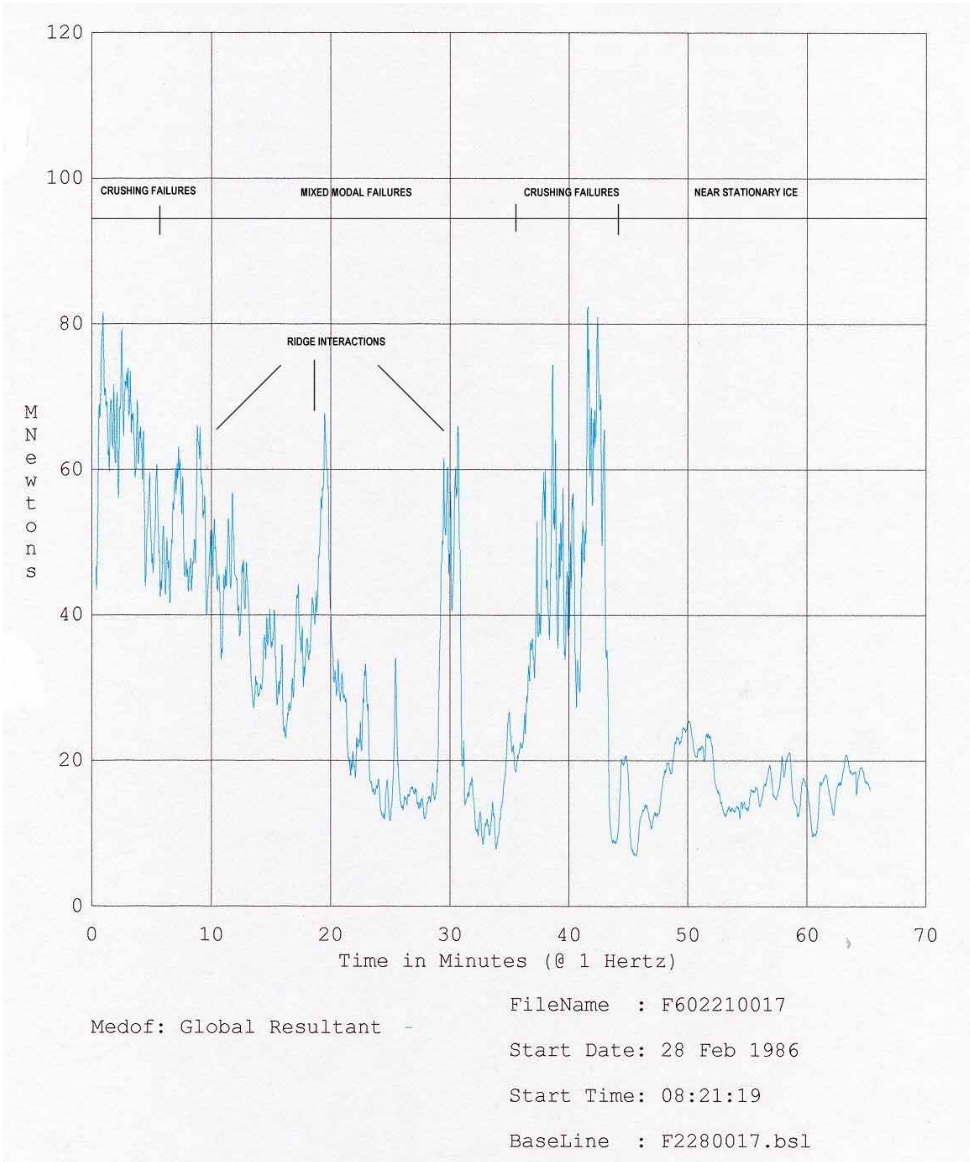

Figure 36 Ice load data from a fast file showing ridge interaction events, together with the other ice failure mechanisms that occurred during the time period.

Failure Modes

The first question that was addressed with the Molikpaq data involves the full scale failure behaviour of ridges. As will be outlined in chapter 5, most analytic theories suggest that when first year ridges move against a vertical structure, the initial failure is comprised of crushing of the ridge's consolidated layer and local passive failure of its keel, occurring simultaneously. At larger penetrations, a shear plug is expected to form through the keel rubble. Generally, these theories assume idealized ridge geometries that are long and linear with respect to the structure, and ridges moving perpendicular to the interaction front. However, observations from the Molikpaq suggest that the nature of the first year ridge interaction process, at least for wide structures, is considerably more complex.

Based on a review of the Molikpaq video tapes, there appear to be a number of characteristic failure behaviours involved in the ridge interactions that were experienced. Since the ridge failure mechanisms often involved a sequence and/or a combination of failure modes, they are generally referred to here as failure behaviours, rather than failure modes. The main ridge failure behaviours that were identified from the video review are summarized as follows, supplemented by representative video frames that were obtained during specific ridge interactions. Although causal relationships have not been quantified, these behaviours appear to depend upon a variety of factors, which include the parent ice sheet thickness, the size and apparent age of the ridge, its continuity, orientation and speed relative to the structure, the boundary conditions at the ridge interaction front, and the length of the Molikpaq face (ie: broadside versus corner) over which the interaction occurs. It is important to note that these failure behaviours are relevant for the top portion (or consolidated layer) of first year ridges, because the underwater deformations and failures of the keel rubble could not be seen.

Spine Failures

Many ridges were observed to fail along the central portion of their sails or "spine", as shown in Figure 37, at distances of a few metres to tens of metres away from the caisson

This type of failure behaviour was most common in small to moderately sized ridges embedded within relatively thin ice, and was largely independent of the orientation of the ridges (relative to the caisson wall against which they were moving)

Slow to moderate ice drift speeds tended to favour this failure behaviour, although it sometimes occurred during higher drift speed events

The weight of the rubble debris caused by the ice failure and clearance process at the caisson wall often tended to bend the oncoming ice cover downwards and seemed to contribute to the occurrence of these spine failures, but this was not a necessary condition

Once a spine failure was observed, the "backside" of the ridge and oncoming ice sheet would frequently ride under the leading portion of the failed ridge

For long ridges that were sinuous and not linear, this type of failure behaviour was sometimes observed in conjunction with other failure mechanisms that occurred at different locations along the ridge

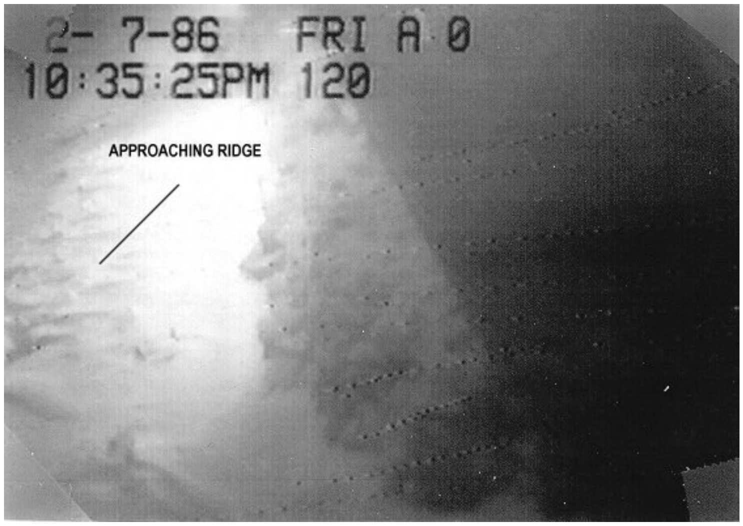

Figure 37 A small ridge approached the Molikpaq's north face and failed along its "spine", in its sail and consolidated layer portions.

Recognizing the high degree of variability that is present in the geometry and consolidated layer thickness of most ridges, spine failures are not surprising, since these variabilities, acting in combination with various in and out of plane stresses, can lead to substantial bending in many areas of the consolidated layer

Figure 38 shows a schematic illustration of the type of ice deformation that may have occurred during spine failures of ridges, with the consolidated layer breaking apart along the ridge crest

- Figure 38a, a ridge which presumably has a variable or discontinuous refrozen layer under its spine interacts with the structure
- Figure 38b shows the initial spine failure as the refrozen layer is pushed up and down
- this failure behaviour continues as the advancing ice sheet is pushed under and/or over the ridge (Figure 38c)
- finally, there is general rubble building and clearing as the ridge fragments rotate and slide along the caisson face (Figure 38d)

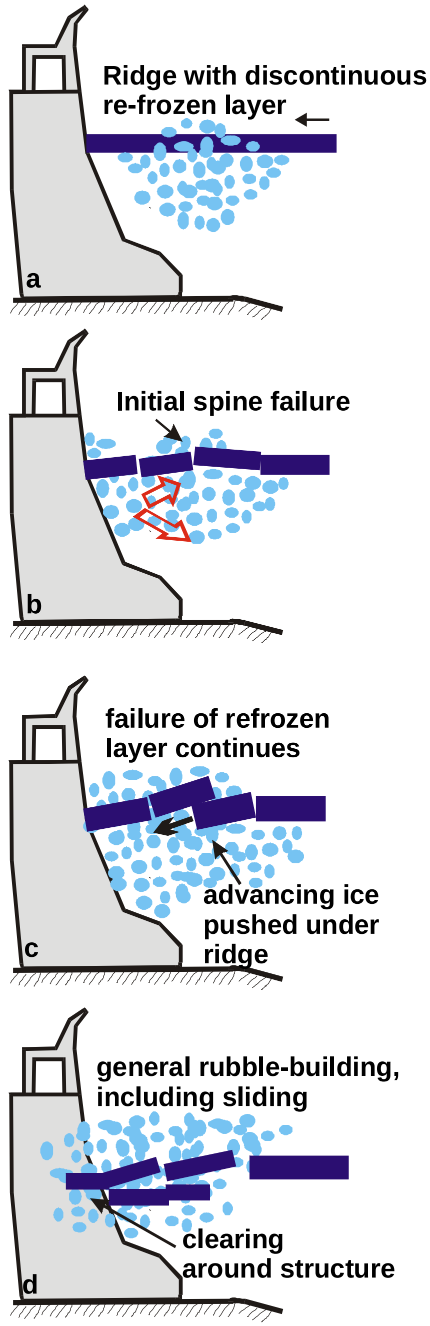

Figure 38 Conceptual sequence illustration of a ridge “spine” failure.

Failing Behind

For a large portion of the ridges that interacted with the Molikpaq, failure tended to occur in the parent ice sheet behind the ridge, rather than in the ridge itself, as shown in Figure 39.

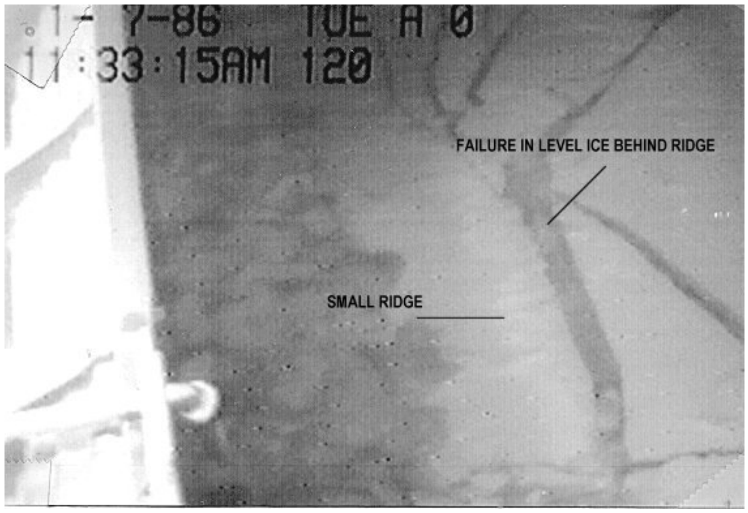

Figure 39 Typical example of a failure in the parent ice sheet behind a small first year ridge.

This type of failure behaviour was seen for ridges in all size categories and for parent ice sheets over a wide range of thicknesses, and represents the single most common failure behaviour that was observed

Ridge interactions that were characterized by failures in the level ice behind the ridge usually involved parallel or near parallel ridge approach angles (with respect to a long face of the Molikpaq caisson)

The ice drift speed did not seem to be a significant factor in generating this type of failure behaviour, although failures of this nature appeared to be more common when large ice rubble piles were present immediately adjacent to the caisson, particularly in the thicker level ice sheets

Typically, the first failure in the level ice behind ridges was estimated to occur prior to or near the time when their keels first began to interact with the structure, with little evidence of significant penetration into thicker portions of the ridge

Many of the ridges appeared to slump immediately after the ice failed behind them, and often, were overridden by the oncoming ice sheet as the interaction proceeded
In some cases, this failure behaviour may suggest some element of ridge keel ride up on the relatively steep slope of the Molikpaq, at least for the thicker ridges

Some of the moderate and larger sized ridges also seemed to "pop up" just before ice failure occurred behind or around them, particularly when less rubble was present at the caisson wall

Figure 40 shows a schematic illustration of the type of ice deformation that may have occurred during ice failures behind ridges

- in Figure 40a, a ridge with a relatively thick consolidated layer, frozen into a thinner parent ice sheet, moves against the structure
- the initial failure occurs in the thinner ice behind the ridge, as the ice is deformed out of the plane of the ice cover (Figure 40b)
- this process continues (Figure 40c), until there is general rubble building and clearing.

Shearing

Some of the ridges appeared to "shear" or fracture, with one or more relatively large cracks forming perpendicular to the face of the caisson and propagating out from it, as shown in Figure 41.

This type of failure behaviour was usually observed in ridges that were moderately sized or large, and was less likely to occur when the ice was moving quickly

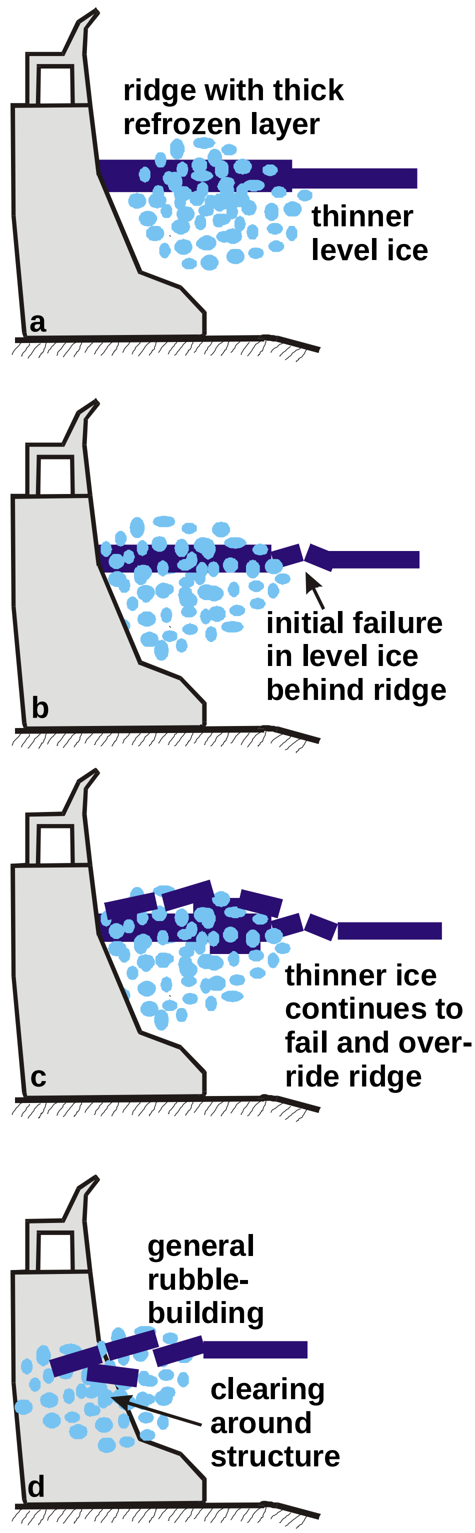

Figure 40 Conceptual sequence illustration of a ridge interaction with the parent ice sheet "failure behind".

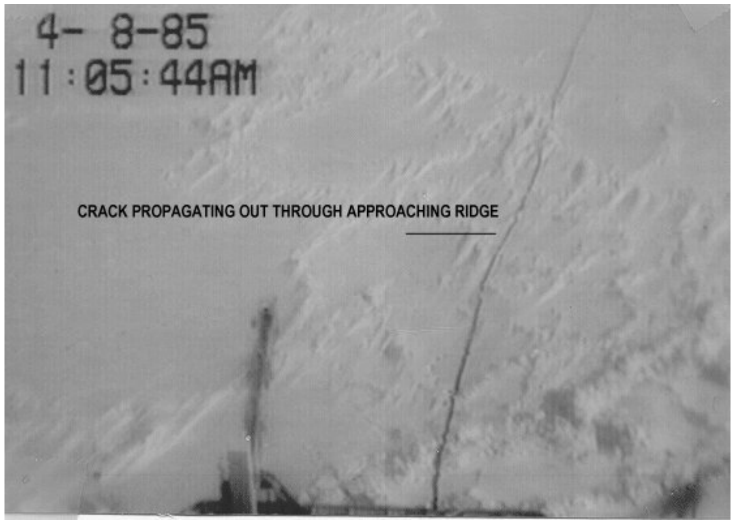

Figure 41 An example of a shear ridge failure, with a crack propagating out from one of the caisson's long faces.

Typically, only one crack would form through the ridge at a time as it moved against the caisson wall, with one portion of the ridge stopping and the remainder of the ridge continuing to move, and then failing in another way at a slightly later time

This led to sections of the ridge acting independently on the caisson since one (or more) ridge fragment(s) would usually stop, with other sections continuing to advance and then failing

This type of failure behaviour is perhaps the closest to traditional concepts of ridge failures and again is not surprising, recognizing the high degree of variability in the cross-sectional geometries of most ridges, together with natural variations in the thickness of their consolidated layers

A schematic illustration of this type of ridge failure behaviour is shown in Figure 42.

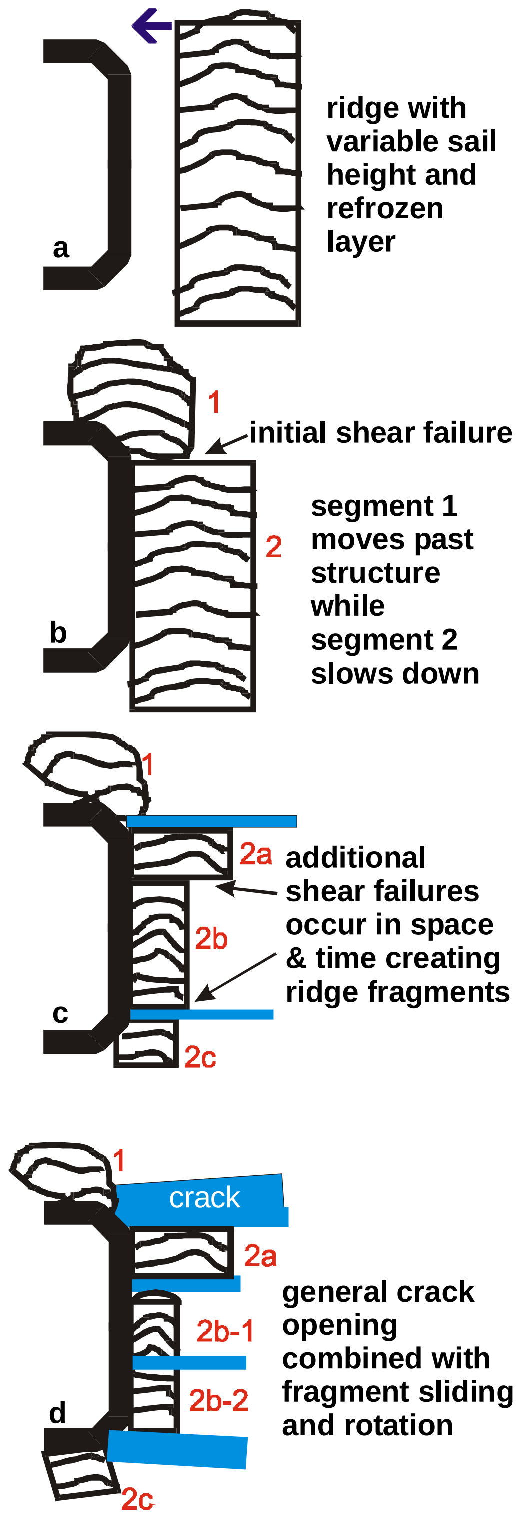

Figure 42 Sequence illustration of a ridge failing in shear.

Stopping

A few of the ridges that interacted with the Molikpaq did not fail in any observable way during their initial contact, but appeared to simply stop until the stress levels became high enough to induce a subsequent failure, as shown in Figure 43.

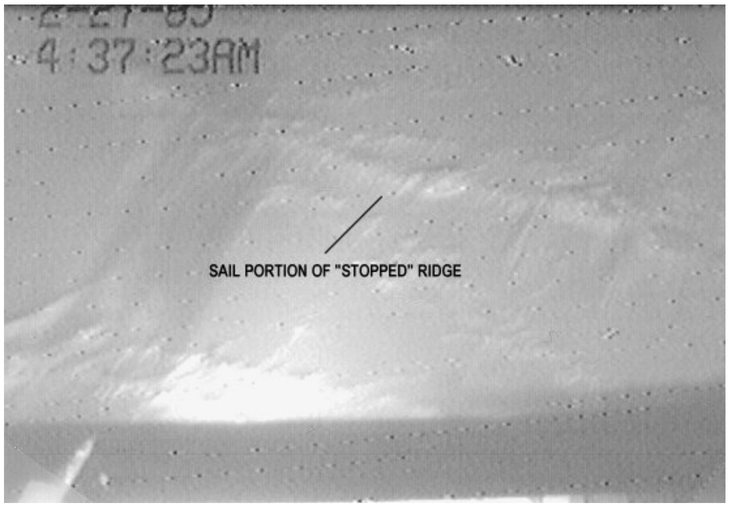

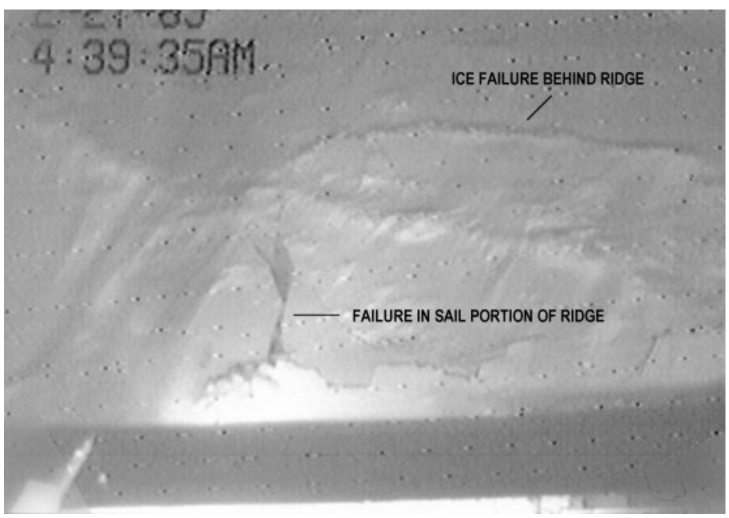

Figure 43 Some ridges stopped, then appeared to fail around their boundaries, as shown here.

This type of behaviour was limited to moderately sized and larger ridges that were frozen into a thicker parent ice sheet, and was favoured at low to moderate ice drift speeds

Ridges that stopped were the least common type of ridge/structure interaction event, most likely due to the relatively infrequent occurrence of ridges that were large (sail heights of several metres)

After these ridges had stopped for periods of tens of seconds to minutes, they tended to fracture into several large fragments, with a number of cracks forming through them, most often perpendicular to the caisson face

These fractures formed at different times and displayed no particular pattern, and in turn led to ridge fragments of various sizes

It is interesting to note that some of the larger, wider ridges appeared to "bounce" as they failed into fragments during this type of failure process

Some of the ridges in the size category typified by this failure behaviour were probably lodged against the Molikpaq's steeply sloped face prior to failure

Figure 44 shows a schematic illustration of this type of ridge failure behaviour

Corner versus Longside

The majority of the ridge failure behaviours that are outlined above involved ridge interactions with the Molikpaq's long faces (60 m), since these were the areas of best video coverage

However, the video records did contain several events where ridges moved against the caisson's shorter corner sections (22 m) and appeared to indicate a different type of initial ridge failure behaviour

Although there are only several examples which involve small to moderately sized ridges, these ridges tended to fail when one crack formed in a near normal direction with respect to the caisson's corner, splitting the ridges into two sections that would subsequently clear around it (see Figure 45)

This observation suggests horizontal bending failures, at least for ridges having their long axis parallel to the caisson's corner and relatively long lengths in comparison to this corner width

A schematic illustration of this ridge failure behaviour is shown in Figure 46.

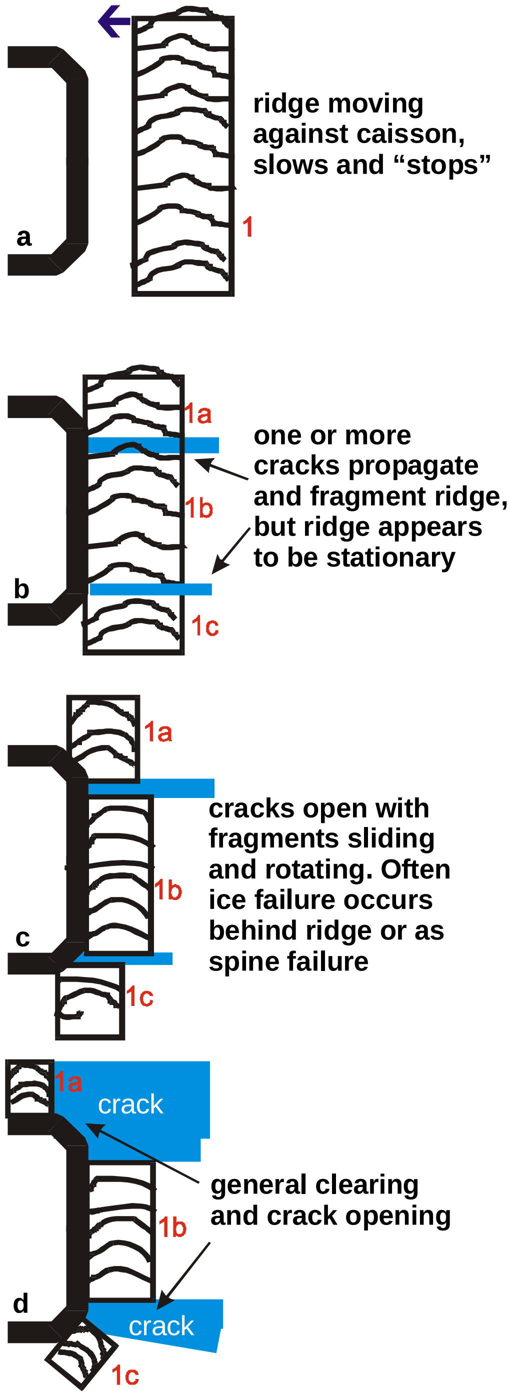

Figure 44 Sequence illustration of a "ridge stopping" failure mechanism

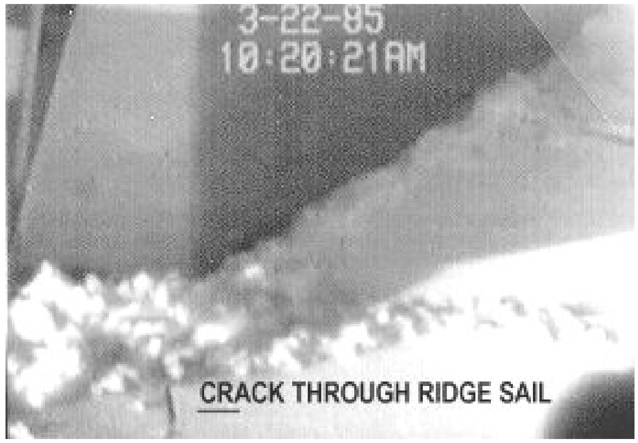

Figure 45 A moderately sized ridge moving against the NE face of the Molikpaq, with a crack propagating out from the caisson's corner.

Mixed Modal

Most of the ridge interactions were not limited to one failure behaviour but were mixed modal, and involved the non simultaneous occurrence of a combination of the failure mechanisms outlined above, along the Molikpaq's relatively wide interaction front

Combinations of "spine and behind" failures and "shear and stopping" failures were most typical

It is interesting to note that in many cases, the approaching ridges, segments of them, or of the ice cover into which they were frozen seemed to pause for a moment, prior to the onset of any particular failure behaviour

By way of summary, the nature of the first year ridge interactions that the Molikpaq has experienced in full scale is complex, and is normally characterized by a complicated sequence of ice failures that are largely dependent on the particulars of the ridge and the interaction event.

Distribution of Ridge Failure Behaviours

Because there seemed to be a number of characteristic ridge failure behaviours, the next question that was considered involved their relative frequencies of occurrence, and the typical conditions under which they occurred. To assess the distribution of ridge failure behaviours and confirm some of the visual trends that were suggested, eleven time lapse video segments (ranging from 6 to 24 hours in length) were reviewed in a slightly more quantitative manner. In total, this sample represented more than 100 hours of pack ice movements against the Molikpaq and included more than 360 ridge interactions, which showed a variety of failure behaviours. The objective of this assessment was not to become overly quantitative but rather, to gain some perspective about the distribution of first-year ridge failure behaviours and any associated trends.

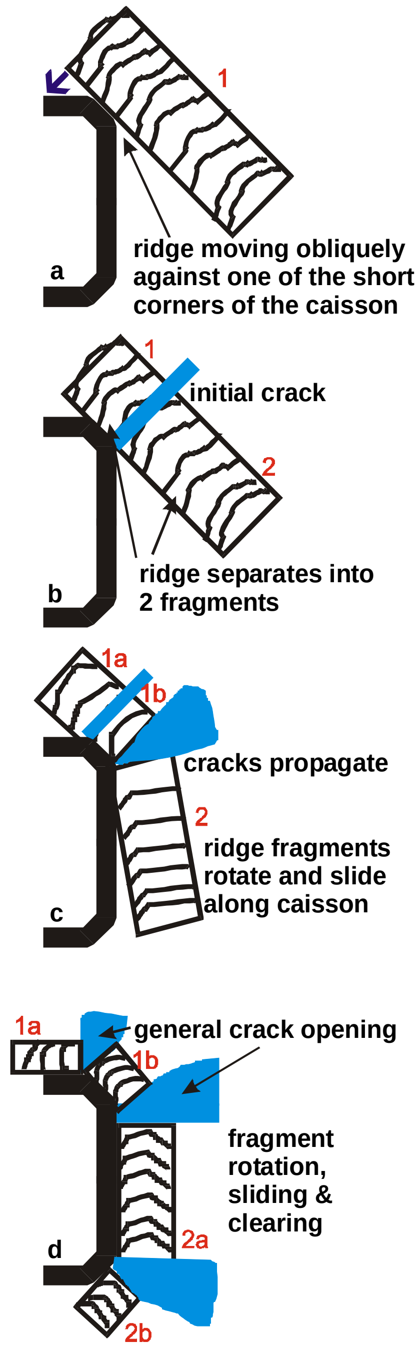

Figure 46 Sequence illustration of ridge failures at the corners of the caisson.

For this review, ridge sizes were visually estimated from the video sample, subdivided into small, medium and large size categories, which reflected approximate sail heights in the 0.5 to 1 m, 1 to 2 m, and >2 m ranges. For each ridge interaction contained in the video, the main type of failure behaviour was then identified, and histograms developed for each failure behaviour and ridge size category. The results of this assessment are shown in Figure 47.

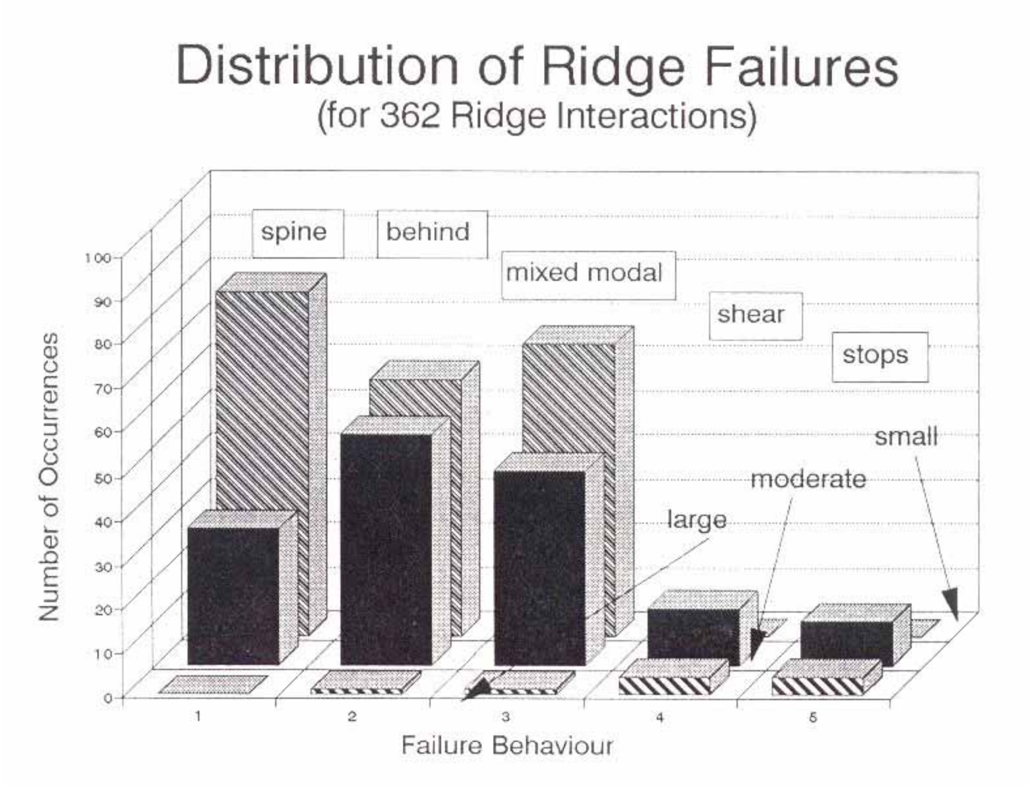

Figure 47 Distribution of first-year ridge failure behaviours based upon an assessment of 362 ridge interaction events

It may be seen that the trends in the distribution of ridge failure behaviours tend to support the observations given in the last section. In addition to being of basic interest, this type of information may be of considerable importance for probabilistic analyses of ridge load levels.

4.2.1.3 Ice Loads from Ridge Interactions

Data Base

As noted earlier, ice load time series that were obtained from the Molikpaq's Medof panel data have been used to evaluate ridge load levels. For the purposes of this review, nine fast file records were selected to form the ridge loading data base, with eight coming from the winter of 1985/86. These fast files covered time periods of about an hour, each containing a variety of first year ridge interactions that were reasonably well documented on time lapse video tapes. A number of case histories that "walk through" some of these fast files and ridge interaction events have been presented in an earlier report (Croasdale et al, 1995) and will not be repeated here. Instead, a more concise presentation of the ice load levels that were associated with ridge failures against the Molikpaq is given, based upon the 23 ridge interaction events that were contained within the nine fast file records.

Ridge Load Levels

The peak ice loads that were associated with the 23 first year ridge interactions are shown in Table 9, along with information on ridge sail height, parent ice sheet thickness and drift speed, the width of loading, the time to peak load and event duration, the parent sheet load, and the primary ridge failure mode. The estimated sail heights for these ridge interactions ranged from 0.5 m to 2.5 m and the global loads from 30 MN to 89 MN. These ridge load levels are in the "low to moderate range" in terms of the Molikpaq's overall experience in Beaufort sea ice, and are lower than many of ice loads experienced during crushing failures in level first year ice (Wright & Timco, 1994). An additional point to make at this stage is that the ice loads experienced during ridge interactions were "quasi-static, and did not exhibit any significant cyclical dynamics.

Table 9 Summary of first year ridge loading events on the Molikpaq.

Ridge Sail Height	Parent Sheet Thickness	Ice Drift Speed	Width of Loading	Peak Ridge Load	Time to Peak Load	Duration of Load Event	Parent Ice Sheet Load	Primary Ridge Failure Mode
(m)	*(m)*	*(m/sec)*	*(m)*	*(MN)*	*(sec)*	*(sec)*	*(MN)*	
1	0.7	0.75	75	45	34	64	20	fails behind
0.5	0.9	0.4	75	52	22	31	20	spine
1	0.9	0.4	75	43	15	55	18	fails behind
1.5	0.9	0.4	75	56	43	49	18	shear (& fails behind)
2	0.9	0.4	75	72	101	150	20	stops
1.5	1.1	0.3	60	46	68	120	20	stops (& fails behind)
1	1.0	0.1	105	67	63	115	30	fails behind
1	1.0	0.1	105	54	40	75	25	fails behind
1.5	1.0	0.1	105	70	108	170	25	fails behind
0.5	1.0	0.1	105	44	73	117	20	fails behind
1	1.0	0.1	105	37	122	139	15	spine (& fails behind)
1	1.1	0.1	105	55	123	158	15	spine
1	1.1	0.1	105	50	98	108	20	spine (& fails behind)
0.5	1.1	0.1	105	42	48	121	20	fails behind
0.5	0.8	0.1	60	30	120	190	15	fails behind
1	0.8	0.1	60	39	160	240	18	spine
1	0.8	0.1	105	89	56	87	35	fails behind (& spine)
1.5	0.8	0.1	105	88	37	60	35	shear (& fails behind)
2	1.1	0.2	75	81	112	277	25	spine
1	0.9	0.1	105	68	106	167	45	spine
1	0.9	0.1	105	66	31	78	30	fails behind
1.5	0.9	0.1	75	60	90	200	20	fails behind
2.5	1.3	0.1	60	75	-	-	35	stops

Figure 48 show the peak ridge interaction loads as a function of ridge sail height, based upon this data set. In the figure, the primary ridge failure mode that was associated with each one of the load values is also indicated, by the plotting symbol used.

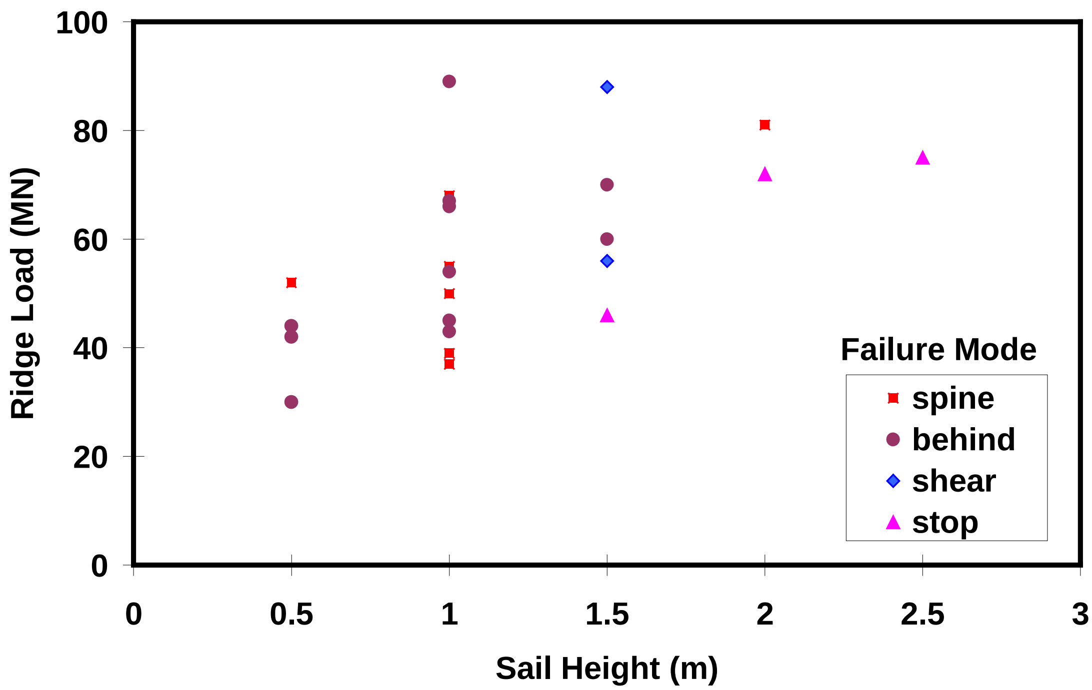

Figure 48 Peak ice loads from first year ridges as a function of sail height

Although the results show a considerable amount of scatter, there is a weak trend towards increasing load levels with increasing ridge size. There does not appear to be any strong or systematic influence of different ridge failure behaviours on the load levels seen, although the larger ridges that sheared and/or stopped are typically seen near the upper end of the ice load spectrum.

Figure 49 shows these peak ridge loads normalized by the width of ice loading on the Molikpaq, as viewed from the videos. Again, the global line load is shown as a function of the estimated sail height of the ridge.

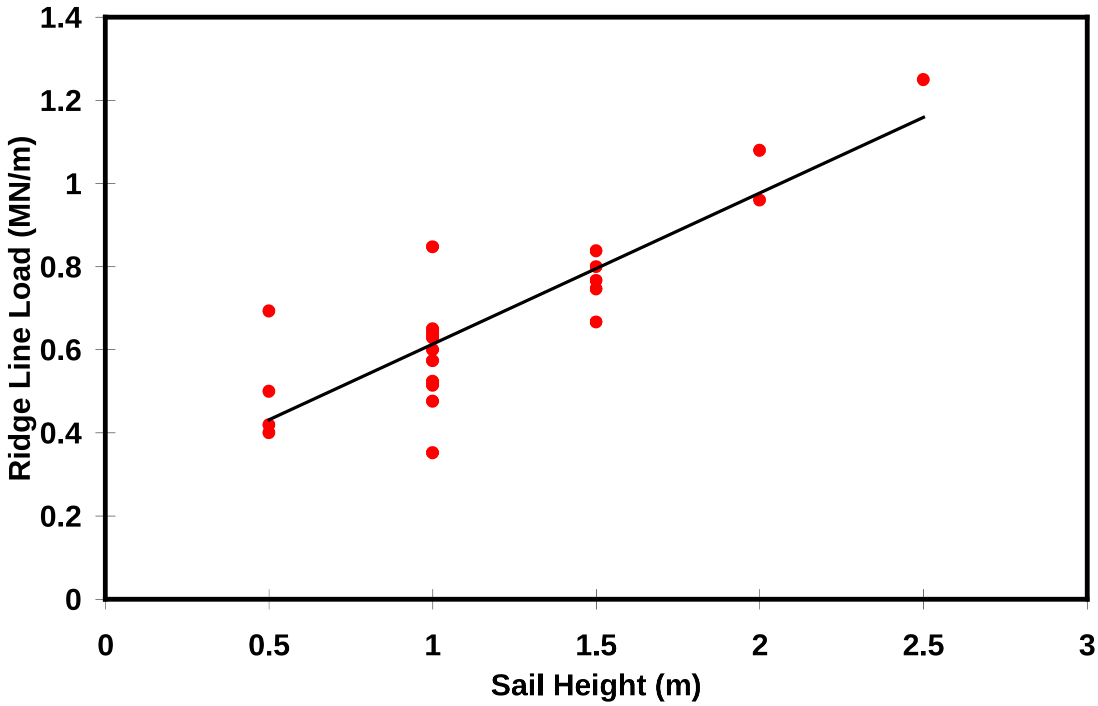

Figure 49 First year ridge line loads as a function of sail height.

This figure shows a fairly strong trend towards increasing line loads with increasing sail heights. For sail heights between 0.5m and 2.5m, the following regression line can be fit to the data:

$$R_{LL} = 0.36\, H_s + 0.25 \qquad \textbf{4-1}$$

where R_{LL} is the ridge line load in MN/m, and H_s is the ridge sail height in metres

This is simply an empirical fit and should be used with a high degree of caution, particularly when extrapolating to larger sail heights. This being said, it is still of interest to get some feel for the ice load levels that would be estimated for larger ridges, on the basis of this empirical relationship.

Assuming that a ridge with a sail height of 5m (which implies a keel depth of about 20m) interacts with a 100m wide structure, this relationship suggests a ridge load of about 200 MN. It is interesting to note that this empirically based ice load level is in the same range as some of the “more current analytic models” would predict, for similarly sized ridges and structures.

Still with empiricism, ridge loads are sometimes expressed in terms of a ridge factor, which indicates the probable increase in load levels because of ridge interactions, over and above that caused by the parent ice sheet. This approach is most commonly used by Russian practitioners, with a ridge factor value of 1.5 specified in Russia's VSN code for the design of offshore structures. It is noteworthy that this ridge factor value is independent of ridge size.

Figure 50 shows the Molikpaq ridge load data expressed as a ridge factor, again plotted against sail height. Here, the load from the parent ice sheet immediately before and after the ridge interaction was taken as the mean load level, since failure mode variations in the level ice over the course of a fast file can have a significant influence on mean load levels.

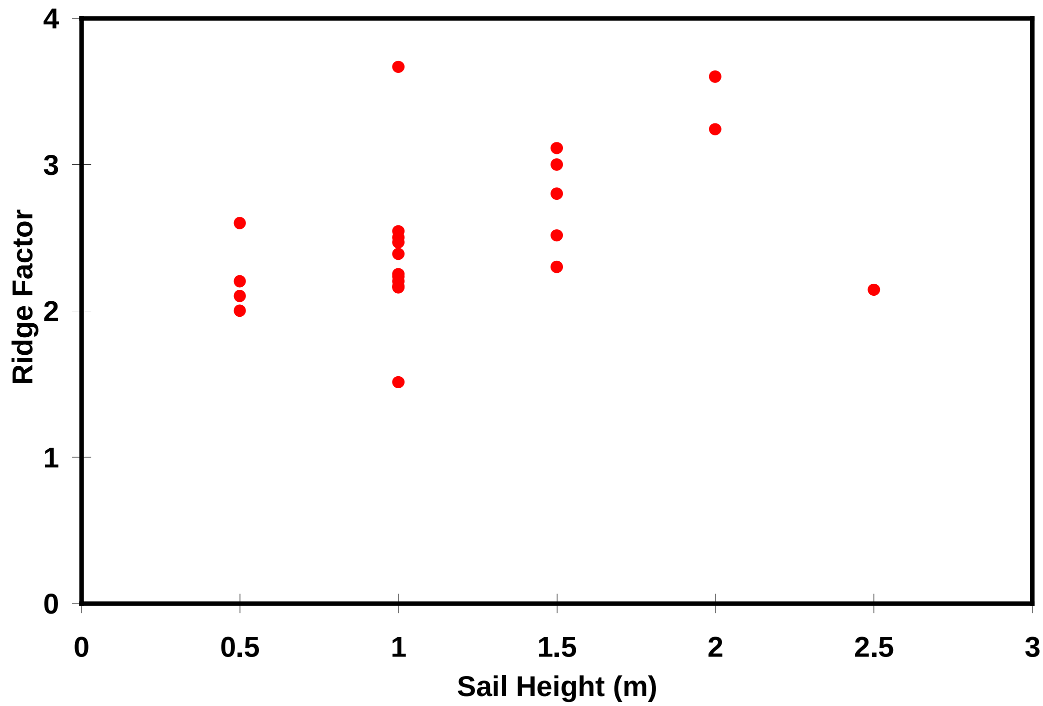

Figure 50 Molikpaq ridge loads expressed as a ridge factor.

It can be seen that the ridge factors typically range between 1.5 and 3.5, and are consistently higher than the 1.5 value that has been specified in the Russian codes. However, the mean load levels reflect mixed modal failures in the parent ice sheet around the ridges, with lower ice failure pressures, that tend to drive up the ridge factor value. If crushing failures of the level ice sheet are assumed at a pressure of 1 MPa, the ridge factors that are shown in Figure 51 result.

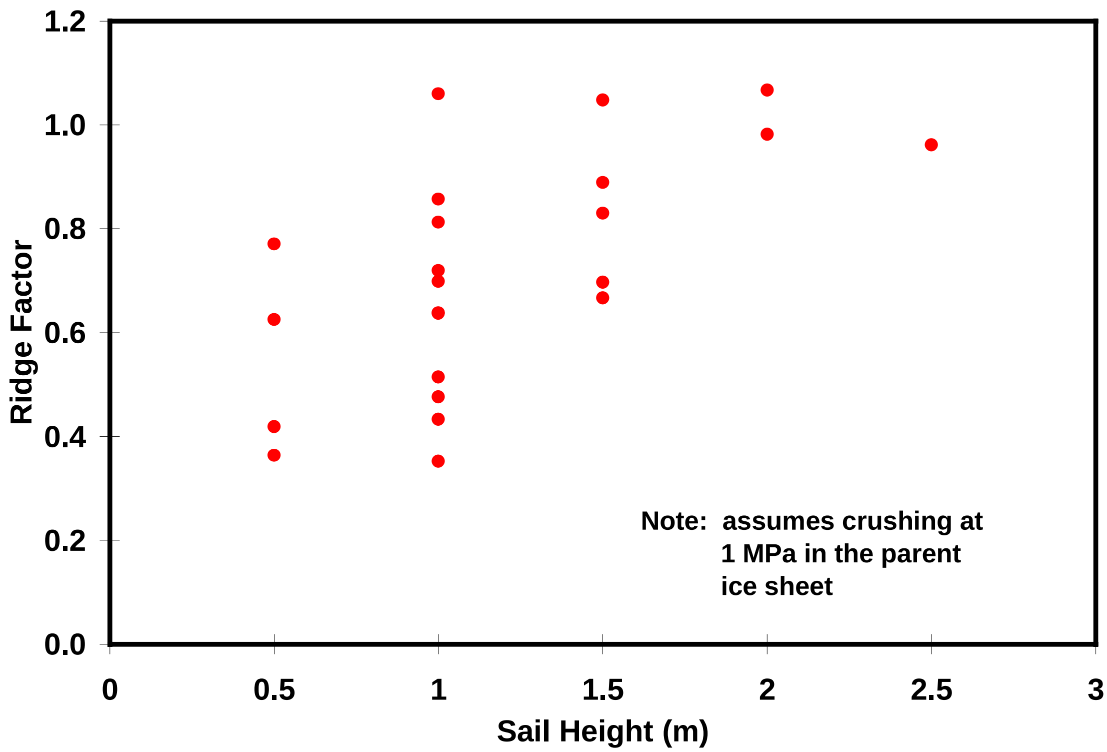

Figure 51 Molikpaq ridge loads expressed as a ridge factor, with crushing failures in the level ice surrounding the ridges assumed at a failure pressure of 1 MPa.

These ridge factors are typically less than one, and are reasonably well bounded by the 1.5 ridge factor value that is assumed in the Russian codes. However, if larger ridges were contained in the data base with load levels following the empirical line load versus sail height relationship given earlier, there is little doubt that the ridge factor would exceed 1.5, even when crushing of the parent ice sheet is assumed.

Some of the temporal aspects of the ridge interactions have also been on the basis of the ridge loading data. In Figure 52 and Figure 53, the time to peak load and total load duration value for each ridge interaction event are shown as a function of sail height.

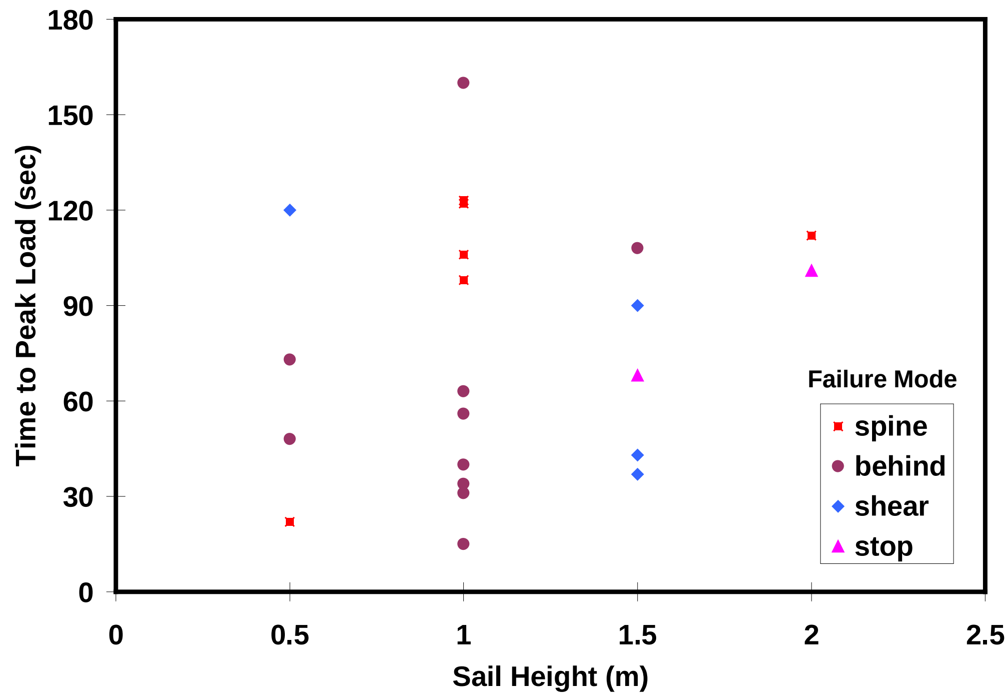

Figure 52 Time-to-peak-load versus sail height for different failure modes.

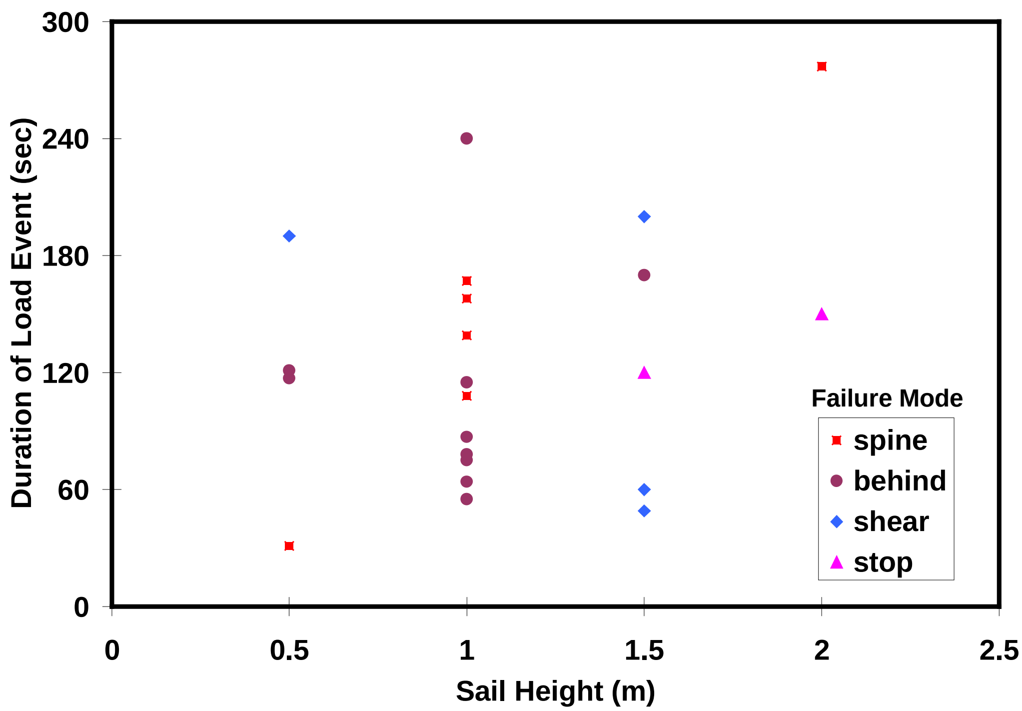

Figure 53 Duration of loading Event versus sail height for different failure modes.

These figures do not show any discernible trends and are not particularly revealing, but do indicate that the typical time frame for ridge failures and ridge interaction events are in the order of tens of seconds to several minutes. It can be seen that most of the ridge failures involving shearing and stopping behaviours tend to have slightly longer time frames than many of the spine and "behind" failures.

The ridge interaction information has also been considered from the perspective of "ridge penetration distances", although this assessment should be recognized as very rough. Figure 54 shows the estimated ridge penetration distance to peak load, plotted against a ridge width estimate. Here, the following points should be noted:

- ridge penetration values are based upon the time to the peak load and the ice drift speed for each ridge load event. Because the drift speed was measured in the general vicinity of the Molikpaq, it is not necessarily accurate for the ridge interaction zone. In addition, some of the ridges appeared to fail away from the caisson face, at least in their surface portions. Recognizing these factors, the ridge penetration distances shown are, at best, only ballpark values.
- ridge width values are based upon the sail height estimates that were obtained from video records, and the empirical relationship between sail height and ridge width given in Chapter 2. Accordingly, these values must also be acknowledged as very crude.

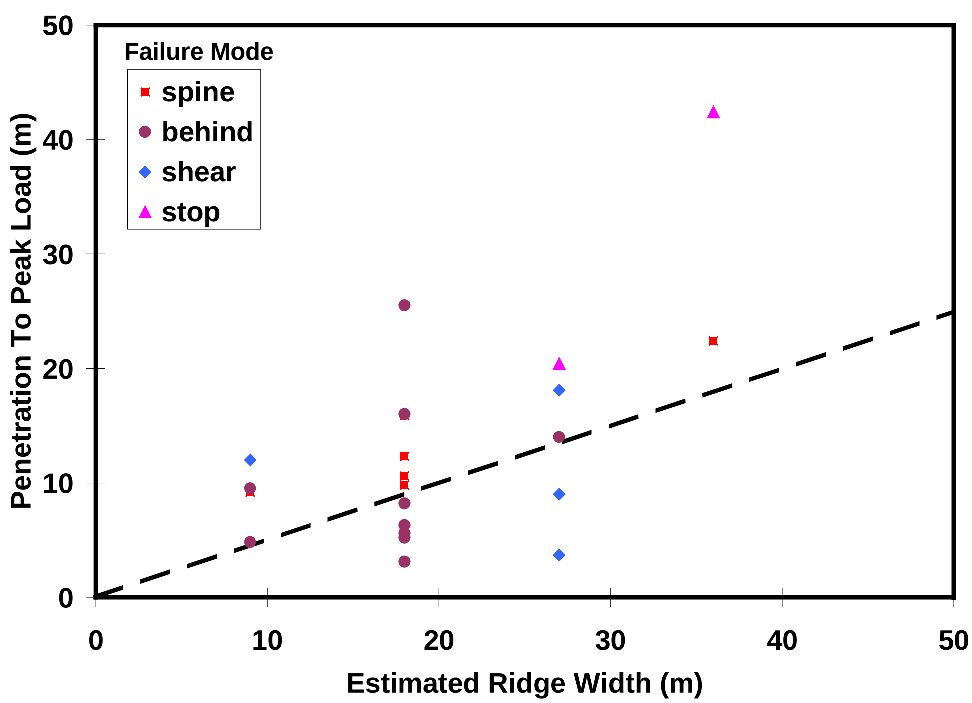

Figure 54 Penetration length to the peak load versus the ridge width for different failure modes. The dashed line represents the "half-width" of the ridge.

The line that is shown in Figure 54 represents the "half width" of the ridges that interacted with the Molikpaq. Penetration points falling below this line suggest that the ridges failed prior to penetration into their central portions. Although the accuracy of the data can easily be challenged, this figure seems to indicate that many of the ridges failed prior to or around the time their midpoint sections were reached. Several of the outlying points (ie: those above the line) involved shear and stopping ridge failure behaviours, where penetration distances are probably overestimated (because the general ice drift speed value was used).

Figure 55 shows ridge penetration distance over the total duration of these ridge loading events, plotted against the estimated ridge width. The line that is contained in this figure represents the "one to one" boundary for ridge width and penetration distance. If all points fell on this line, the influence of ridge interactions in terms of load levels would only be experienced while the structure was moving through them. In a very approximate sense, this appears to be the case, although there is a large amount of scatter in the data. Again, some of the outlying points reflect shear and stopping ridge failure behaviours, where penetration distances are undoubtedly overestimated.

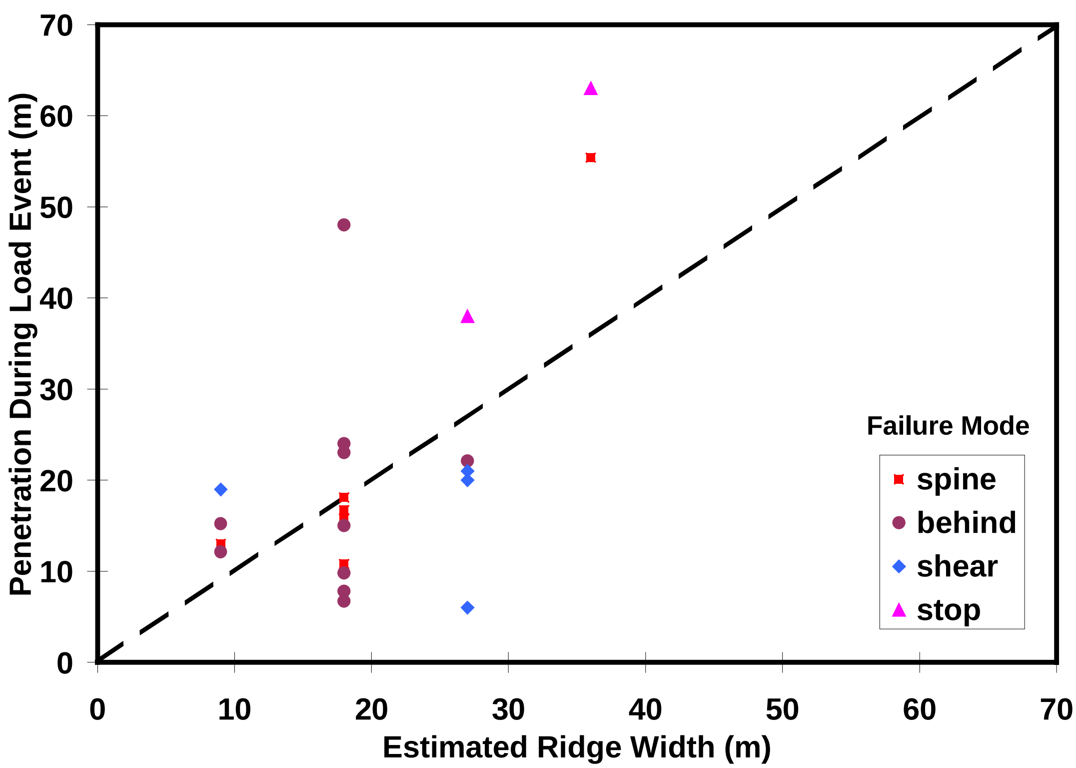

Figure 55 Penetration during the loading event versus the ridge width for different failure modes.

Keel Load Levels

It is important to recognize that the foregoing ridge loading information reflects the ice loads imposed by the sail, consolidated layer and keel portions of the ridge features encountered by the Molikpaq. Clearly, the individual load components from the different "sections" of the ridges, particularly their keel rubble portions, are of high interest.

In terms of keel loads, there is not a lot of information that can be gleaned from direct load measurements on the Molikpaq with any degree of reliability, because of limited Medof panel coverage "at depth". However, the caisson did have deep load panels on its E, NE and N faces which provided an indication of loads from about 3 m to 6 m below sea level, but only over one panel width (1.14 m). Since these panels were located below the consolidated layer depth of most ridges, they should provide some indication of typical "small area" load and pressure levels in the uppermost portions of keel rubble (Figure 56).

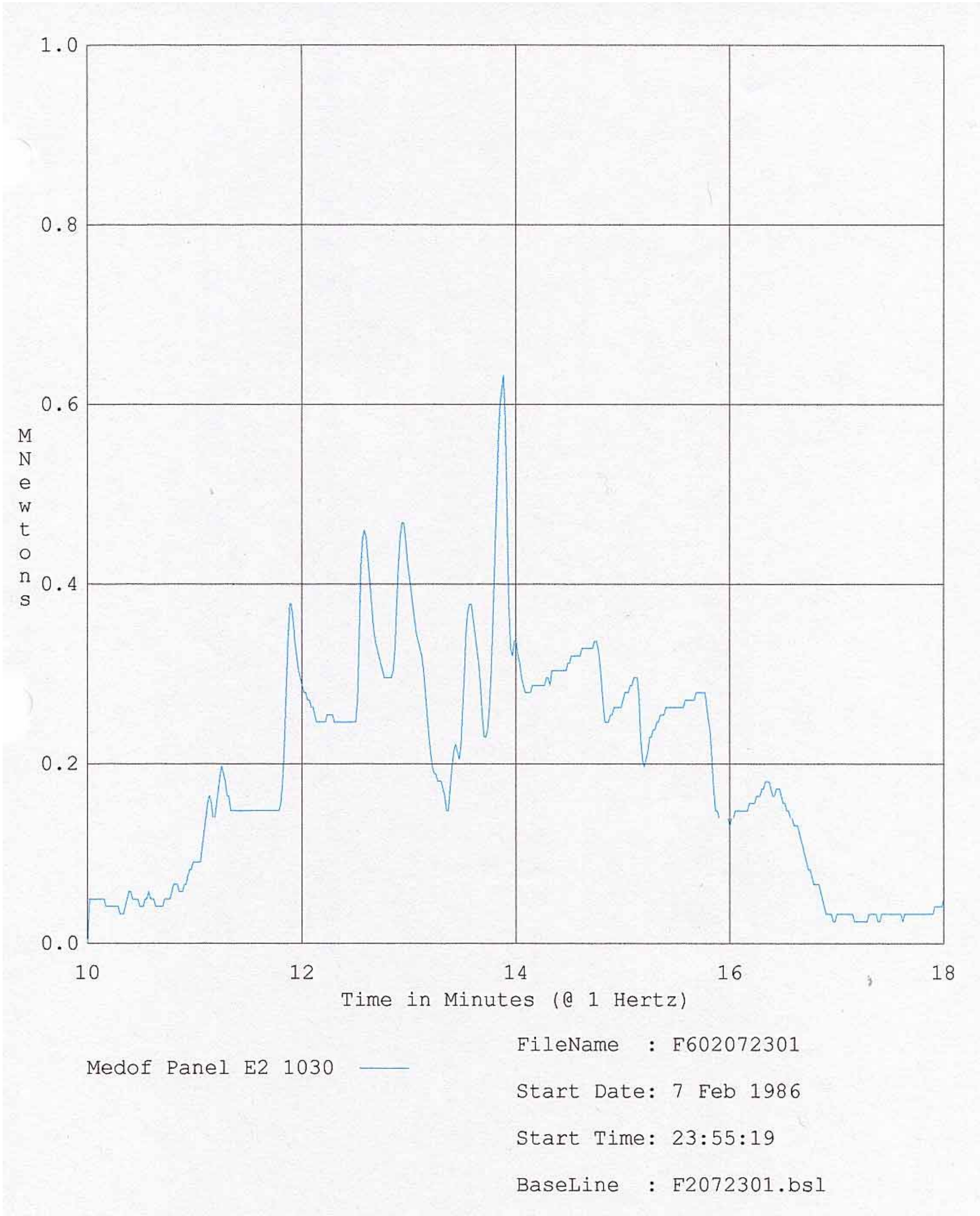

Figure 56 A typical example of the ice loads measured on a deep Medof panel during a ridge interaction event. The schematic of the load panel cluster (on the left) shows that the lower panel should be exposed to the keel rubble portion of most first year ridges.

Ice load data from these lower Medof panels has been reviewed during ridge interaction periods, to obtain some feel for the range of keel rubble pressures being applied, at least over the area of the panel (~ 3 m^2). Figure 57 shows the peak pressures that were obtained from these panels during ridge interactions plotted against sail height, assuming the entire area of the panel was loaded by keel rubble.

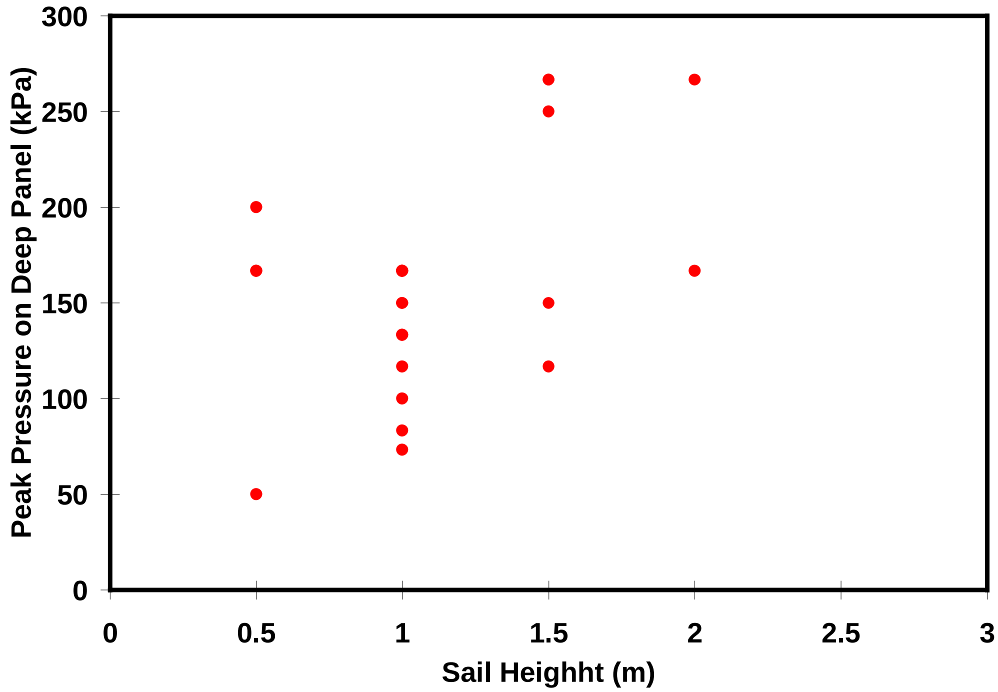

Figure 57 Peak small area pressure estimates for the upper portions of first year ridge keels versus sail height.

Although there is a considerable amount of scatter in the data, it does show that ice pressures were generally in the range of 100 to 200 kPa in "what should be" the upper levels of the keel rubble, during most ridge interactions. A weak trend towards higher pressures with increasing sail (and keel) sizes is also apparent, as one might expect due to keel buoyancy effects. These keel rubble pressure estimates should be recognized as very crude, since they are solely based on peak load measurements over very small areas. In all likelihood, averaging load levels over larger areas (if the panel coverage was available) would result in lower mean values, by a factor of two or more.

Figure 58 shows the mean pressures that were estimated over the duration of each ridge loading event, again assuming the panels were fully loaded by keel rubble. These pressures in the order of 50 to 125 kPa and interestingly, are in the same order of magnitude as one would expect from some of the more recent analytic models for determining keel loads.

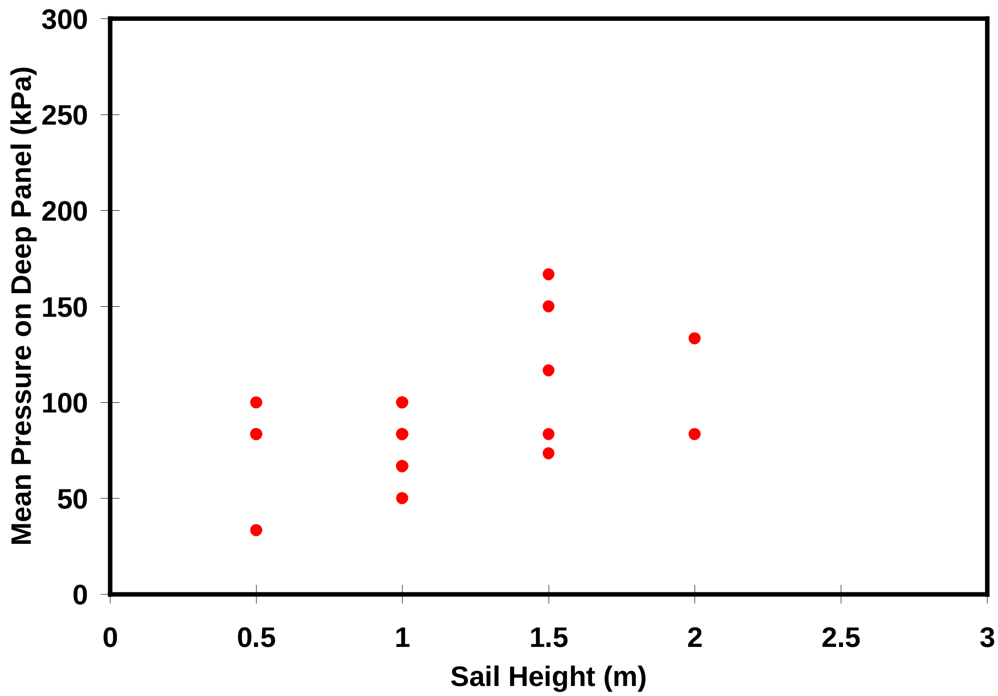

Figure 58 Mean small area pressure estimates for the upper portions of first year ridge keels over the duration of each ridge loading event versus sail height.

Various projections could be made with this "keel ice pressure" information, but are not attempted here, in view of the limitations of the data and the "speculations" that would be involved. Instead, rough estimates for the keel rubble component of each ridge load have been made from the global ice loading data, based upon some pragmatic assumptions. The keel load estimation method and the assumptions that have been used for this purpose at best approximate, and are highlighted as follows:

- the consolidated layer of each ridge is assumed as 1.5 times the parent ice thickness.
- the mean load from the parent ice sheet "around the time" of each ridge interaction is multiplied by 1.5 to estimate the load contribution from the consolidated layer
- this consolidated layer load is then subtracted from the overall peak ridge load to give a keel load estimate

The results of this rough assessment are given in Figure 59, where keel load versus keel depth estimates are shown, assuming a sail height to keel depth ratio of 1:4.5. To account for differences in the ice loading widths that were observed in the Molikpaq ridge interaction events, these keel load estimates have been normalized to a loaded structure width of 75m.

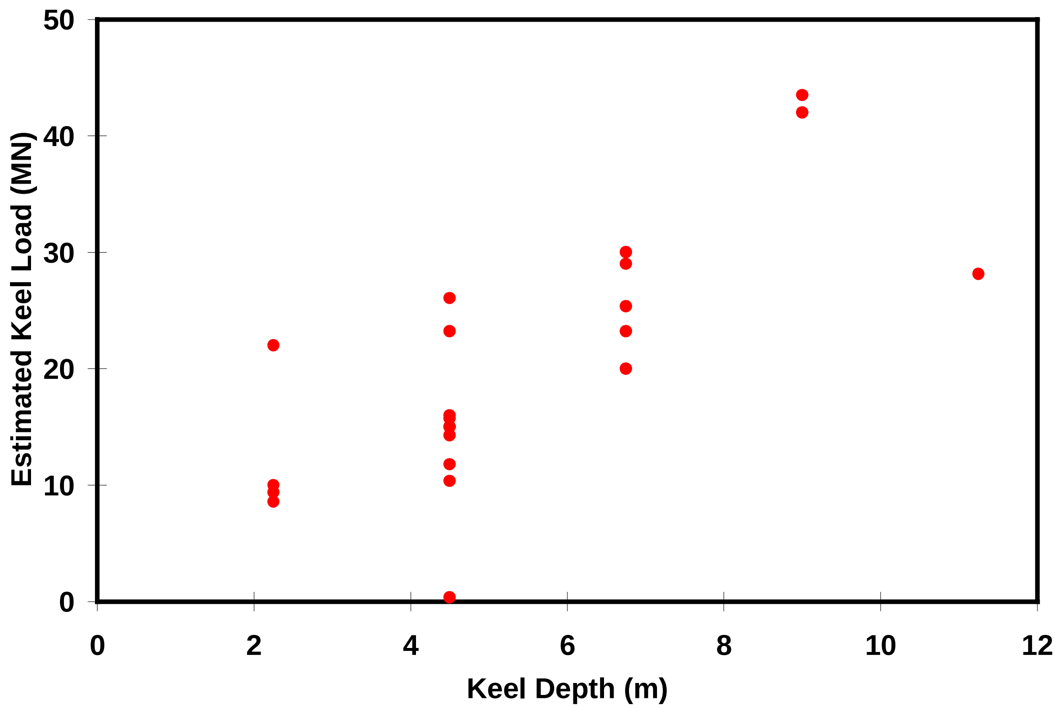

Figure 59 Rough estimates of keel loads experienced during Molikpaq ridge interaction events as a function of keel depth, normalized to a structure width of 75m.

Although the load estimation method that has been used is at best approximate, and there are many limitations in the data, it can be seen that the keel load values seem to follow a logical trend. For small ridge keels, these estimates are in the order of 10 MN, increasing to values of about 40 MN for larger ridge keels. It is interesting to note that these keel load levels are slightly high, but not too far out of line when compared to predictions from some recent keel load models, as will be discussed later in this report.

By way of summary, the full-scale data that was acquired during the Molikpaq's Beaufort Sea deployments provides some good insights into first year ridge interactions and loads for wide structures. Although many questions and uncertainties remain, it should be recognized that this data is the best and in fact, the only good information that is now available. As such, any other ridge interaction observations are best compared to this Molikpaq data and its implications, since it is "benchmark information". This is the approach that is used in the remainder of this chapter, where "snippets" of full scale information about first year ridge interactions with other structures, both wide and narrow, are highlighted and compared to the Molikpaq's experience in Beaufort Sea ridges.

4.2.2 *Observations from Other Beaufort Sea Structures*

4.2.2.1 Artificial Islands

Well before the Molikpaq had entered the Beaufort Sea, artificial islands had been used to support exploratory drilling activities in the area, beginning in the early 1970s. These islands were first constructed in the shallow nearshore waters of the Beaufort, in water depths of a few metres, and were covered by landfast ice throughout the winter period. As experience was gained, this technology was extended into the deeper waters of the landfast ice zone, with the deepest island built at Issungnak, in 19m of water (Figure 60).

Figure 60 A view of the Issungnak O-61 artificial island in the winter of 1980. A large grounded rubble field that formed around the island during freeze-up can be seen. This island was located near the outer edge of the landfast ice, in 19m of water, and did not experience much ice movement against its protective rubble annulus over the course of the winter.

The design of these islands was dominated by the Beaufort's severe ice environment, and was driven by expected loads from thick level first-year ice, and from potential multi-year ice floe interactions. Most of the information that was obtained about their performance in Beaufort sea ice has been summarized in a report entitled "Ice Load Transmission through Grounded Ice Rubble" (Croasdale et al, 1994). With regard to first year ridge interactions with artificial islands, only "anecdotal observations" are available, and little can be said. However, the following points should be noted:

- first year ridges were never a significant design concern for artificial islands, because of the shallow water areas and limited ice movement regimes in which they were located, and the protection afforded by their shallow "beach slopes"
- grounded rubble fields that consistently formed around these islands in the "thin ice" freeze-up period also protected them from direct interactions with ridges, even during the late break-up time frame
- any free floating ridges that did happen to move against these islands during ice movement events were "folded" into the rubble fields that surrounded them, and did not create high ice load levels
- a few *ad-hoc* observations of first year ridges moving into the grounded rubble fields around islands tended to indicate the same types of ridge failure behaviours as were seen on the Molikpaq, particularly the spine and failing behind modes (Figure 38 and Figure 39).
- any scouring on the sand beaches of these islands because of first year ridge and/or rubble interactions was of little significance (for both new and remnant islands)
- this suggests that the forces from the lower keel portions of the rubble in first year ridges were probably low and/or the rubble quite weak, at least in relation to the resistance of the sand material

4.2.2.2 Shallow Caissons

As exploration proceeded into the intermediate to deeper waters of the Beaufort Sea (20m or more), shallow caisson retained islands were introduced, as a cost-effective alternative to artificial islands. These structures (the Tarsiut caisson and the Esso CRI), were placed on submerged berms, which reduced sand fill requirements and the associated dredging costs, and created a quick means of penetrating the waterline, to reduce the risk of experiencing the adverse effects of storm waves as construction was nearing completion.

Any experiences that were gained with shallow caissons in first year ridges are similar to those with artificial islands, since these structures were also protected by grounded rubble fields (Figure 61).

Figure 61 A view of the Esso CRI at the Amerk location during the winter of 1982.

Despite this limited experience, an anecdotal point should be made that when large ridges and ridge fields were seen moving against the Tarsiut CRI during a summer ice intrusion in 1983 (after the CRI had been abandon), they were observed to have fractured in both the vertical and horizontal planes

4.2.2.3 Deeper Caissons

There is basically nothing reported for the SSDC or CIDS unit, in terms of significant ridge interactions. This is quite understandable, since the SSDC was always set on a berm (-9 m) and was rarely exposed to direct action from moving pack ice, and the CIDS unit was always deployed in shallow waters and never experienced significant ridge interactions

4.2.3 Molikpaq Observations off Sakhalin Island

In the early 1990s, the oil industry lost interest in Canadian Beaufort Sea activities and Gulf Canada decided to sell the Molikpaq to Sakhalin Energy Ltd.[1,] for use as a

1 a consortium led by Marathon Oil.

production platform off Sakhalin Island. The caisson was towed from the Beaufort Sea to Korea in the summer of 1996, where it underwent structural modifications and received "production topsides". Because its deployment location off Sakhalin Island was in 30 m of water, a decision was made to deepen the original structure by adding a new steel pontoon, called the "Spacer", rather than placing the Molikpaq on a large sand berm. This spacer section was constructed in Russia and the Molikpaq, after undergoing modifications in Korea, was mated with it and then installed off Sakhalin Island in the summer of 1998 (Bruce et al, 1999).

The Molikpaq is now operating at the Piltun-Astokskoye field on a year round basis. From an environmental perspective, the offshore Sakhalin area is severe, since it is subject to strong seismic activity, large storm waves and heavy seasonal pack ice. During the summer period, the region experiences maximum wave heights that can exceed 15 m. In winter, it is covered by rough and heavily deformed first year sea ice, and is normally ice covered for about 7 months of the year. First year ridges and rubbled ice areas with keel depths as large as 25 m are representative of the design ice features for the Molikpaq's deployment location. However, extreme wave loads governed its deployment design.

The Structure

- a schematic cross-section of the Molikpaq and its new "spacer base section", as deployed at the Piltun-Astokskoye location in 30 m of water, is shown in Figure 63.

- the overall geometry of the Molikpaq caisson is the same as the "Beaufort version" shown in Figure 32, except that it is now seated on the spacer, which has a 15 m height, and also has new topsides and ice/wave deflector sections

- as compared to its first two Beaufort Sea deployments (which had ≈20 m set down drafts), the Molikpaq has basically been placed on the spacer at a set down draft of 15 m, resulting in a slight increase in its waterline width (to ≈100 m from 90 m) and a sizable increase in its freeboard (to ≈20 m from 13.5 m, to prevent significant wave overtopping in open water storms)

- at this set down draft, the caisson's walls are 23° off vertical through the waterline (from +1.5 m to –10 m, relative to mean sea level), flaring out at an angle of about 40° to the 15 m depth, where they meet the vertically sided spacer section

Figure 62 A photograph of the Molikpaq in moving pack ice conditions at the Piltun-Astokskoye location, off the northeast coast of Sakhalin Island. This photo was taken in mid-May 1999, when a subsea flowline from the Molikpaq to a tanker loading facility was being installed. At the time, icebreakers had managed (or fragmented) the pack ice in the general vicinity of the caisson, to support construction operations from the ice capable vessel being used for the flowline installation. However, the heavy character of the pack ice cover, and the ridge and rough areas contained within it, are still evident. (photo courtesy of Rick Weiss).

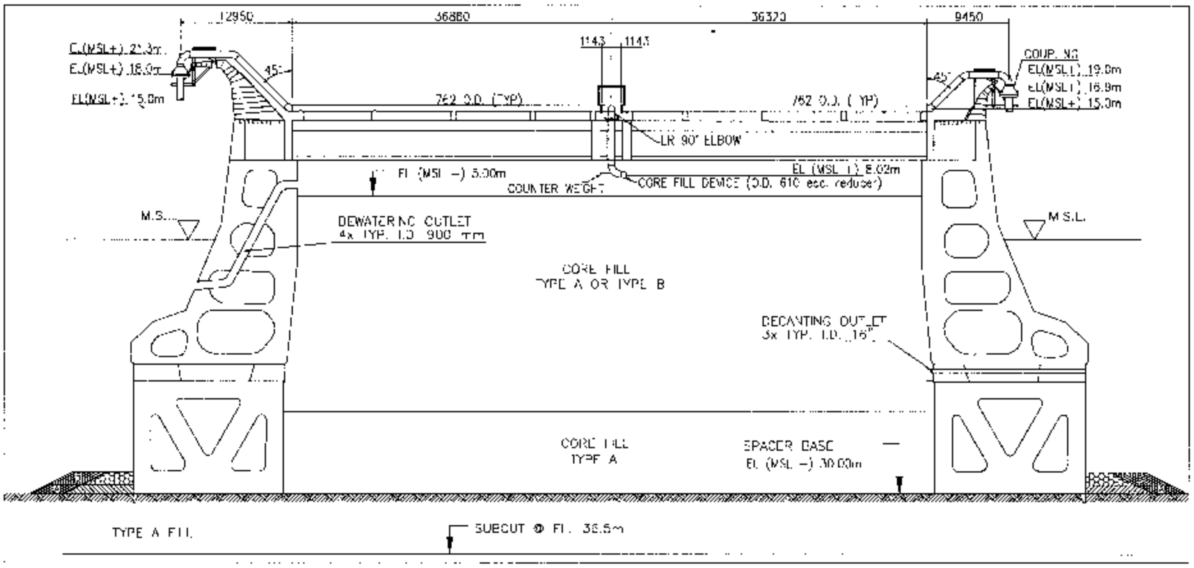

Figure 63 A schematic illustration of the Molikpaq's deployment configuration off Sakhalin Island (after Hollowell et al. 1999).

- in terms of the first year ridge interactions with the Molikpaq, this deployment configuration suggests:
    - the consolidated layer of ridges will move against a 23° face
    - the upper keel portion of most ridges will also move against a 23° face
    - the mid to lower portions of large ridge keels will interact with the more sloped section of the Molikpaq's base and the vertical walls of the spacer

Instrumentation & Monitoring

- for this long term deployment off Sakhalin Island, the Molikpaq structure is again well instrumented, to measure ice and wave loads, and various platform responses to these loads and to seismic events

- sensors that were installed on the caisson for its Beaufort Sea operations have been refurbished, while some new sensors have been installed on the Molikpaq and spacer and their sand core and foundation soils.

- direct observations of ice conditions that the structure is experiencing off Sakhalin are also being acquired by onboard monitoring personnel, and by video coverage of ice interactions with the caisson (as they were in the Beaufort)

- again, in terms of ridge interaction and loads, the most important components of the instrumentation and monitoring systems are those which provide information on ice loads, the ice conditions that are causing these loads, and the associated ice failure behaviours

- as in the Beaufort, ice loads on the Molikpaq are being measured by three separate systems, which include clusters of ice load panels on the caisson's N face, strain gauges on the main bulkheads, and extensometers that sense the overall deformations of the caisson

Ridge Interactions & Loads

- because of its inclined faces at the waterline, bending failures are commonly seen in the pack ice that moves against the Molikpaq, and small free floating rubble accumulations are frequently seen along its updrift face
- general observations suggest that these floating rubble accumulations, combined with some "looseness" in the Sakhalin pack ice, often buffer direct interactions between ridges and the structure
- some of the initial data from ice load panels located between 6 m and 8 m below sea level suggest that peak keel rubble pressures can be moderately high) similar to keel rubble pressures seen in the Beaufort Sea), when pack ice with high ridge and hummock frequencies was moving against the Molikpaq
- no significant dynamics have been noticed during ridge interaction events or in fact, during any ice interactions
- it is interesting to note that these generalized observations are not "out of line" with the knowledge gained about first year ridge interactions with the Molikpaq in the Beaufort Sea

Analysis of the Molikpaq ice loading data that is being acquired off Sakhalin Island is just beginning, and the results of this work remain proprietary to Sakhalin Energy Ltd. However, it is important to be aware of this data collection effort on the Molikpaq, because it will be a key source of information on ridge interactions with wide structures for many years to come.

4.3 Narrow Structures

4.3.1 Observations from Confederation Bridge Piers

Observations that are currently being obtained from the Confederation Bridge piers are the best source of full-scale information about first year ridge interactions with narrow offshore structures. This bridge is located in Northumberland Strait, in the southern part of the Gulf of St. Lawrence, spanning a distance of more than 11 km between the coastlines of New Brunswick and PEI (Tadros 1997). The region is subject to moving pack ice in every winter, usually from late December until late April. Because the pack ice contains significant numbers of ridges and is highly dynamic (Brown, 1997), the bridge piers experience a large number of ridge interactions each year (Figure 64). First year ridges with keel depths in the range of 10 m to 15 m are not uncommon, while the level ice cover can approach maximum thicknesses of about 1 m by late winter.

Since first year ridge loads governed the design of the Confederation Bridge piers and were the subject of considerable debate during the design process, “real life interactions” between these features and the piers are of high interest. In view of this, a five-year ice monitoring program was initiated in the winter of 1997/98, which will continue to collect ice load and ice/structure interaction data through the winter of 2001/2002 (Cheung et al. 1997). The database that is being acquired within this program is providing a wealth of information about first year ridge interactions and loads on narrow structures. Unfortunately, this information is proprietary to the government departments and companies that are funding the work, and cannot be discussed in any more than qualitative terms in this report. However, it is important to be aware of this monitoring program, because it will be a key source of information on ridge interactions and loads for years to come.

Figure 64 Video image showing rough first-year pack ice moving against one of the Confederation Bridge piers.

The Structure

- the Confederation Bridge is supported by a large number of piers, the majority of which are located in water depths of 25 m to 40 m. A schematic illustration of a typical pier from the Confederation Bridge is shown in Figure 65.

- each pier consists of a conical base section that houses a cylindrical pier shaft, which rises to within 4 m of the mean sea surface. This cylindrical shaft is 10 m in diameter and supports a conical icebreaking collar, with a cone angle of 52° and a waterline diameter of about 15 m.

- the base of the conical section lies about 5m below mean sea level and rises to a height of 2.6 m above the sea, where there is a transition to a 78° cone that reaches to +7 m. The main pier shaft above this cone is octagonal to the underside of the box girder that forms the bridge.

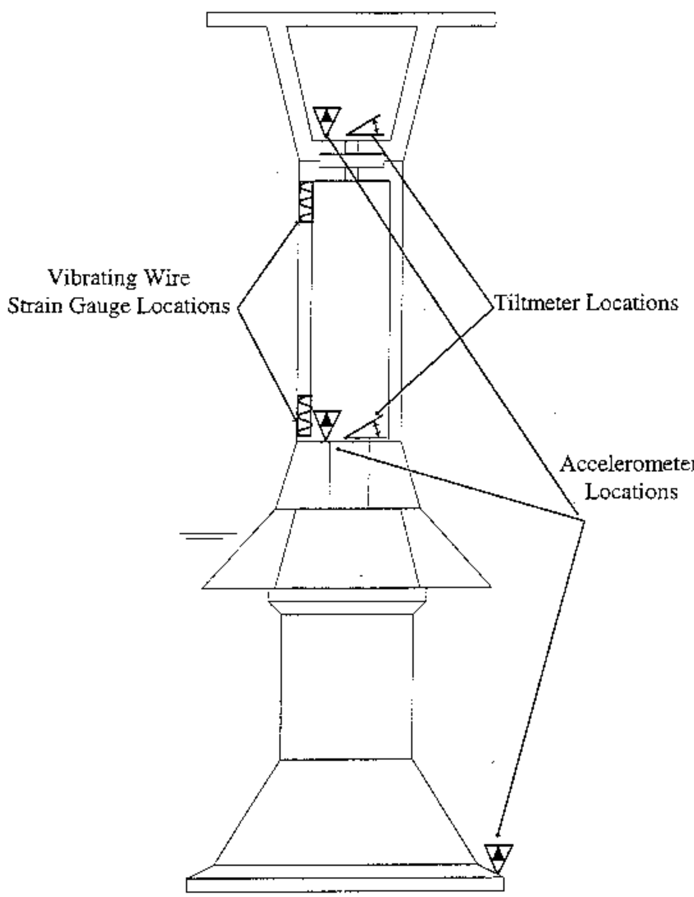

Figure 65 Schematic illustration of a Confederation Bridge pier showing the location of some of the instrumentation used to determine ice loads.

- in terms of the first year ridge interactions with the bridge piers, this configuration suggests:

- the consolidated layer of ridges will move against the 52° conical collar
- the upper keel portion of most ridge keels will also move against this collar
- the mid to lower portions of larger ridge keels will interact with the more narrow cylindrical shaft under the conical collar

Instrumentation & Monitoring

- Two of the main piers (P31 and P32) on the Confederation Bridge have been extensively instrumented to measure ice forces, and to observe and document the ice moving against them piers, along with its failure behavior (see Figure 65).
-
- The ice force measurement program consists of five main components. These are:

  1. indirect measurements of global ice loads on the instrumented bridge piers from observed structure responses
  2. direct measurements of local ice loads on the conical collar and cylindrical shaft of the piers with ice load panels
  3. video recording of interactions between the oncoming ice cover and the piers
  4. measurements of the level ice thicknesses and ridge keel depths in the ice that is moving against the piers, from upward sonars placed on the seafloor in close proximity to them
  5. measurements of the prevailing weather conditions

Ridge Interactions & Loads

Although the Confederation Bridge has only been in place for three years, the instrumented piers have experienced several thousand ridge interaction events to date. Little can be said about the data that has been acquired, because it remains proprietary to the participants of the monitoring program. However, a few qualitative comments about ridge interactions with the bridge piers can be made, on the basis of recent papers and general knowledge. These points are summarized as follows.

- the consolidated portion of many ridges have tended to fail against the conical section of the bridge piers in a "classical manner", by riding up the cone and failing in flexure. However, ice rubble accumulations on or near the cone (formed from earlier level ice pile-ups or as part of the ridge interaction process) have often complicated this failure behaviour.

- a variety of other "surface failure modes" have also been observed during ridge interactions with the Confederation Bridge piers (Brown et al, 1999), including:

  - wedge or plug failures (somewhat akin to shear failures against the wider Molikpaq structure)
  - spine failures (also seen on the Molikpaq)

- local failures and some "splitting" failures
- buckling failures in the sheet ice adjacent to ridges (somewhat akin to the failures seen behind ridges at the Molikpaq)

- Figure 66 shows several representative examples of these first-year ridge failure modes.

- Similar to the Molikpaq, the full nature of ridge interactions are difficult to define from the videos, because only the surface characteristics of the ridge interaction can be seen, and not the keel failure modes.

- the load levels that ridge interactions have caused are well within the bounds of those predicted from design ice load calculations

- it is noteworthy that the total loads from fairly small ridges are sometimes higher than the total loads from larger ridges, presumably because of differences in the consolidated layer thicknesses of individual ridges, the manner in which this layer fail, and the relative magnitudes of the consolidated layer load (which represent the major ridge load component).

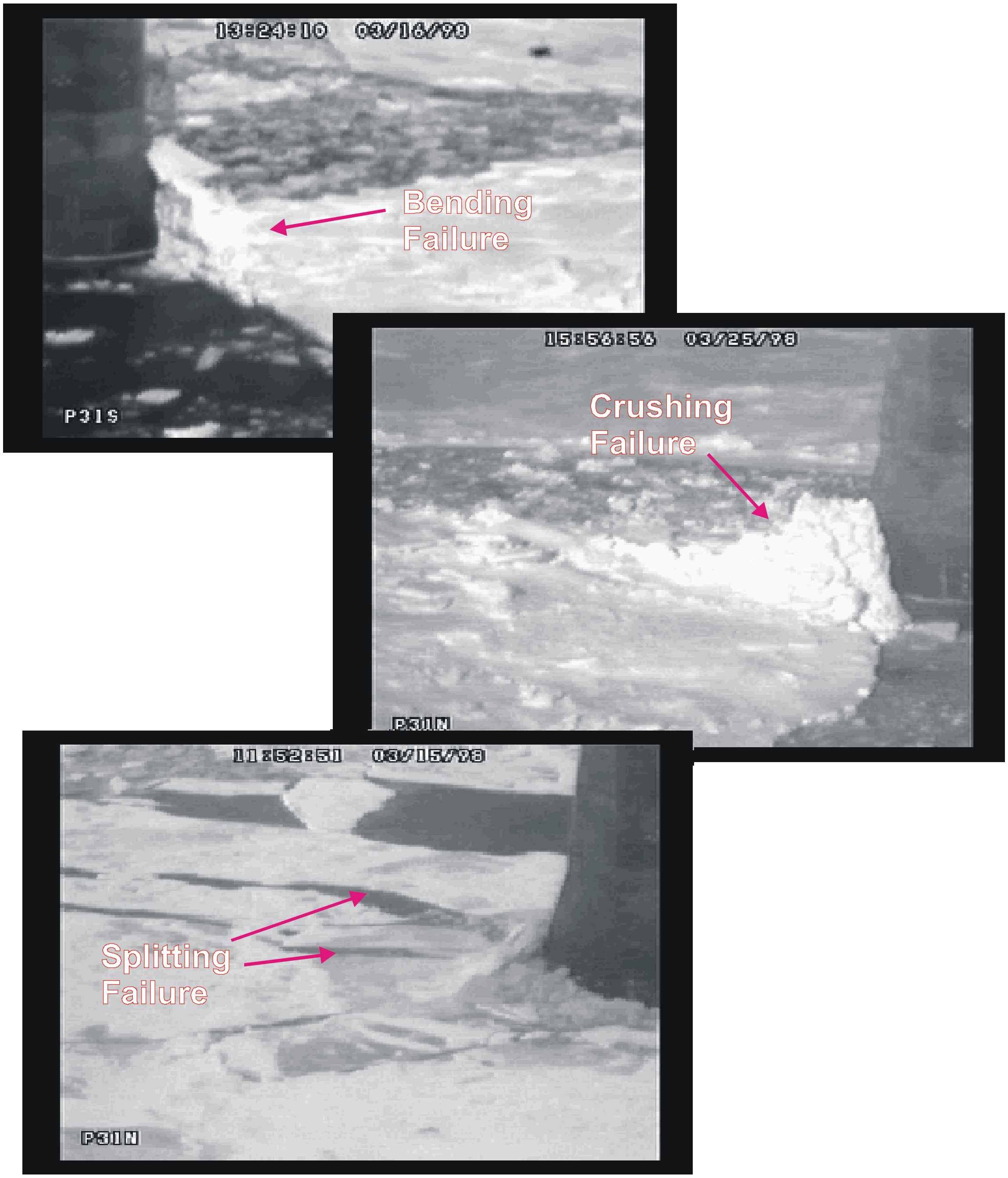

Figure 66 Video photos showing different failure modes observed on the Confederation Bridge piers.

4.3.2 Observations from Cook Inlet Platforms

The first offshore structures that were designed for use in moving pack ice conditions were those developed for oil and gas production operations in Cook Inlet, Alaska, which began in the early to mid 1960s. These structures were designed to accommodate a variety of environmental influences including relatively deep waters (30 m – 40 m), high tides (10 m), strong seismic activity, and seasonal pack ice. The Cook Inlet platforms were basically an extension of previous open water designs and for the most part, were four legged structures that were piled into the seafloor. Bracing between their leg columns was placed well below low water level, to avoid ice action on relatively small structural members. Presumably, this was dictated by the maximum depth of ridge keels. Several variations of the four-legged platform were also designed and deployed, including monopod and three column structures. All of these platforms had fairly narrow vertical columns through the waterline which were circular in form, with column widths varying from about 4 m to 10 m. As such, they fall into our narrow structure category.

The pack ice conditions that are found in Cook Inlet are quite mild when compared to many other areas, but were unprecedented at the time. The typical ice design condition that was identified for these structures involved level first year ice with maximum thicknesses approaching 1 m, floe sizes in excess of 1 km, and ice drift speeds of up to 3 m/sec. Other types of ice features were also observed in Cook Inlet, which included first year ridges (with maximum keel depths of 7 m), small low relief rubble fields, and thicker ice areas that were generated by nearshore tidal processes. Although their presence was recognized, it appears that ridges and these other ice features were not explicitly considered in terms of design ice load levels.

Throughout the 1960s, the Cook Inlet platforms received a considerable amount of R&D attention, in terms of the type of ice action and ice load levels that were experienced. In fact, these measurements and observations represent some of the most important pioneering efforts in the field of ice mechanics. Key results from the Cook Inlet experience have been published in a variety of papers (eg: Peyton, 1968), where the ice crushing failures and pressures that have been seen on these narrow vertical structures are described, along with the ice induced dynamics that have been experienced. Although no quantitative discussion of ridge failure modes or load levels has been given, a few key points are highlighted as follows:

- ridge loads (expressed as a ridge factor), were reported to be two to three time higher than level ice crushing loads on the Cook Inlet platforms

- the maximum line loads measured on the narrow vertically sided columns in ridges were in the range of 60,000 to 70,000 lbs/ft (or about 1 MN/m)

It is interesting that these summary points are not “out of line” with what has been inferred from the Molikpaq ridge interaction data.

4.3.2 Observations from Lighthouses

There have been a number of very important ice load monitoring programs that have been carried out at lighthouses, particularly in the Baltic Sea. These efforts have been underway for a number of years, and have been described in various reports and papers (eg: Hoikkanen, 1984; Määttänen 1986; Määttänen and Hoikkanen, 1990). Although load measurements have been obtained during level ice interactions, these lighthouses have encountered few ridges, because they are generally located in landfast ice. Määttänen (1986) describes the failure behaviour of the ice around the Kemi-I lighthouse as follows:

> Qualitative results of ice failure patterns, rubble pile formations and clearing in different ice conditions have been recorded by video, photographed, and written in log books. The ice failure and subsequent clearing is strongly velocity dependent. With low velocity the ice behaves in a ductile manner, breaks in bending mode and rides up the cone in a single layer. With high velocity the ice failure is brittle in a combination of bending, crushing and shearing modes, rubble pile formation occurs and the riding up layer is thicker. During pressure ridges the clearing mechanism of broken ice mass appears to be efficient. The rubble pile is alive with pieces climbing up the cone and being pushed sideways. A stationary false bow formation will not take place usually. It was observed only a few times with thin ice during temperatures below - 20 °C.

Other than this one case, it appears that little information about ridge interactions with Baltic lighthouses has been collected to date. There is, however, a fairly recent R&D initiative called the "LOLEIF Project", in which an array of ice load panels has been placed on a Baltic lighthouse. This project may lead to some data on first year ridge interactions with the lighthouse, depending upon how much exposure its location gets to moving pack ice conditions.

4.4 References

Brown, T.G. 1997. The Confederation Bridge: Analysis of Environmental Impacts Related to Ice. Can. J. Civil Eng., Vol. 24, No. 6, pp 908-914.

Brown, T. et. al, 1999. Year Two of the Confederation Bridge Ice Monitoring Program. Proceedings OMAE'99, Paper OMAE99-1171, St. John's, Nfld. Canada.

Cheung, M.S., Tadros, G.S., Brown, T., Dilger, W.H., Ghali, A. and Lau, D.T. (1997) Field monitoring and research on performance of the Confederation Bridge, Canadian Journal of Civil Engineering, NRC, 24: 951-962.

Croasdale, K. et al., 1994. Load Transmission through Grounded Ice Rubble. Report to the National Research Council, Ottawa, Ont., Canada.

Croasdale, K. et al. 1995. Ice Load Models for First-Year Pressure Ridges and Rubble Fields. Phase 1 Report. Report to PERD/NEB, Calgary, Al., Canada.

Frederking, R., Timco, G.W. and Wright, B.D. 1999. Ice Pressure Distribution from First-Year Sea Ice Features Interacting with the Molikpaq in the Beaufort Sea. Proceedings 9th International Offshore and Polar Engineering Conference ISOPE'99, Vol II, pp 541-548, Brest, France.

Hollowell, J.A. and L. C. Visser. 1999. Installation of the Vityaz Production Complex. Proceedings Offshore Technology Conference, OTC'99 Paper OTC 10820.

Jefferies, M.G. & Wright, W.H. 1988. Dynamic Response of Molikpaq to Ice-Structure Interaction. Proceedings OMAE'88, Vol. IV, pp 201-220, Houston, TX, USA.

Määttänen, M. and Hoikkanen, J. 1990. The Effect of Ice Pile-up on the Ice Force of a Conical Structure, in Proc. of the 10th International IAHR Symposium on Ice, pp 1010-1021, Espoo, Finland.

Määttänen, M. 1986. Test Cone Project. Proceedings of Polartech'86, Vol. 2, pp 749-761, Espoo, Finland.

Hoikkanen, J. 1984. Measurements and Analysis of Ice Pressure against a Structure in Level Ice and in Pressure Ridges, in Proceedings 7th International IAHR Symposium on Ice, Vol. 3, pp.151-160, Hamburg, Germany.

Peyton, H.R. 1968. Sea Ice Forces. NRC/DBR Technical Memorandum No. 92, pp 117-123, Ottawa, Ont., Canada.

Rogers et al., 1998. DynaMAC: Molikpaq Ice Loading Experience. Klohn-Crippen Report to the National Research Council of Canada.

Tadros, G. 1997. The Confederation Bridge: an overview. Canadian Journal of Civil Engineering, NRC, 24: 850-866.

Timco, G.W., Wright, B., Johnston, M. and Frederking, R. 1999. First-Year Ice Ridge Loads on the Molikpaq. Proceedings 4th International Conference on Development of the Russian Arctic Offshore, RAO99,Part II, pp 172-179, St. Petersburg, Russia.

Wright, B., Pilkington, G.R., Woolner, K.S. and Wright, W.H. 1986. Winter ice Interactions with a Arctic Offshore Structure, IAHR Symposium on Ice, August 18-22 1986, Iowa city, Iowa, USA, III: 49-73.

Wright, B.D. and Timco, G.W. 1994. A Review of Ice Forces and Failure Modes on the Molikpaq. Proceedings of the 12th IAHR Ice Symposium, IAHR'94, Vol. 2, pp 816-825, Trondheim, Norway.

5.0 METHODS FOR PREDICTING RIDGE LOADS

There have been a number of different approaches used to predict the loads that ridges could exert on offshore structures. These can be catagorized into 3 groups:

1. Model Tests
2. Analytical Models
3. Numerical Models

Each approach will be discussed in this chapter.

5.1 Model Tests

Physical modelling has been carried out to investigate the failure behaviour of ridges and the associated loads during interaction with fixed structures. In this approach, the important forces on the prototype (full-scale) structure are maintained in the same ratio on the model structure, but at a reduced scale. In this way, the interaction process can be investigated in a controlled laboratory environment with reduced loads. Special procedures must be used to correctly simulate the interaction behaviour. In particular, it is important to have the correct geometric, kinematic and dynamic characteristics for reliable results.

Model test programs of ridge interaction have been carried out by a number of different investigators including Abdelnour (1981), Lewis and Croasdale (1978), Wang (1984), Kamesaki and Yoshimura (1987), Eranti et al. (1992), Timco and Cornett (1995), Brown et al. (1995); Croasdale (1999).

For accurate modelling, the linear dimensions of the full-scale or prototype (p) structure are reduced to model (m) scale by a geometric scale factor λ. For these tests, the inertial, gravitational and crushing forces are of particular importance, and so the scaling is performed using Froude and Cauchy scaling (see Timco (1984) for a review of ice modelling techniques). The use of physical modelling requires special techniques and precautions in order to obtain reliable results. Based on the modelling laws, the materials used to model both the ice and the structure must have certain well-defined characteristics and values. In addition, the techniques used to measure the ice loads must not interfere with the interaction process.

One of the most challenging aspects of tests involving ridges is the production of a realistic ridge in the model basin. A number of approaches have been developed to produce the ridges including the “dump truck” method and the “closing chute” method. In both cases, a level ice sheet is grown to the desired thickness. For the dump truck method, ice at one end of the tank is broken and scoped with a “bucket” and the ice is poured into a pile where the ridge to be located in the ice tank. In some cases, the ice is poured between parallel plates that act as guides, and it other cases, the ice is poured with no guide walls. This approach produces a large pile of broken ice that will naturally equilibrate to the desired shape. In the “closing chute” approach, two parallel plates are inserted vertically into the ice tank and the ice between them is broken. Then, the plates are moved together to form a large pile of broken ice. In both cases, care is taken to ensure that the feature is linear and uniform across the width of the tank. Following the ridge building process, a level ice sheet is grown to confine the ridge and provide realistic boundary conditions for the tests.

Both of these approaches produce ridges that have geometric similitude with full-scale ridges. However, problems arise with tempering the ridge to the correct strength. There are 2 reasons for this. First, the strength of full-scale ridges and its components are very poorly known and understood, so the lack of a representative full-scale value is problematic. Second, the growth of the level ice sheet often significantly strengthens the consolidated layer due to the movement of the chemical dopants in the ice. Thus, often this layer is too strong, based on expected strength of the consolidated layer. These factors must always be borne in mind in viewing and analyzing the test results.

Figure 67 Photograph showing a model test of a first-year ridge interacting with a pier from the Confederation Bridge (after Timco and Cornett, 1995).

As an example, Timco and Cornett (1995) performed a model test program of the interaction of first-year ridge with a pier from the Confederation Bridge.

Figure 67 shows a photograph of the tests. Note that the ridge is linear and well defined and spans the width of the ice tank. In this test program, there were a number of observed failures mode for the ridge including:

Large-scale Lifting of the Ridge - In this case, the central portion of the ridge was lifted as it slid up the face of the cone. The ridge had an appearance of a large-scale "heave". This mode was only observed when the consolidated layer was very strong. In this case, the ridge had sufficient strength to enable it to be lifted from the water. Ridge failure finally occurred through either a large circumferential cusp failure, or a splitting of the ridge. This failure mode produced high loads.

Splitting of the Ridge - In some cases, the ridge split across its full width. This mostly occurred part way through the ridge-pier interaction. In some cases secondary cracks occurred across the ridge, usually, but not always, at a large distance from the pier. This mode of failure produced very large ice pieces.

Circumferential Cusp Failure - In most cases, the conical section of the pier induced circumferential cracks in the consolidated layer of the ridge (see Figure 67). This failure created a number of semi-circular shaped ice pieces that were pushed up the face of the cone as the ridge advanced towards the pier. The ice pieces were often split into smaller pieces while riding-up on the conical section of the pier. This was a very prevalent failure pattern. In general it appeared that the size of the cusp was related to the strength of the ice. With weaker ice, the cracks occurred closer to the pier.

Ploughing Failure - In a few cases, a "ploughing" type of failure pattern was observed. In this case, relatively small pieces of ice were broken in the region close to the pier. This mostly occurred with weaker ice.

Model test programs provide excellent insight into the interaction of pressure ridges with offshore or coastal structures. With suitable instrumentation, it is possible to measure global loads as well as component loads on the structure. These results can be used with the appropriate scaling laws to predict full-scale ice loads from ridges. Model tests have an additional advantage in the fact that the interaction and failure processes can be readily observed in the tests. This makes them invaluable for a thorough study of ridge loads on structures.

5.2 Analytical Models

Most analytical models of ridge failure divide the ridge into separate components (consolidated layer, sail and keel), and loads are determined for each section of the ridge. This approach has definite advantages in terms of simplicity, but assumptions must be made on the failure process, and the temporal and spatial distributions of failure in each section. A number of different theories have been used for predicting ridge loads, and they are discussed in the following sections.

5.2.1 Consolidated Layer

The failure process for the ridge is important in defining the type of approach that should be used for calculating the failure loads. The type of approach used depends upon the shape of the structure. For vertical-sided structures, most approaches assume that the consolidated layer will fail by crushing, and the Korzhavin Equation (Korzhavin, 1971) is used. For sloping structures, a number of different algorithms have been postulated.

1.1.1.1 Vertical-sided structures

The Korzhavin equation was originally developed to estimate the force on vertical-sided bridge piers. The Korzhavin approach, which assumes a crushing failure of the ice against the structure, is based on the concept of ice indentation. Although it was derived for very narrow structures (i.e. bridge piers), it is the only common approach for estimating the forces due to ice crushing. The Korzhavin equation is given as

$$F = p\ D\ h_i \qquad \textbf{5-1}$$

where F is the force, p is the ice pressure, D is the width of the structure and h_i is the ice thickness. The ice pressure is related to the uniaxial compressive strength (σ_c) by

$$p = I\ m\ k\ \sigma_c \qquad \textbf{5-2}$$

where I is an indentation factor, m is a shape factor and k is a contact factor. This equation has been adopted for use in the American Petroleum Institute (API) Bulletin on ice loads (API 1982, 1994).

Although this approach appears to be quite straightforward, the choice of the coefficients presents difficulty. The contact factor can vary over a wide range, typically between 0.3 and 1, depending upon the amount of contact between the structure and the ice. Generally, it is low for cold, brittle ice and closer to 1 for warmer, ductile ice. The value for the shape factor is usually expressed as m = 1 for a flat structure and m = 0.9 for a round structure. The indentation factor I incorporates the effects due to both the aspect ratio (i.e. structure width to ice thickness ratio) and ice grain anisotropy. The factor takes into account the fact that the surrounding ice laterally confines ice in an ice sheet, and this can influence the failure stress. Plasticity theory has shown that the indentation factor is a very strong function of the grain structure (Ralston 1978). For columnar ice it is ~4.5 for low aspect ratios, and decreases to ~3 for high aspect ratios. For granular ice, it is ~3 for low aspect ratios and ~1.2 for high aspect ratios. To estimate the uni-axial strength of the ice, it is necessary to know the strain (loading) rate since it is well known that the compressive strength of the ice is a function of strain rate. Thus, to use this approach, the strain rate must be known. Usually the strain rate is defined as either v/2D or v/4D where v is the ice velocity (Ralston 1978). On the other hand, Kry (1981) has proposed a strain rate proportional to v/h, where h is the ice thickness. Thus, the load calculated using the Korzhavin equation could vary over a wide range depending upon the choice of empirical coefficients. Clearly, the use of this equation involves many assumptions, and consequently the predicted load can vary significantly.

In fact, it has been shown that its use can lead to extremely conservative ice loads, especially when applied to wide arctic structures. For example, Croasdale (1988) applied the indentation equation to an extreme event, as measured on the Molikpaq platform. Using plausible inputs, the indentation equation gave a load of 3,564 MN compared to the measured load of about 500 MN.

So, although the indentation equation method is quoted in the all the codes for ice loads (CSA, 1992, API, 1995), its use by practitioners is becoming less and less popular. The preferred approach for ice crushing loads is to use empirical methods derived from full-scale measurements on actual structures.

These are usually expressed in terms of nominal ice crushing pressure (p) as a function of either contact area (A), width (D), ice thickness (h), aspect ratio (D/h) or a combination of these. For example, Wright and others (in Croasdale & Associates, 1996a) used the expression:

$$p = 1.5\, h^{-0.17} \qquad \textbf{5-3}$$

as an upper bound fit to the Molikpaq global ice pressures for non-simultaneous crushing. In the equation, h is in metres and p is in MPa. For thick ice as might occur in a consolidated layer (3.5m), this equation gives a crushing pressure of about 1.2 MPa and is independent of width.

Another approach is to use pressure area as discussed by Sanderson (1986). He plotted a large amount of experimental data and suggested an equation of the form:

$$p = C\, A^{-0.5} \qquad \textbf{5-4}$$

If this equation is calibrated using 1.5m thick ice and the Molikpaq measurements (assuming a 60m face width), then A = 13.3 and the equation becomes approximately:

$$p = 13.3\, A^{-0.5} \qquad \textbf{5-5}$$

where A is in square metres and p is in MPa. Applying this to a 3.5m thick consolidated layer acting on a 100m wide structure gives a crushing pressure of about 0.7 MPa.

A more conservative approach was suggested by Metge (in Croasdale & Associates, 1996a) in which he proposed using an exponent of -0.33 rather than -0.5. With this approach, the crushing pressure for the 3.5m thick refrozen layer becomes 0.9 MPa.

Blanchet and Kennedy (1996) suggested that width was the most important parameter and developed an upper bound plot to measured data. The curve gives about 0.9 MPa for a 100 m wide structure, and it is suggested the ice pressure is independent of thickness.

Another approach is to use an aspect ratio relationship (Aspect ratio is structure width (D) divided by thickness). A typical aspect ratio equation might be:

$$p = 0.9\left[1 + 80\,(h/D)\right]^{0.3} \qquad \textbf{5-6}$$

This gives a crushing pressure of about 1.25 MPa for a 3.5m thick refrozen layer acting on 100m width.

As illustrated in this section, different investigators have used various relationships to fit the same data and this can give divergent results when extrapolated to different load cases. This is the main disadvantage of the empirical approach. However, at present, the empirical approach is considered to be the best approach.

The values discussed above are derived from level sea ice data. There are additional considerations when considering crushing loads due to a ridge consolidated layer. These are:

1. The effects of the variable thickness of the layer
2. Whether there should be a discounting of the crushing pressure relative to level sea ice
3. Whether there is a change in the failure mode from crushing to out of plane failures.

Issue 1) has been discussed in Chapter 3. A reasonable approach is to average the thickness across the width of the structure. Judgement has to be used with regard to local thickenings which may only extend over a few square metres or less and which could be due to an upturned ice block protruding below the layer. These would normally be excluded from the averaging calculation unless the structure is very narrow.

An extremely important issue is whether the method used to measure the thickness of the layer gives the true mechanical layer or includes some of the compacted slush that can be present under the layer. The compacted slush should not be included, but allocated to the keel thickness. This point is also discussed in Chapter 3.

Issue 2) has also been discussed in Chapter 3. In summary, there is insufficient evidence to discount the consolidated layer crushing pressure relative to the database composed from level sea ice pressures.

Issue 3) has been discussed in Chapter 4 in the context of the Molikpaq experience. All first year ridge interactions with the Molikpaq in the Beaufort Sea resulted in the consolidated layer failing out of plane or in a mixed mode failure of crushing and bending. In other words, pure crushing was not observed in first year ridges, yet it was seen with level sea ice and multi-year floes. There are several possible reasons for this behaviour. One is that, as first year ridges fail against a structure, the disturbance of the keel by the structure creates local imbalance in the buoyancy forces. These in turn, create additional out of plane forces on the consolidated layer, and cause bending failures. A second potential reason is that thickness variations in the layer lead to eccentric forces within it, which are sufficient to cause out of plane failures. A third possible reason is that the sloping walls of the Molikpaq at the lower levels cause the keel to fail upward and create out of plane forces on the consolidated layer.

Whether, the Molikpaq experience can be transferred to other structures is unknown and requires judgement. If the out of plane failures are caused by the first two of the above processes, then one could transfer the experience - at least to wide structures. Narrow structures might not see the same magnitude of out of plane forces. If the third reason is driving the Molikpaq experience, then it would be inappropriate to assume no crushing on vertical structures which did not have the same lower wall slopes as the Molikpaq.

Until more definitive and unambiguous experience is available, or appropriate work is carried out, it will be prudent to assume that crushing of the consolidated layer of a ridge can occur against a vertical structure.

1.1.1.2 Inclined (sloping) Structures

There have been a number of different approaches used to predict the loads that a level ice sheet will exert on a sloping structure, such as an inclined plane or a cone. These theories have been used to predict the loads due to the consolidated layer on a sloping structure. During a ridge interaction, it is usually assumed that the consolidated layer fails in a manner similar to a level ice sheet (i.e. the influence of the sail and keel on the behaviour are ignored). The different approaches used include:

- Edwards and Croasdale (1976) developed an empirical equation based on small-scale model tests.
- Croasdale (1980) developed an analytical two-dimensional model suitable for wide structures based on the failure of a semi-infinite beam on an elastic foundation.
- Croasdale (1980) also suggested a three-dimensional modification suitable for more slender structures.
- Ralston (1977) developed a formula for load prediction based on a plastic limit analysis for an sheet ice interacting with a cone.
- Kato (1986) developed a set of empirical equations based on his model tests.
- Hirayama and Obara (1986) also developed empirical equations that were based on a series of model tests.
- Nevel (1992) proposed a theory that includes either simultaneous or sequential breaking of wedges, and includes ride-up forces. Both forces and moments can be calculated for a range of conditions.

Each of these seven models include force components due to breaking of the ice sheet and due to ride-up and clearing of ice pieces onto the cone. Each of these models is briefly discussed.

Edwards and Croasdale (1976) developed an empirical formula to predict the horizontal force on a cone based on a number of laboratory experiments on a cone with a 45o slope and friction factor of 0.05. Their equation can be written

$$F_h = 1.6 \ \sigma_f \ h^2 + 6.0 \ \rho_w \ g \ D \ h^2 \qquad \textbf{5-7}$$

where F_h is the maximum horizontal force on the cone, σ_f and h are the flexural strength and thickness of the ice, ρ_w is the density of water, g is gravitational acceleration, and D is the waterline diameter of the cone. The first term in the equation is the force due to ice breaking and the second term is the force due to ice ride-up on the cone.

Croasdale (1980) proposed a theoretical two-dimensional model of the loading on a plane slope due to level ice. The model is based on analysis of a semi-infinite elastic beam on an elastic foundation with geometrical consideration of the force required to push broken ice blocks up an inclined slope. The predictive equation for the horizontal load can be written

$$F_h = C_1 \ D \ \sigma_f \left(\frac{\rho_w \ g \ h^5}{E} \right)^{1/4} + C_2 \ z_f \ h \ D \ \rho_i \ g \qquad \textbf{5-8}$$

where C_1 and C_2 are coefficients that depend on the slope inclination and the coefficient of dynamic friction between the structure and ice (μ_s), E is the strain (Young's) modulus of ice, and z_f is the cone freeboard. In this equation, the first term represents the force due to flexural failure of the advancing ice sheet and the second term represents the force due to the ride-up of broken ice pieces. The coefficients C_1 and C_2 are given by

$$C_1 = 0.68 \frac{\xi_1}{\xi_2} \qquad \textbf{5-9}$$

$$C_2 = \xi_1 \left(\frac{\xi_1}{\xi_2} + \cot\alpha \right) \qquad \textbf{5-10}$$

with

$$\xi_1 = \sin\alpha + \mu_s \cos\alpha \qquad \textbf{5-11}$$

$$\xi_2 = \cos\alpha - \mu_s \sin\alpha \qquad \textbf{5-12}$$

Croasdale suggests that this method is most appropriate for relatively wide structures, since two-dimensional theory is used.

Croasdale (1980) also suggested a modification to his two-dimensional theory to treat the case of a more slender conical structure. This modification involves the characteristic length ι defined by

$$\iota = \left(\frac{E\ h^3}{12\ \rho_w\ g\ \left(1 - \nu^2\right)} \right)^{1/4} \qquad \textbf{5-13}$$

where E = 3 GPa is the Strain (Young's) Modulus and ν = 0.3 is Poisson's ratio for the ice in the consolidated layer. The modified equation for the horizontal load on a cone can be written

$$F_h = C_1\ D\ \sigma_f \left(\frac{\rho_w\ g\ h^5}{E} \right)^{1/4} \left(1 + \frac{\pi^2 \iota}{4D} \right) + C_2\ z_f\ h\ D\ \rho_i\ g \qquad \textbf{5-14}$$

Ralston (1977) presented expressions for the horizontal and vertical loads on a conical structure based on plastic limit analysis for the flexural failure of a level ice sheet. Ralston's equation for the maximum horizontal force is

$$F_h = A_4 \left[A_1 \sigma_f h^2 + A_2 \rho_w g h D^2 + A_3 \rho_w g h (D^2 - D_2^{\ 2}) \right] \qquad \textbf{5-15}$$

where D_2 is the diameter of the top of the cone and A_1, A_2, A_3 and A_4 are dimensionless coefficients that depend on the cone angle α, the ice-structure friction coefficient μ, and the factor $\rho_w g D^2/(\sigma_f h)$.

Kato (1986) published an empirical formula based on a number of physical model tests. Kato's equation for the maximum horizontal load on a cone can be written

$$F_h = A_h \left(D^2 - D_2^2\right) \rho_i\ g\ h + B_h\ \sigma_f\ h^2 \qquad \textbf{5-16}$$

where A_h and B_h are coefficients determined from his tests. Kato provided values of A_h and B_h for four different cone angles.

Hirayama and Obara (1986) developed a formula for the peak horizontal ice load on a cone based on dimensional analysis and a review of physical model tests from several different sources. Their equation can be written

$$F_h = 0.7 \; \rho_i \; g \; h \; D^2 \; \frac{\xi_1}{\xi_2} \; \frac{z_f}{D} \; \frac{\left(1 - \frac{z_f}{D} \tan\alpha\right)}{\sin\alpha} + 2.43 \; \sigma_f \; h^2 \left(\frac{D}{\iota}\right)^{0.34} \quad \textbf{5-17}$$

where ξ_1, ξ_2 and ι are as previously defined.

Nevel (1992) presented a theory based on the elastic bending of truncated wedges to predict the ice loads on a cone that includes forces due to ice breaking and ride-up. Predictions of maximum ice loads by Nevel's theory are obtained computationally using an iterative process, since the theory does not provide a closed form solution for the maximum loads. Load predictions according to Nevel's method depend on whether the flexural failures of the wedges are sequential or simultaneous, and whether the ice action on the cone is assumed to be active or passive. The method differs from the others in that in-plane forces in the wedge as well as an applied moment to the edge of the wedge are included. Nevel's theory predicts a range of peak loads depending on the type of interaction that is assumed.

Chao (1992) compared several of the previously described algorithms with available experimental data. He concluded that at the larger scales, the Croasdale algorithm with the 3D correction gave one of the best fits to the data. In the design of the Confederation Bridge a similar comparison was made and the Croasdale algorithm was chosen for loading calculations. However, based on observations at the Kemi 1 lightpier in the Baltic, there was concern that in full scale, the ice rubble on the cone was more persistent and achieved greater volumes than in model tests (Maattanen and Hoikkanen, 1990. Therefore, it was decided to add additional features to the Croasdale, 1980 algorithm to account for this. In fact, the model was modified not only to include the effects of the rubble pile on the cone slope, but also to account for in-plane stress, and for the additional forces required to turn ice blocks as they met the vertical shaft above the cone slope.

The revised comprehensive model is described in Croasdale and Cammaert, (1993) and in Croasdale and others, 1994. In this model, the total horizontal force (F_h) is is given by:

$$F_h = F_B + F_p + F_R + F_L + F_T \quad \textbf{5-18}$$

where F_B is the breaking force, given by

$$F_B = C_1 \; D \; \sigma_f \left(\frac{\rho_w \; g \; h^5}{E}\right)^{1/4} \left[D + (\pi^2/4)\,\iota\right]/D \quad \textbf{5-19}$$

and F_p is the force to push the ice sheet through the rubble, given by

$$F_p = D\, h_r^2\ \mu_i\ g\ (1-\gamma)\,(1-\tan\theta/\tan\alpha)^2\ (1/2\tan\theta) \qquad \textbf{5-20}$$

where h_r is the height of the ice rubble, μ_i is the ice-ice friction, and θ is the angle the rubble surface makes with the horizontal.

F_R is the force to push the ice blocks up the slope through the ice rubble, given by

$$F_R = D\ P\ (1/[\cos\alpha - \mu_i \sin\alpha]) \qquad \textbf{5-21}$$

where

$$\begin{aligned} P = {} & 0.5\mu_i(\mu_i+\mu_s)\ \rho_i g\ (1-\gamma)\ h_r^2\ \sin\alpha\ (1/\tan\theta - 1/\tan\alpha)(1-\tan\theta/\tan\alpha) \\ & + 0.5\,(\mu_i+\mu_s)\ \rho_i g\ (1-\gamma)\ h_r^2\ \cos\alpha\ (1/\tan\alpha)\ (1-\tan\theta/\tan\alpha) \qquad \textbf{5-22} \\ & + h_r\ h\ \rho_i g\ ([\sin\alpha + \mu_s\cos\alpha]/\sin\alpha) \end{aligned}$$

F_t is the force to turn the ice blocks at the top of the slope, given by

$$\begin{aligned} F_t = {} & 0.5\ D\ h_r^2\ \rho_i g\ (1-\gamma)\ \varepsilon\ ([1/\tan\theta]-[1/\tan\alpha])\ (1-[\tan\theta/\tan\alpha]) \\ & + 0.5\ D\ h_r^2\ \rho_i\ g\ (1-\gamma)\ \varepsilon\ \tan\phi\ (1-[\tan\theta/\tan\alpha])^2 \qquad \textbf{5-23} \\ & + \varepsilon\ c\ D\ h_r\ (1-[\tan\theta/\tan\alpha]) \end{aligned}$$

where c is the cohesion strength of the ice rubble, ϕ is the friction angle of the rubble and $\varepsilon = (\xi_1/\xi_s)$.

One of the few sources of measured data was used by Maattanen (1996) to compare algorithms which can account for additional rubble build up on the cone slope. This comparison is shown in Figure 68. Note that neither the Ralston nor Nevel method have been modified to include a rubble pile, but it is simulated by choosing thicker ice in the ride up and clearing terms.

Since 1996, data is being collected at the Confederation Bridge, which has conical piers at the ice line. The observations support the Baltic experience with rubble build up on the face of the cone (and this process was included in the design load estimates). General observations of failure modes including ice rubble patterns is given in Brown et al. (1999). The data being gathered at the bridge is part of an industry sponsored project and is currently proprietary. Some data is available for university R&D and is being analyzed to compare observations and measurements to current theories (Mayne and Brown, 2000a; 2000b). It is expected that the extensive data from the bridge will lead to further improvements in ice load algorithms for ridges. Figure 69 shows example video stills of ice action on the pier conical face.

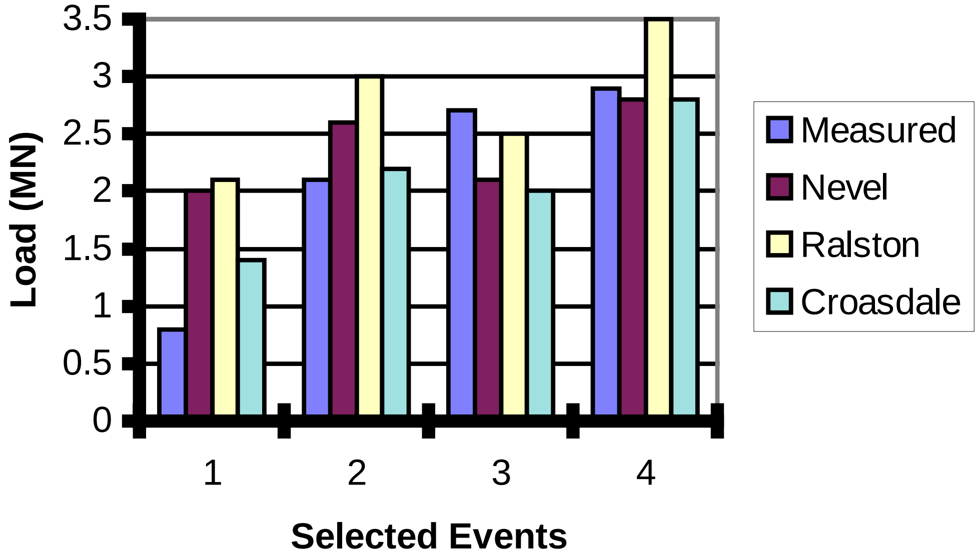

Figure 68 Comparison of Various Methods with Measured Data from the Kemi 1 Lightpier (Maattanen, 1996)

The observations and discussion of failure modes for ridges outlined in Chapter 4 clearly indicated that the overall ridge failure could take many forms. For a vertical-sided structure such as the Molikpaq, the assumption of ice crushing, and thereby using the Korzhavin Equation, appears to be conservative. The observations indicate that, although there can be local ice crushing, the global failure of first-year ridges does not take place with large-scale overall crushing. Similarly, the failure process of the consolidated layer on conical-shaped structures is largely unknown. New approaches are required to calculate the failure of the consolidated layer, based on full-scale observations. For added confidence, much more observation data is required to be able to provide a quantitative description of the frequency of each failure mode, and the factor that dictate the failure mode.

5.2.2 Sail and Keel Loads

A number of different analytical models have been developed to try to predict the loads due to the failure of the sail or keel. In general, these theories can be characterized as either **local failure** or **global failure**.

5.2.2.1 Overview of Analytical Models

Theories for **local** ridge keel or rubble failure modes have been largely based on ideas borrowed from soil mechanics. They treat the failure of the ridge as a number of small local failures. Theories for local failure have been proposed by Dolgopolov et al. (1975), Prodanovic (1979), Mellor (1980), Croasdale (1980), Hoikkanen (1984), Krankkala and Määttänen (1984), Croasdale and Cammaert (1993), Croasdale et al. (1994) and Weaver (1994). Most of these theories provide an estimate of the load due to a ridge keel, but a few produce estimates of the load for both the sail and keel. Each will be briefly discussed in turn.

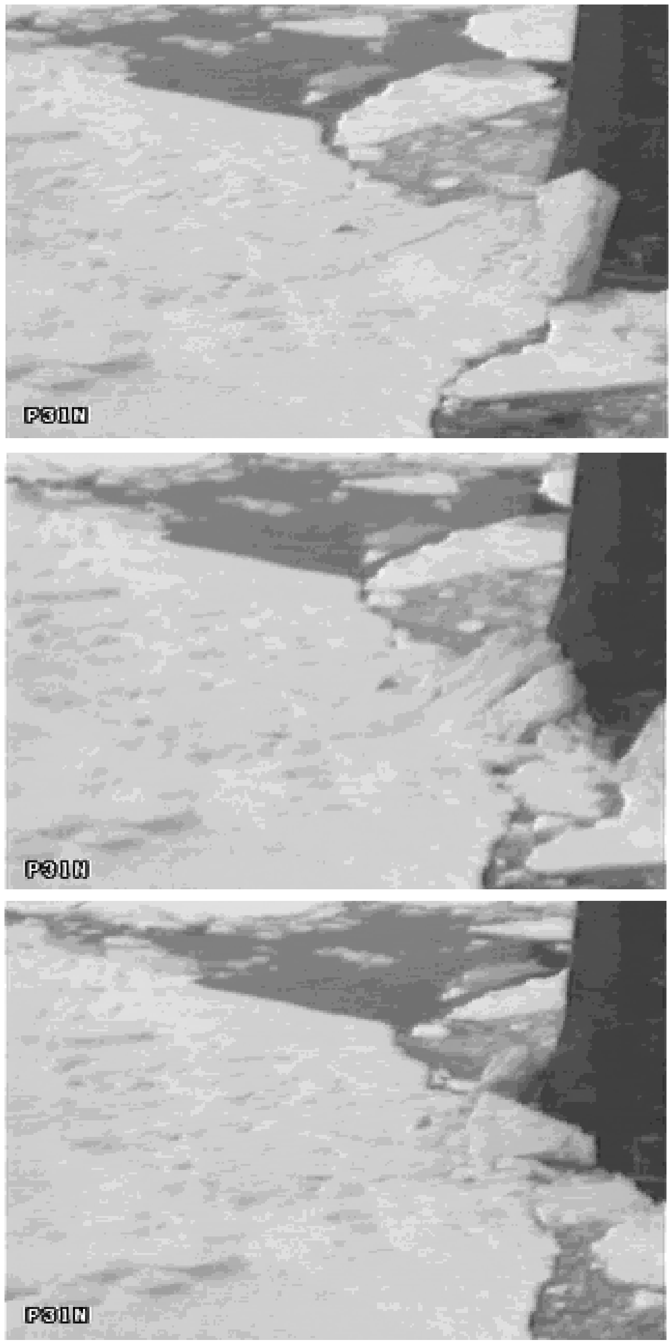

Figure 69 Ice failing on Confederation Bridge pier.

Dolgopolov et al. (1975) developed a theory based on some observations from experiments and parallels with granular material. Their equation for the horizontal force is:

$$F_h = h_k D_e q\left(\frac{h_k \gamma_e \eta^2}{2} + 2\eta c\right) \qquad \textbf{5-24}$$

where h_k is the keel depth, D_e is the effective structure width, γ_e is the effective buoyant density, c is the apparent cohesion, and η is the passive pressure coefficient, which is given by

$$\eta = \sqrt{\frac{1 + \sin\phi}{1 - \sin\phi}} \approx \tan\left(45° + \frac{\phi}{2}\right) \quad . \qquad \textbf{5-25}$$

Equation 3 does not assume any slip planes, but it is based on a Mohr-Coloumb material behaviour producing a trapezoidal pressure distribution on the face of the structure. The factor q is a shape factor that depends on the keel depth and the structure width:

$$q = 1 + \frac{2 h_k}{3 D_e} \quad . \qquad \textbf{5-26}$$

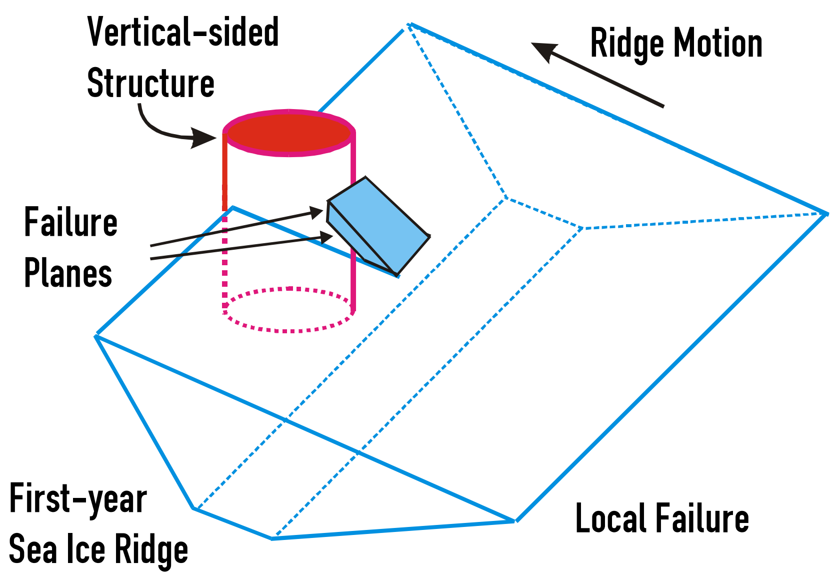

Figure 70 Illustration of local failure in a first-year ridge.

In the original paper, γ_e is described as the ice buoyancy, but it is generally considered to include the effect of the void ratio n, and has been termed the effective buoyancy:

$$\gamma_e = (\rho_w - \rho_i) g (1 - n) \quad . \qquad \textbf{5-27}$$

Dolgopolov et al. also recommended that an increase in the keel depth of between 0 and D/2, caused by the interaction, should be considered. Määttänen (1993) has recommended that the value of q should be taken as unity, based on his experience in the Baltic Sea.

Prodanovic (1979) developed an "upper bound" estimate of the maximum load due to a field of ice rubble based on a linear Mohr-Coulomb material and plastic limit analysis. His equation can be written

$$F_h = \sigma_p D_e h_k \left[1 + a \frac{h_k}{D_e} \left(1 + b \frac{h_k}{D_e} \right) \right] \qquad \textbf{5-28}$$

where σ_p denotes the plane strain compressive strength of the unconsolidated rubble, given by

$$\sigma_p = 2c \tan\left(45° + \frac{\phi}{2} \right) \qquad \textbf{5-29}$$

and *a* and *b* are coefficients that are based on minimizing energy that depend on the effective internal friction, and are given approximately by

$$a = 0.89\left[1 + 1.82 \tan(\phi - 17°) \right]$$
$$b = 0.31[1 + 2.01 \tan(\phi - 8°)] \quad . \qquad \textbf{5-30}$$

This method is recommended by the American Petroleum Institute (API, 1994).

Mellor (1980) proposed that the rubble in the keel and sail slip along planes that make a constant angle with the horizontal. The horizontal force due the sail $F_{h,s}$ is given by

$$F_{h,s} = 0.5 D_e \eta^2 (1 - n) \rho_i g h_s^2 + 2 D_e c \eta h_s \quad . \qquad \textbf{5-31}$$

The horizontal force due to the keel $F_{h,k}$ is given by

$$F_{h,k} = 0.5 D_e \eta^2 (1 - n)(\rho_w - \rho_i) g h_k^2 + 2 D_e c \eta h_k \qquad \textbf{5-32}$$

The total horizontal force due the rubble ice in the sail and keel regions is given by the simple sum of these two components: $F_h = F_{h,k} + F_{h,s}$. This method is also recommended by the American Petroleum Institute (API, 1994).

Hoikkanen (1984) and *Krankkala and Määttänen* (1984) presented equations developed for predicting the maximum horizontal load on a structure due to the sail and keel portions of a ridge based on an assumption of a linear variation of pressure with depth. The pressure due to the sail is assumed to vary linearly between p_1 at the top and p_2 at the bottom of the sail, while the pressure due to the keel varies linearly between p_3 and p_4 at the top and bottom of the keel. The pressures are given by:

$$
\begin{aligned}
p_1 &= 2c_s\sqrt{\eta_s} \\
p_2 &= 2c_s\sqrt{\eta_s} + \eta_s \rho_i g h_s(1-n) \\
p_3 &= 2c_k\sqrt{\eta_k} + \eta_k \rho_i g h_s(1-n) \\
p_4 &= 2c_k\sqrt{\eta_k} + \eta_k\left(\rho_i g h_s(1-n) - \min\left\{\begin{matrix}[\rho_w - \rho_i(1-n)]g h_k \\ \rho_i g(1-n)h_s\end{matrix}\right\}\right)
\end{aligned}
\qquad \mathbf{5\text{-}33}
$$

where c_s and η_s are the apparent cohesion and passive pressure coefficient for the ridge sail, and c_k and η_k are the apparent cohesion and passive pressure coefficient for the ridge keel. These pressures are quite sensitive to the sail height assumed for the design ridge. The forces due to the sail and keel can be written as:

$$F_{h,s} = \left(1 + \frac{\tan\phi}{\tan\beta}\right)\left[0.5(p_1 + p_2)D h_s - \left(\frac{2p_1}{3} + \frac{p_2}{3}\right)h_s^2 \cot\alpha_s\right] \qquad \mathbf{5\text{-}34}$$

and

$$F_{h,k} = \left(1 + \frac{\tan\phi}{\tan\beta}\right)\left[0.5(p_3 + p_4)D h_k + \left(\frac{p_3}{3} + \frac{2p_4}{3}\right)h_k^2 \cot\alpha_k\right] \qquad \mathbf{5\text{-}35}$$

where $\beta \cong 45°$ is half of the leading angle of the "pseudo bow" formed in front of the structure, α_s and α_k represent the slope angles of the structure interacting with the sail and the keel. (For the present comparison to the Molikpaq structure, $\alpha_s = \alpha_k = 83°$). According to this method, the keel load is strongly influenced by the sail height through the pressures p_3 and p_4 in a manner that does not seem realistic. The total force due to the ice rubble in a first-year ridge is given by the sum of these two components: $F_h = F_{h,k} + F_{h,s}$.

Croasdale (1994) developed a wedge failure theory in which the keel was assumed to fail locally in a wedge limited by a 45° plane down through the rubble from the intersection of the keel and the consolidated layer, and two vertical side planes. Figure 70 illustrates the failure planes. The maximum force is determined as:

$$F_h = c_e(2h_k D_e + h_k^2) \qquad \mathbf{5\text{-}36}$$

where c_e is the effective shear strength of the rubble in the form of a cohesive strength. This can be obtained from the keel properties as:

$$c_e = \frac{h_k}{2}\gamma_e \tan\phi + c \quad . \qquad \mathbf{5\text{-}37}$$

Weaver (1994) modified an equation originally developed by Broms (1964) which is based on frictional resistance theories for the lateral resistance of piles in granular media. For cohesive materials, Weaver recommends an approach based on the Prandtl equation with a load reduction factor based on the work of Vesic (1973). The resulting equation for the maximum frictional resistance can be written as:

$$F_h = 1.5\, D_e \gamma_e h_k^2 \eta^2 \,. \qquad \textbf{5-38}$$

The equation for cohesive resistance is

$$F_h = 5.14(0.32 + 0.12\frac{D_e}{h_k})\, c\, D_e h_k \qquad \textbf{5-39}$$

where c is the apparent cohesion of the ice rubble.

There are a few theories that have been developed that treat the failure of the ridge in a **global** sense. These include those by Croasdale (1980), Prodanovic (1981) and Croasdale and Cammaert (1993).

Croasdale (1980) proposed an equation for the maximum horizontal load on a vertical cylinder due to the "plug" shear failure of a triangular wedge of ice-rubble. The ridge keel is assumed to fail as a plug bounded by two vertical failure planes which initiate at the sides of the structure, and a horizontal failure plane which is at, or adjacent to, the underside of the consolidated layer (see Figure 71). Croasdale's equation can be written as:

$$F_h = \frac{2}{3} W_R h_k^2 \left(\rho_w - \rho_i\right) g \tan\phi \qquad \textbf{5-40}$$

where W_R is the width of the ridge and h_k is the maximum height of the triangular keel. According to this equation, the force does not depend on the diameter of the structure or the apparent cohesion of the ice rubble.

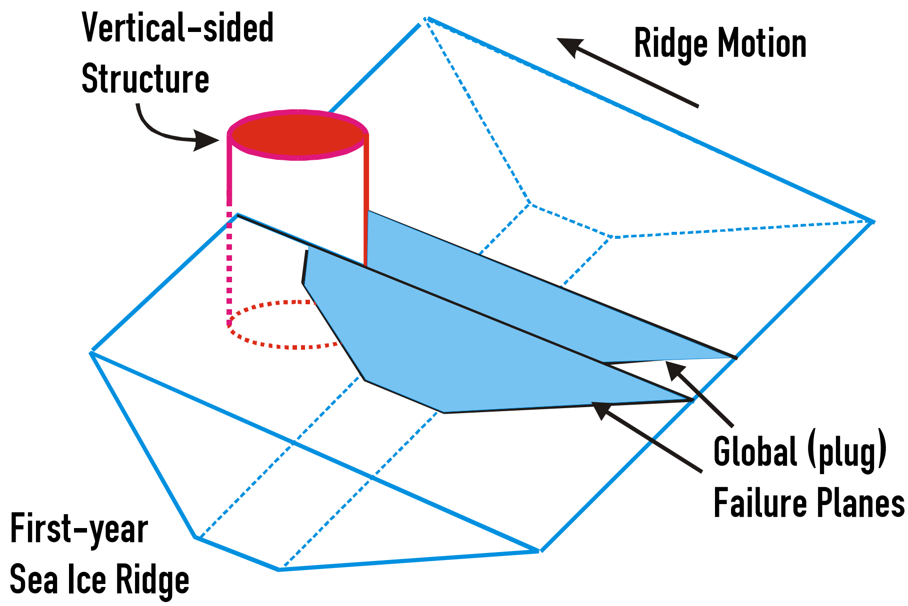

Figure 71 Illustration of global failure of a first-year ridge.

Prodanovic (1981) proposed a simple equation for the force required to initiate a global shear failure of ice rubble based on a plasticity upper bound analysis. His equation is

$$F_h = 2c\,A_k \qquad \textbf{5-41}$$

where A_k is the cross-sectional area of the rubble in the ridge keel. This formula suggests that the force is independent of the internal friction angle of the ice rubble and the size of the structure.

Croasdale and Cammaert (1993) modified Croasdale's early approach to take into account the orientation of the ridge. This was done since the global plug failure theory of Croasdale (1980) assumed that the vertical failure planes were oriented parallel to the direction of motion of the ridge. There was no provision for oblique ridge impacts. Croasdale and Cammaert (1993) determined the force due to plug failure as:

$$F_h = \left(\frac{W_r D_e h_k}{2} + \frac{W_r h_k^2}{3}\right)\gamma_e \tan\phi \qquad \textbf{5-42}$$

where the symbols are as previously defined.

5.2.2.2 Application of Models for Load Predictions

Timco et al. (1999) compared the predictions of each of these models to a number of full-scale load measurements for first-year ridges on the Molikpaq. To do this, a number of assumptions were required about the physical properties of the ice and ridge, and the ice-structure contact. The results of this analysis are presented below.

The consolidated layer of a ridge produces the highest loads on a structure during the interaction process. The use of the Korzhavin equation for load prediction was found to be quite poor, since a large number of assumptions is required. It was possible to use the equation to get almost any load value, depending upon the choice of the coefficients. It was found that the Korzhavin equation, which was developed for loads on bridge piers, was not suitable for predicting loads on wide offshore structures.

Solution methods used to determine failure forces of ridge keels are also a source of uncertainty. Most methods used in practice are based on assuming a failure surface, then multiplying its area by some average stress. That would give an upper-limit (plastic) solution. Such methods are popular because of their simplicity, but they involve several assumptions. Choosing a failure mechanism of ridge keels has been completely arbitrary. The main problem, however, is choosing a stress to apply over the assumed failure surfaces. Failure usually occurs progressively with stress distributions far from the simple average values that are assumed to act over the "hypothetical failure planes". At times, empirical formulas developed for particular soil mechanics applications have been used. Those formulas do not take into account the differences between ice rubble properties and soil properties. Also such formulas are usually based on specific assumptions (e.g. boundary conditions and stress levels) that do not apply in the ridge failure case. The keel loads predicted using the various models show substantial differences (Timco et al, 1999). Generally the global load models predict lower loads than the local load models.

The *local failure models* of keels are generally taken from soil mechanics practice. The Dolgopolov model was extensively used in the early stages of the analysis of keel loads on the Confederation (PEI) Bridge in Canada. It includes structure width, keel depth, keel buoyancy with porosity, keel properties of friction and cohesion, and it introduces the passive pressure coefficient from soil mechanics. It does not consider keel width. The Mellor and Hoikkanen models include both the sail and keel, and take the same input properties as the Dolgopolov model. It is interesting to note that the Dolgopolov and Mellor keel models produce identical results, but the Hoikkanen keel model yields loads almost twice those of Mellor. The Hoikkanen model takes into account a “pseudo bow” of ice rubble and the actual slope angle of the face of the structure. The Hoikkanen model is the most complex, taking into account the most factors, and gives the highest loads of any of the models. Croasdale (1994) assumed local wedge failure at 45° (see Figure 2) and an “effective” shear strength to calculate keel loads. The model takes into account all factors except keel width and structure slope. Weaver (1994) developed two models, one based on friction and the other on cohesion. His friction model, while having some similarity to Croasdale (1994), yields substantially higher forces. On the other hand, his cohesion model produces keel forces which are relatively insensitive to keel depth for wide structures. It should be pointed out that none of the keel load models were developed for wide structures such as the Molikpaq, so their application for such cases should be done with caution. The Prodanovic (1979) model is an upper bound solution including keel depth and structure width, as well as keel properties, and it yields the lowest keel forces. Note that none of the calculation models take into account the 3-dimensional shape of the structure or velocity effects. They are all essentially static models.

With respect to the *global load models*, the Prodanovich (1979) model can be rejected as being inappropriate for wide structures since it does not take into account structure width. Also it predicts unrealistically low forces. The Croasdale (1980) model is also independent of structure width, but it takes into account the buoyant force of the submerged keel and width of the keel; However, it also predicts very low forces. The Croasdale model was modified to include structure width in Croasdale and Cammaert (1993). Keel porosity was also taken into account, reducing the buoyant force of the keel. The model was further modified by Brown and Croasdale (1996) to include cohesion and the option to orient the vertical failure planes of the plug at angle ω.

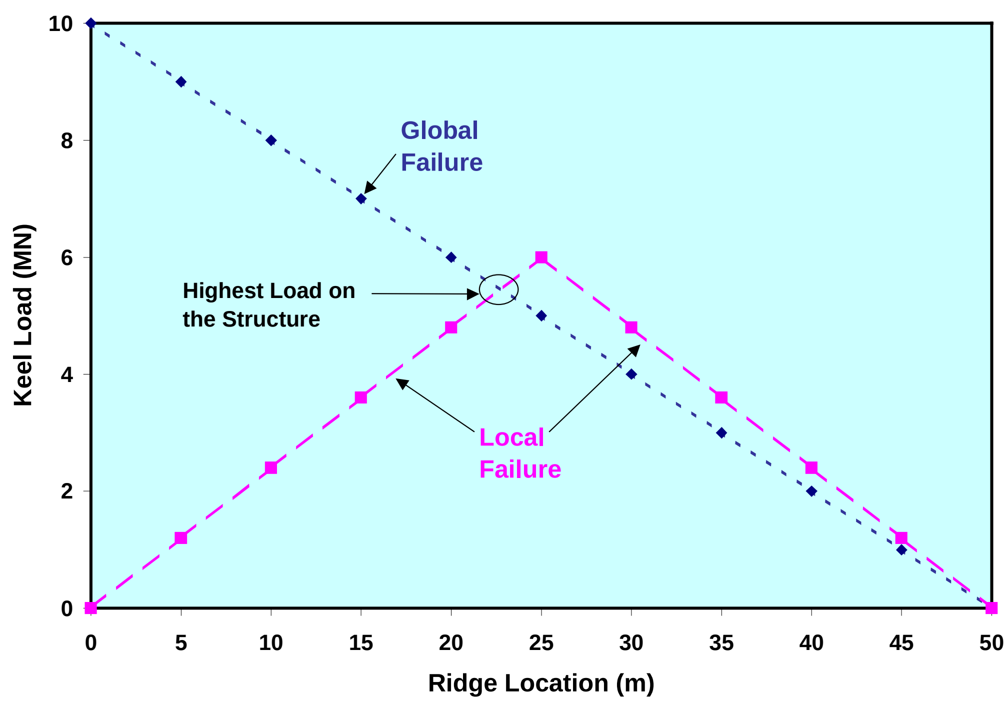

Figure 72 Variation of global and local failure loads during ridge interaction for a hypothetical case.

A number of these models have been used over the years to predict the loads due to first-year ridge loading on a structure. In their application, it is usually assumed that local failure governs the rubble load during the early stages of an interaction as the pier begins to penetrate into the ridge, but that global failure dominates at later stages. This behaviour can be incorporated into the determination of a design load by considering the variation in loading through the width of the ridge for various local and a global failure modes. Figure 72 illustrates this principle with two simple load plots for a hypothetical ridge interaction. The load predicted by the global failure model is initially 10 MN at the beginning of the interaction (ridge location = 0 m) and decreases linearly with distance to zero as the ridge travels past the pier. The load curve predicted by the local failure model takes on a triangular shape, reaching a maximum of 6 MN at the centre of the ridge, reflecting the variation in the depth of keel encountered by the structure as it passes through the ridge. The load on the pier at each stage of the interaction would be the minimum load predicted by these two models, and the overall highest load for the interaction would be the maximum of these minima, which is 5.5 MN for the hypothetical case shown in Figure 72. Thus, although the global and local failure models independently predict maximum loads of the 10 MN and 6 MN, this analysis indicates that the highest load for the structure, considering the load variation across the ridge, is only 5.5 MN. This value is less than the minimum of the two maxima for each of the failure models when considered independently. The reduction in overall load from this form of analysis obviously depends on the nature of the two load plots.

These simple analytical theories provide a means of estimating the loads on a structure. They have been used in Monte Carlo simulations for defining probabilistic loading on a structure. However, the assumptions involved in their use limit their application and confidence in the results.

5.2.2.3 Comprehensive Keel Load Models

All the models described so far relate either to local passive failure of the ridge keel or global plug failure as depicted in Figure 73. Depending on ridge width and depth, the actual ridge failure load can never be higher than the local passive failure load, but can be less. This is because a plug failure can occur at some value of penetration of the keel by the structure prior to the full keel depth being reached.

Combined Dolgopolov/Croasdale Method

An improved approach has been described by Brown, Croasdale and Wright (1996) and Croasdale (1997). The analysis proceeds by stepping through the ridge in convenient increments, and determining the two loads at each location. For the analysis, the actual keel depth at each location (with appropriate surcharge) is used for the Dolgopolov model, while the unpenetrated cross sectional area is determined for use with the plug model. The minimum of the two loads is then selected as the ridge keel failure load for the structure at that position in the ridge. The peak load occurs when the Dolgopolov and the shear plug loads are equal. In most cases, the peak keel load obtained from this method is less conservative than either the Dolgopolov load based on maximum keel depth or the Croasdale plug load based on full cross sectional area. It is illustrated in Figure 74, which is the output from a spreadsheet that combines the two failures.

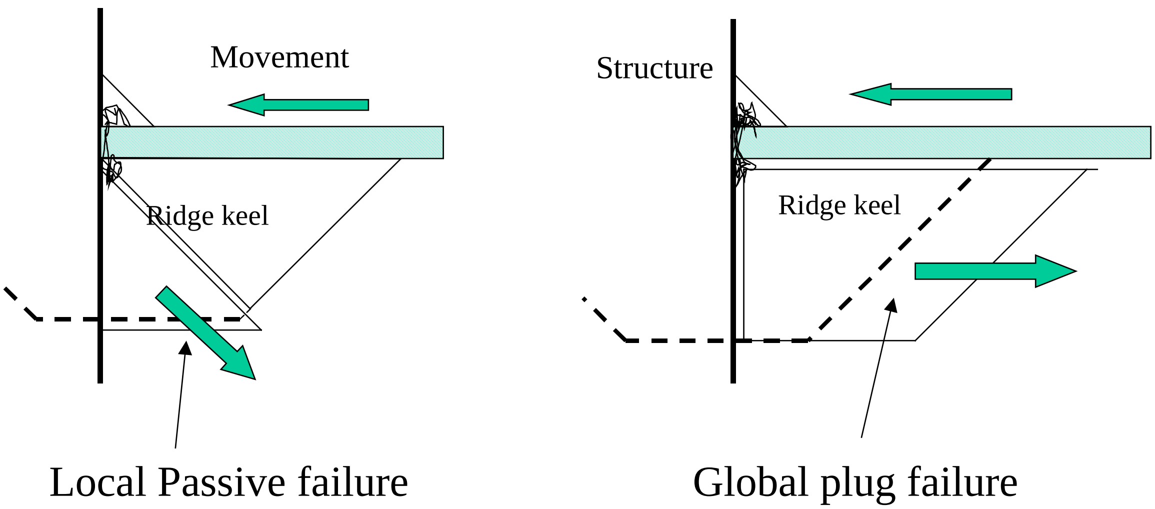

Figure 73 Ridge Keel Failure Modes

The General Passive Failure Model (GPF)

A generalized passive failure method was developed by Weaver in Croasdale & Associates (1996b). A schematic of the GPF model is shown in Figure 75. It is based on classical soil mechanics theory for a compressible but linear Mohr-Coulomb material. At any given structure penetration into the ridge, the model resolves all of the forces acting on the failure wedge and determines the resultant horizontal force for a given β (the vertical inclination of the primary failure plane). At every penetration level, the model searches for the critical β which corresponds to the minimum horizontal force. This value defines the true failure load at that level of penetration.

The model assumes that the vertical walls of the failure wedge diverge at an angle ω to the direction of ice movement. The lateral earth pressure coefficient, K acting normal to the vertical side shear planes is defined by the user. An upper bound solution to the ice load may be taken as the lower of the following two limit cases:

a) $\omega = 0$ and K=Kp
b) $\omega=\phi$ (K falls out of the equations when $\omega=\phi$)

The model also accounts for a non-vertical structure, wall friction, inertia and the buildup of a surcharge in front of the pier during penetration. These additional components are, at least in theory, very important in calculating loads due to extreme ice ridges. The surcharge factor, varies from 0 for no surcharge to 1 for a full surcharge, it is defined as the fraction of broken rubble that accumulates in front of the structure. A hydrodynamic added mass factor, is used to model inertia. In theory, this factor can vary between 0 and 2. The method used to account for inertia is approximate. The GPF calculations are performed in an Excel spreadsheet.

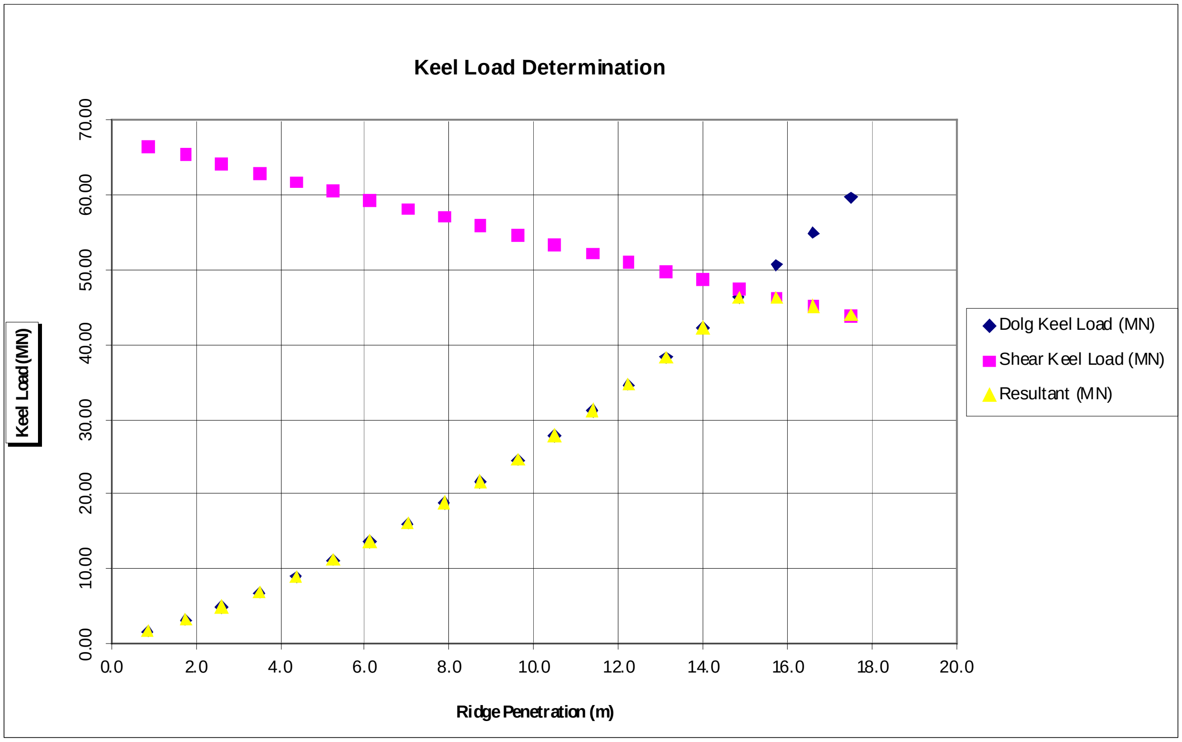

Figure 74 Results from Combined Dolgopolov/Croasdale Keel Load Models. Actual Keel Failure Load is at Cross-over Point

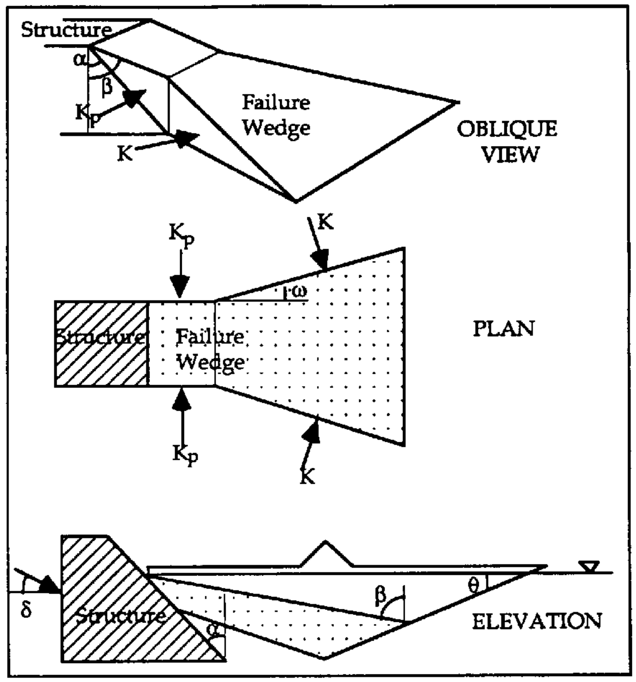

Figure 75 General Passive Failure Model for Ridge Keel Failure

5.2.2.4 Verification by Small Scale Tests

In order to better understand the failure modes of first year ridges against structures and to provide measured loads against which to test the load algorithms, a number of small scale tests were performed. These were conducted in the ice basin at the National Research Council in St John's, Newfoundland.

The tests were conducted using the model structure shown in Figure 76. Two shaft diameters (0.8m and 1.8m) could be tested by adding the cylindrical collar. With the narrow shaft, the shape of the structure was very similar to that of a PEI Bridge pier. The general aim of the tests was to obtain load data due to the action of ridge keels on vertical structures of cylindrical form in the presence of a boundary condition representative of the refrozen layer in a ridge. The cone was added to fail the refrozen layer in bending on a part of the structure which could be independently instrumented, so that keel loads on the cylinder could be separated from loads caused by the refrozen layer. Even though the tests were not to be interpreted as scale model tests, the ice properties were adjusted to represent the flexural strength of fairly weak sea ice at a reduced scale of 12.5 which leads to a full scale pier shaft diameter of 10m, as on the PEI bridge.

A total of 12 ice sheets were used during the test program that consisted of two test series. For each sheet, a single ridge was constructed across the width of the tank. The ridge widths ranged between 1.75 to 6m and their depths from 0.46 to 1.15 m. Twenty-nine separate keel structure interaction data sets were obtained.

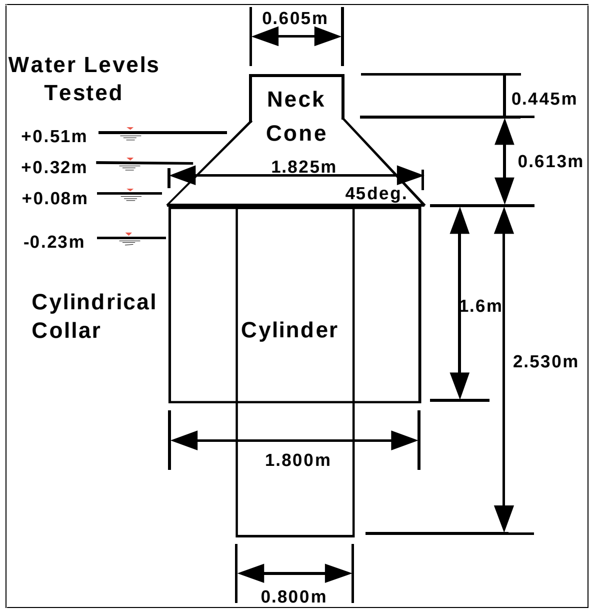

Figure 76 Test Structure used in Verification Model Tests for Ridge Keels

Each ridge was constructed from breaking up level ice about 50 mm thick. After rubble was dumped to form the ridge, the ambient air temperature was reduced in order to freeze a surrounding ice sheet and create a thin refrozen layer in the ridge. At the time of testing the surrounding ice thickness was about 60 mm thick and the refrozen layer about 40 mm. The intent was to keep the refrozen layer as thin as possible, just sufficient to form an appropriate boundary condition for the keel failure. Flexural strengths of the refrozen layer averaged about 75 kPa. The average flexural strength of the surrounding ice sheet at test time was also about 75 kPa. The average flexural strength of the submerged ice blocks at test time was about 20 kPa. Ridges keels were profiled using an upward looking sonar system that was also checked against manual readings from the working carriage.

To properly evaluate the validity of the keel load algorithms, it was of prime importance to have knowledge of the shear strength properties of the ridge keels. Ice rubble made from the same generic model ice had been separately tested to measure friction angle and cohesion (e.g. Sayed and others, 1992, Case, 1991). However, as will be discussed later, these tests are subject to a range of interpretations. For example, the tests appear to give results that are dependent on effective pressures and aging times. Therefore, for this project it was decided to try an in-situ test method that could be performed in the ridge just prior to the test.

The test chosen was based on the full-scale test approach described by Lapparanta & Hakala, (1992), and can be described as a punch shear. A vertical force is applied to a horizontal platen and pushed through the ridge to achieve large displacement of the keel material. After correcting for buoyancy effects, the maximum force measured is governed by the in-situ shear strength of the keel material. Based on preliminary tests, it was decided to conduct the punch tests with a 50 cm diameter platen at a speed of 0.07 m/s. A detailed description of the method is given in McKenna and others (1996).

For each ridge in the test program, three punch tests were conducted immediately after ridge construction (unconsolidated), and three immediately prior to the test, after formation of the refrozen layer (consolidated). For the consolidated tests, the refrozen layer was first cut into approximately 15 cm squares so that failure of the refrozen layer was not a contributor to the load measured. Interpretation of the punch tests is based on soil mechanics theory. Note that this method has been used subsequently as a large scale field test in Canada and in Russia (see Smirnov and others, 1999). In addition to ridge width, other parameters were varied. These included speed, ridge orientation, shear strength and water level.

Only limited results are discussed here. The main interest was to use the tests to assess the load algorithms. From the punch tests, it was established the keel rubble had an average friction angle of 46.5º. Individual strengths were also measured for each ridge test. These were used in both algorithms together with specific ridge geometries to calculate loads for all tests. Also examined was how well the load algorithm matched the measured loads as a function of penetration by the structure into the ridge. A typical result for the GPF model is shown in Figure 77. In this test, the ridge width was 3.5m, ridge depth 0.97m, the cylinder diameter was 0.8m and the speed was 0.07m/s.

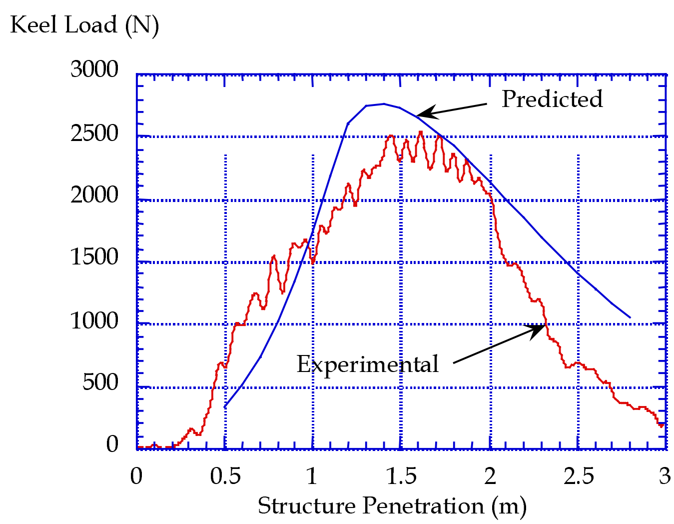

Figure 77 Comparison of Model Test results with GPF Calculated Values as Function of Penetration

A comparison of measured and calculated loads for the Dolgoplov/shear plug algorithm is shown in Figure 78 using measured friction angles for each ridge. A best-fit slope of 0.992 was obtained. For the GPF model a regression slope of 1.145 was obtained (see Figure 79). On the basis of the above, the GPF model appears to be slightly more conservative over the range of parameters relevant to the model tests. But both algorithms give reasonable agreement with measured loads.

It was concluded that, for model ice ridges and vertical structures, the improved keel load algorithms, developed in this study, have been validated. Several other conclusions can be drawn from the tests, namely:

- Speeds up to the equivalent of about 1.5 m/s full scale were tested, and an increase in keel loads of up to about 17% was detected over slower speeds. This increase was matched by the GPF model, which can account for inertia. However, the 17% is within the experimental scatter of the data in the tests, so care should be exercised in drawing any firm conclusions from these comparisons.
- The ridge keel load was not sensitive to angle of attack of the ridge.
- The keel load increases with increasing ice - structure friction. However, the increase was not as much as predicted by the GPF model.
- Keel loads are higher on a sloping structure than on a vertical cylinder of the same water line diameter. However, in its present form, the GPF model does not properly handle an upward breaking cone except by calculating the load on a vertical structure with an effective diameter greater than the water line diameter.

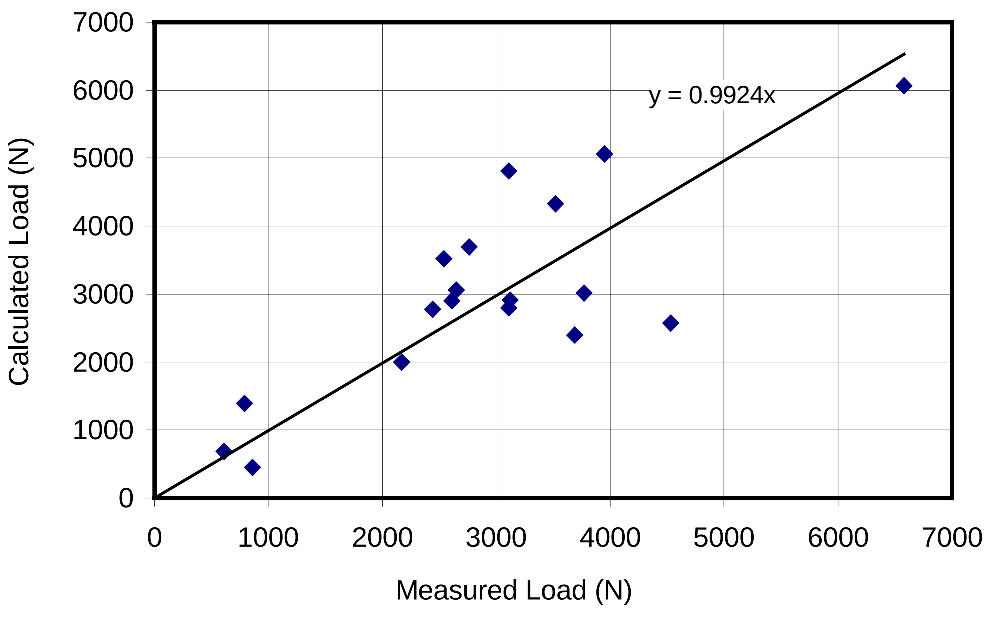

Figure 78 Comparison of Model Test Results with Dolgopolov/Croasdale Calculated Values

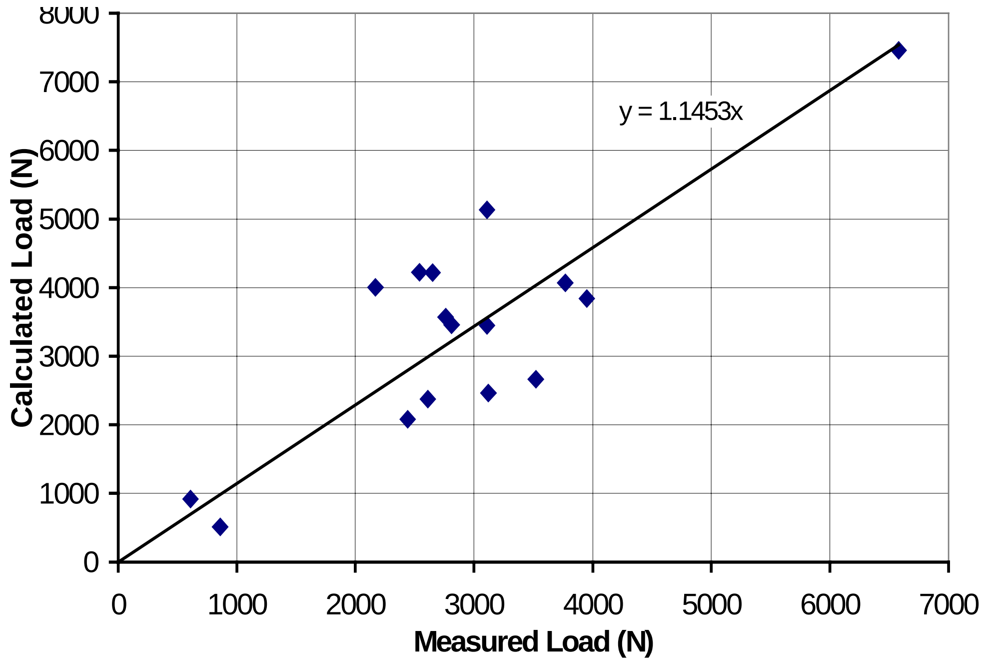

Figure 79 Comparison of Model Test Results with GPF Calculated Values

5.2.2.5 Keel Load Models and Full Scale Data

Keel loads and ice pressures due to keels acting on the Molikpaq have been evaluated in Chapter 4. Figure 59 showed how the estimated measured keel loads vary with keel depth. The highest keel load was 45 MN and the accompanying keel depth was about 9 m. It is of interest to use one of the keel load algorithms previously reviewed to compare with the inferred measured load. This calculation requires the input of several unknown parameters. These include keel top width, keel bottom width, friction angle, cohesion etc.

In Table 10, several trial values for these inputs are used and loads estimated for each combination. The load calculations are performed using the Dolgopolov/Croasdale cross-over method.

Table 10 Calculated keel loads with various assumptions of keel properties and geometry for a 9m deep keel

		Frictional strength ($c = 0$)			Cohesive strength ($\phi = 0$)		
Keel bottom width (m)	Keel top width (m)	$\phi = 45$	$\phi = 55$	$\phi = 60$	c top = 10 c bot. = 4	c top = 12 c bot. = 4	Molikpaq measured loads
0	35	11.4	16.72	21.0	22.4	26.7	45
20	55	27.0	39.2	45.53	39.8	46.34	45

In the above calculations, it was assumed that porosity of the keel rubble was 0.3, and the surcharge factor in the Dolgopolov load was 0.2 m in width. The relevant structure width is 75 m as used in Chapter 4 to derive the measured load of 45 MN for the 9 m deep keel.

Clearly, the results are sensitive to the assumptions relating to keel shape, which are unknown. Even so, the load comparisons provide some insights. For example, if only frictional strength for the keel is assumed, it requires a friction angle of at least 60 degrees for the calculated load to be close to the measured load. If a more “acceptable” value for ice rubble friction of 45 degrees is used, the implication is that the keel load algorithm under predicts the measured load.

On the other hand, we know from the in-situ keel strength measurements referred to in Chapter 3, that keel rubble appears to be dominated by cohesive strength. A relationship established for keel rubble in the Northumberland Strait was:

$$c = 4.0 + 0.68H \qquad \text{(in kPa, with H the keel depth in m)}$$

The above equation yields a cohesive strength of 10 kPa at the top of the keel and 4 kPa at the bottom. This is one strength used in Table 10. The other strength is 2 kPa higher at the top. Using a higher strength for Beaufort ridge keels is intuitively correct, although the rubble temperatures would be similar (the sea water temperature). However, Beaufort ridges would likely be older because the ice season is longer, and cohesive bonds likely increase with time. In any case, it is of interest to note that using the in-situ measured cohesive strengths for ice rubble and the Dolgopolov/Croasdale algorithm, gives reasonable agreement with the measured load for the 9 m deep keel.

Using the same strength relationship for a range of keel depths gives the range of loads shown in Table 11.

Table 11 Keel loads as a function of keel depth assuming cohesive rubble strength

Keel depth (m)	Top width (m)	Bottom width (m)	Cohesion at top of keel (kPa)	Keel load (MN)
2.0	28	20	7.4	15.3
4.5	38	20	9.1	25.35
6.0	44	20	10.1	31.77
7.5	50	20	11.1	39.4
9.0	56	20	12.1	47.01
18.0	92	20	18.2	111.0
23.0	112	20	21.6	165.8

5.2.2.6 Keel Pressures

In Chapter 4, data is presented on measured ice pressures on the lower ice panels that would see the top layer of ice rubble in the keel. These do generally increase with sail height (keel depth) to about the 70 to 160 kPa range. The predicted keel load for the 9 m keel is about 47 MN. This translates into an average keel pressure of 67 kPa. It would be expected that the pressure distribution would be higher at the top of the keel. If in this exercise a triangular distribution is assumed, then the theoretical pressure at the top of the keel is 134 kPa. This value agrees well within the range inferred from the panel measurements on the Molikpaq.

5.3 Numerical Models

There have been a few studies of ridge loading using more powerful numerical techniques. To date, two different approaches have been used:

1. Finite Element Modelling;
2. Discrete Element Modelling.

Each will be briefly discussed below.

5.3.1 Finite Element Modelling

There have been a few studies of ridge interaction failure using the finite element approach (Brown and Bruce, 1995). In these studies, a finite element grid is established with an idealized geometry, and different material properties are assigned to each region.

For example, Brown and Bruce (1995) modelled the interaction of a ridge with a pier from the Confederation Bridge (see e.g. Figure 80). The FE model included the structure (cone and cylinder), the keel and the consolidated layer, as well as the interface elements between the keel & structure, the consolidated layer & the structure, and the keel & consolidated layer. Both structure components were modelled as rigid elements. The keel material was modelled as a continuum. However, there are no material representation that can model the behaviour of the keel. Therefore an idealized, Mohr-Colomb representation was used. The material properties were specified by an internal friction angle and cohesion, and they modelled a failure surface which was symmetric about the line corresponding to hydrostatic pressure and which resulted in increasing deviatoric strength as the hydrostatic pressure increased. There was difficulty in describing the behaviour of the consolidated layer, since modelling the elastic-brittle behaviour of ice flexural failures is not straightforward. The FE model was developed for both 2D and 3D formulations.

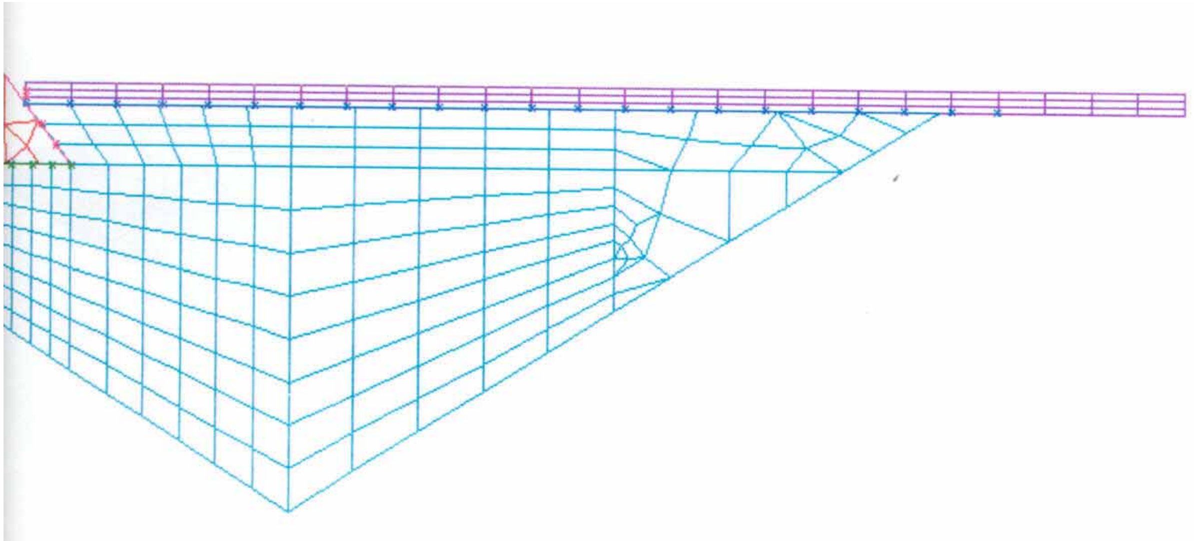

Figure 80 Finite Element grid for ridge interaction with the Confederation Bridge pier (after Brown and Bruce, 1995).

Although the FE approach can be used to provide estimates of global loads, it does not realistically represent the ridge failure process. The model assumes, for example, that the keel is homogeneous and this is clearly not correct. In nature, the inhomogeneity and discontinuities will ensure that the failure is affect, and possibly dominated by local effects within the ridge material. The continuum finite element approach, because it does not permit this behaviour, will over-estimate the loads generated by the keel. Further, the problems with modelling the material properties of the consolidated layer also leads to uncertainties in load estimates using this approach. Therefore their use for load predictions are quite limited.

5.3.2 Discrete Element Models

Recently, discrete numerical methods have been used to model the behaviour of broken ice with a wide range of applications. For example, Savage (1992) and Sayed et al. (1995) developed a discrete model of Marginal Ice Zone dynamics. Hopkins et al. (1991) developed two-dimensional simulations of ice ridging. Sayed (1995, 1997) has used discrete element methods to investigate the failure of a ridge against a pier in the Confederation Bridge in Canada.

Discrete models have several advantages:

1. they provide a realistic simulation of the interaction conditions between ice blocks;
2. they provide an accurate description of the ice edge;
3. they can deal with large deformations;
4. they can also handle the discontinuities that usually arise during failure; and
5. they are based on simple assumptions and avoid the uncertainty regarding complex constitutive equations.

The major limitation has been the need to use very large numbers of elements in order to deal with any problem of practical interest. However, with new advances in computer speed and numerical solvers, this limitation is now largely a thing of the past.

The discrete element approach was used by Sayed (1995) to predict the forces on the Confederation Bridge piers. Sayed modelled the ridge keel as an assembly of random-sized inelastic disks. A “soft-particle” approach was used, where each disk may have multiple contacts that could persist for an extended duration. At the contacts between disks, normal forces and tangential forces arose as the disks approach, rotate and slide. A schematic of one contact force acting on one disk is illustrated in Figure 81. The simulations kept track of the movements and forces on every disk. Normal and tangential forces also developed at the contacts between the disks and the structure. Thus the disks were prevented from crossing the fixed boundary, which represented the structure.

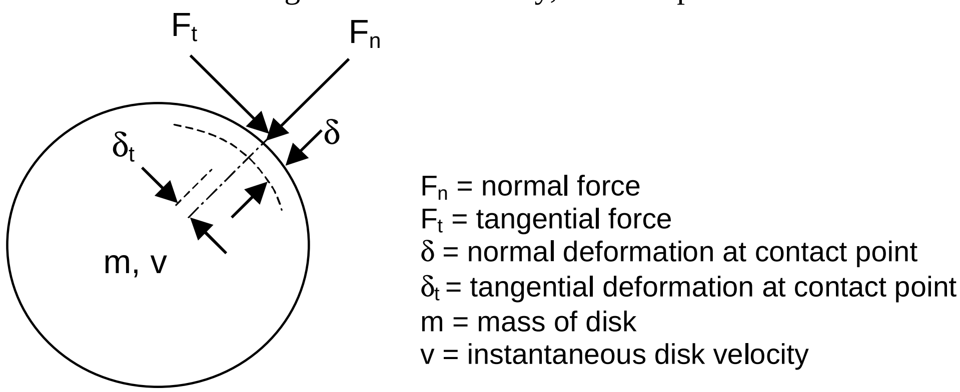

Figure 81 Illustration of the forces acting on a particle in the Sayed (1995) model.

The balance of linear momentum for each disk may be expressed as

$$m\frac{du}{dt} = \sum_{i=1}^{N} F_i + mg \qquad \textbf{5-43}$$

where m is the mass of the disk, u is the velocity vector, t is time, $\sum_{i=1}^{N} F_i$ is the vector sum of contact forces due to N contacts with other disks, and mg is the buoyancy force. The balance of angular momentum is given by

$$I\frac{d\omega}{dt} = \sum_{i=1}^{N} T_i \qquad \textbf{5-44}$$

where I is the moment of inertia of the disk, ω is the angular velocity, and $\sum_{i=1}^{N} T_i$ is the sum of the torques due to N contacts.

At the contact between two disks, compressive normal forces increase as the centres of the disks approach each other. Sayed's model can also account for tensile forces, which may develop if the disks move apart. In that case, the tensile force is reset to zero when it reaches a maximum value representing the tensile strength. Such a broken contact is not allowed to sustain tensile forces afterwards throughout the simulation. This approach was used by Sayed (1995) to model the tensile strength of frozen (or consolidated) ice rubble of the ridge. However, in the keel, the tensile strength of the rubble was zero.

The normal force, F_n at the contact in the keel was modelled using a linear spring and a linear dashpot as follows

$$\begin{aligned} &\text{Compression:} \quad F_n = k\delta - bv_n \\ &\text{Tension:} \quad F_n = 0 \end{aligned} \qquad \textbf{5-45}$$

where k is the spring constant, δ is the relative normal displacement, v_n is the relative normal velocity, and b is the dashpot constant. In this model, the spring prevents disks from overlapping, and the dashpot accounts for energy dissipation during the contact.

The tangential force, F_t was calculated using a tangential spring until it reached its maximum allowable value according to Coulomb friction law

$$F_t = \min\{\ k_t\delta_t\ ,\ \mu F_n\ \} \qquad \textbf{5-46}$$

where μ is the coefficient of friction, k_t is the tangential spring constant, δ_t is the tangential relative displacement, and the tangential force acts in a direction opposite to that of the relative tangential velocity. This approach prevents spurious fluctuations in the tangential force when the relative tangential velocity is near zero.

Sayed (1995, 1997) used this model to predict the forces from a trapezoidal ridge of 20 m keel depth that impacts a cylindrical bridge pier of 10 m diameter. The geometry of the initial configuration is shown Figure 82. The ridge, was 50 m in length, was represented by spheres which are initially placed in hexagonal packing. Then each sphere was given a random displacement of ±0.15 of its diameter. The consolidated layer at the water level was accounted for by using higher stiffness and tensile bond values than for the keel. The total number of spheres was approximately 7000.

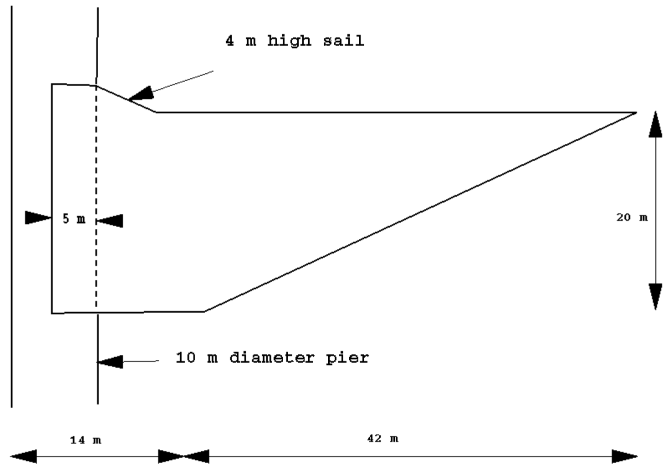

Figure 82 Initial ridge and pier geometry for a 3-dimensional discrete element simulation (after Sayed 1995).

The sides of the ridge were subjected to plane strain conditions; i.e. over the cross-section at each end of the ridge, velocity components perpendicular to the plane of the cross-section are set to zero. A 2 m wide part of the far end of the ridge moved at constant velocity, thus simulating a constant velocity of the pack ice. All spheres in the ridge start at the same initial velocity of the driving boundary (or pack ice). The consolidated layer thickness is approximately 2 m. The tensile strength of the consolidated layer was 400 kPa, and that of keel rubble is 5 kPa. Random components (20% of mean values) were added to the spring constants and tensile strengths. Parameter values were: sphere diameter 2.0 m, velocity 0.5 m/s, spring constant (keel) 2.65 MN/m, spring constant (consolidated layer) 26.5 MN/m, spring strength (keel) 2.3 kN, spring strength (consolidated layer) 184.8 kN, dashpot parameter 12.9 kN s/m, friction coefficient (ice-ice) 0.2, friction coefficient (ice-pier) 0.1, and ice specific gravity 0.9. The corresponding bulk elastic modulus for the keel rubble is approximately 7 MPa, and that for the consolidated layer is 70 MPa.

The resulting forces are plotted versus time in Figure 83, for a number of velocities. Note that the velocities, ridge dimensions, and initial contact area were chosen to give conservative (high) forces. Figure 83 shows that the maximum force is reached after an indentation distance of between 0.5 m and 1m. The clearing and flow of rubble around the pier afterwards produces relatively small forces. A view of the bottom side of the ridge keel from the 3-dimensional representation is shown in Figure 84. It shows ice blocks starting to break-out from the keel in front of the pier. Such a beak-out takes place after the force had considerably dropped. A parametric study examined the role of keel depth, ice-pier friction coefficient, and rubble stiffness. In other cases, a fixed boundary was used at the water level, instead of a breakable consolidated layer, to increase rubble confinement. The observed failure modes show that rubble flows around the pier without forming “fixed wedges”. There was no evidence of the formation of shear planes, along which rubble deforms. This behaviour was also observed during the ice basin models of Timco and Cornett (1995). The conclusions indicate that the maximum forces are lower than those calculated using empirical soil mechanics formulas.

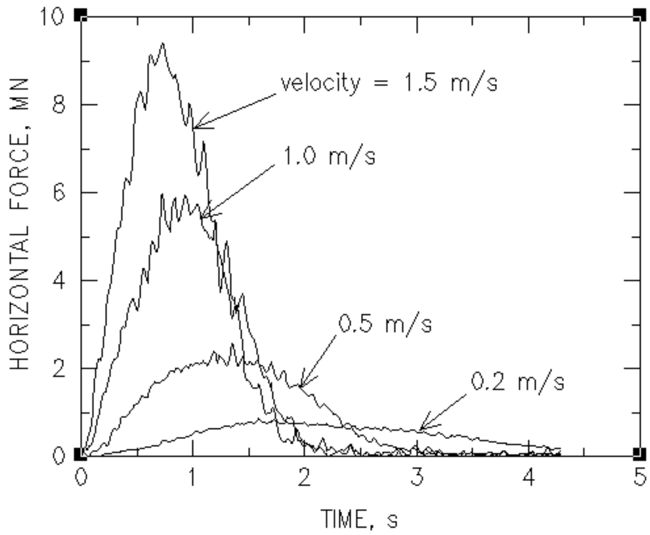

Figure 83 Total horizontal force on the pier (after Sayed 1995).

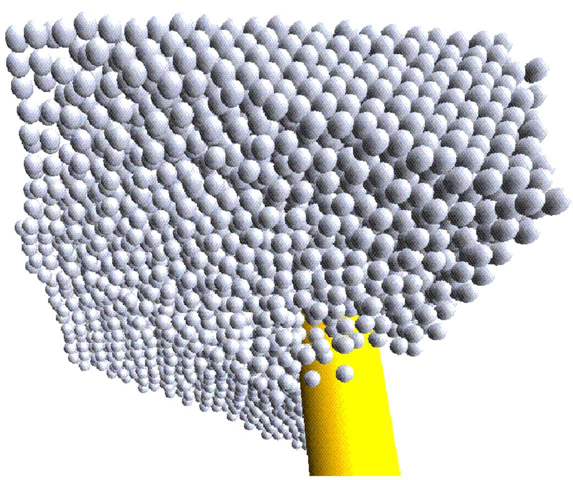

Figure 84 View of the bottom of the keel after 10 seconds. using 3-dimensional discrete element model (after Sayed 1995).

The numerical approach can also be used to provide insight into the stresses and stress distribution within the ridge. Figure 85 shows a sequence of views of the stress distribution in the keel of the ridge during the interaction process (after Sayed 1995).

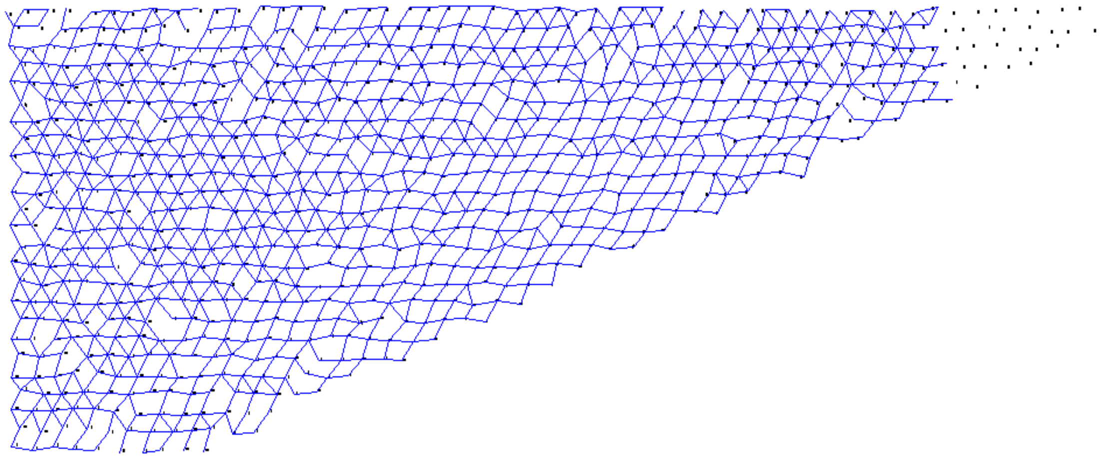

Time = 0 seconds

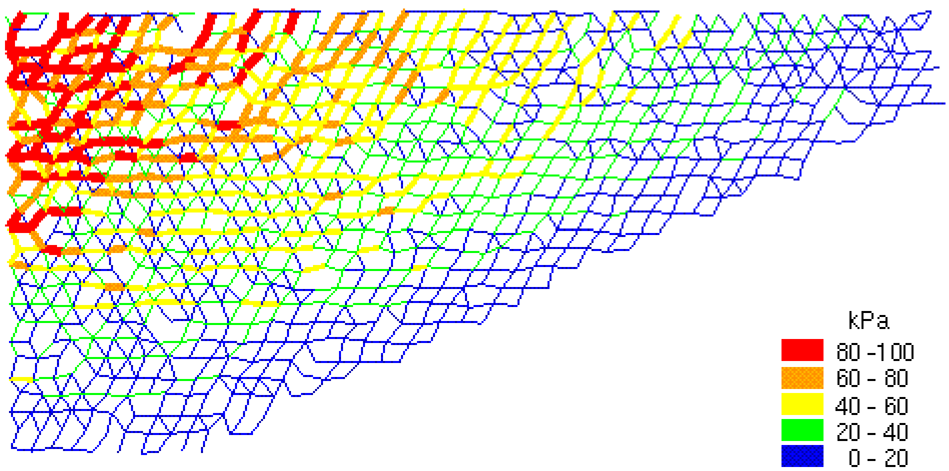

Time = 0.5 seconds

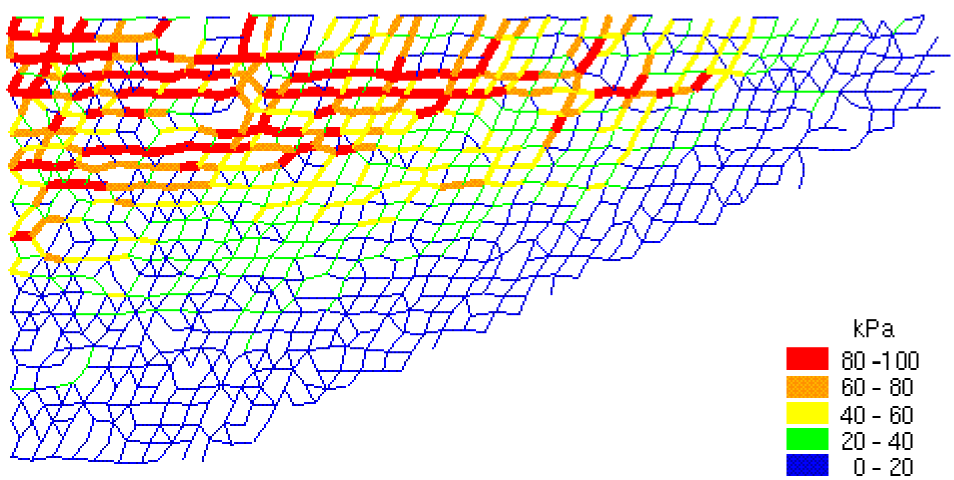

time = 1.0 second

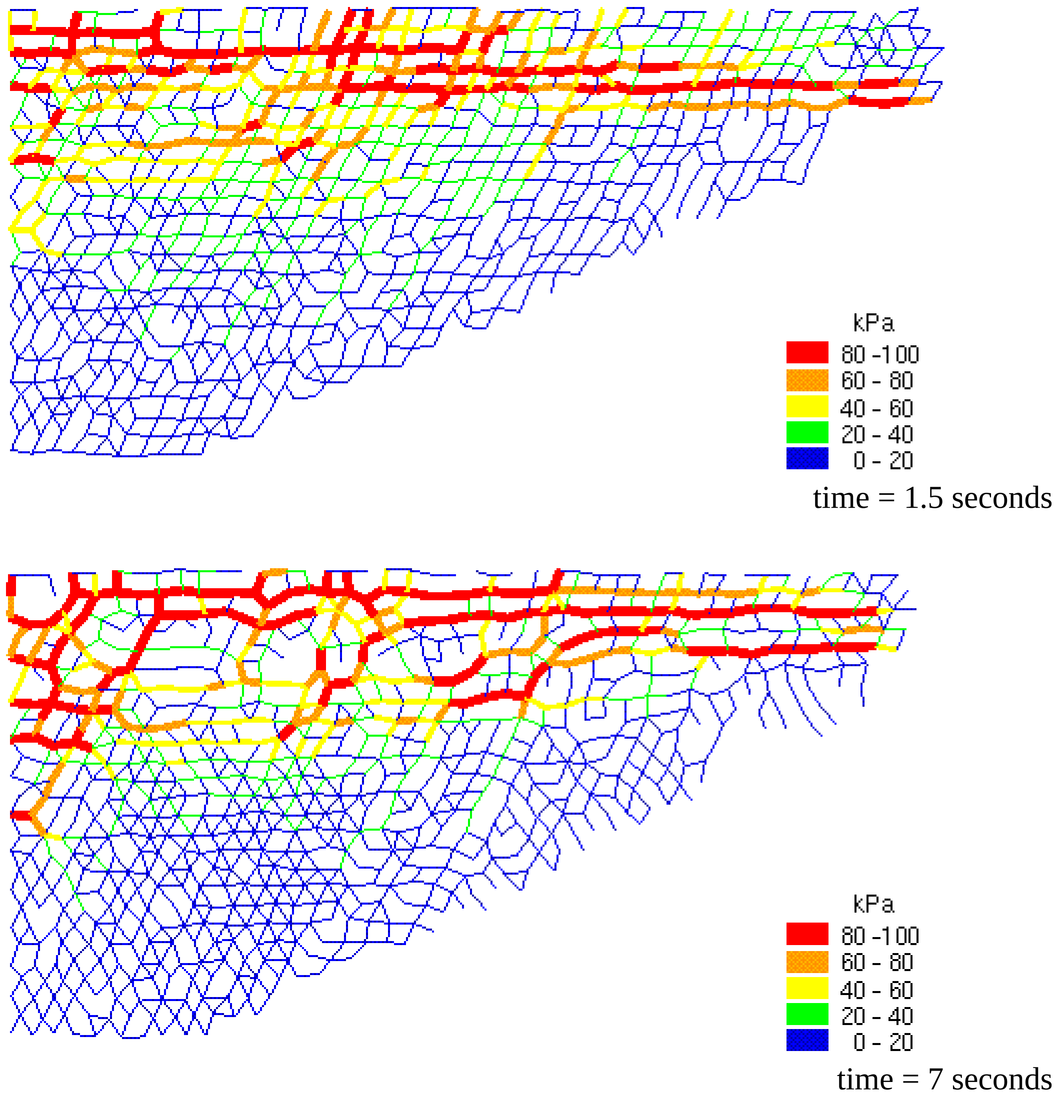

Figure 85 Time-series sequence showing the stress distribution in the keel of the ridge during interaction with fixed structure (after Sayed 1995).

The discrete element approach offers several advantages over the other approaches since it appears to give reasonable load predictions, it is based on relatively few assumptions and it provides additional insight into the failure process.

5.4 References

Abdelnour, R. 1981. Model Tests of Multi-year Pressure Ridges Moving onto Conical Structures. Proceedings IAHR Ice Symposium, Vol. 2, pp 728-751, Quebec City, Canada.

Blanchet, D. 1990. Design criteria for wide Arctic offshore structures. Canadian Geotechnical Journal, Vol. 27, No. 6, pp. 701-725.

Blanchet, D. 1998. Ice Loads from First Year Ice Ridges and Rubble Fields. Canadian Journal of Civil Engineering. 25: 206 – 219.

Chao, J. C. (1992). Comparison of Sheet Ice Load Prediction Methods and Experimental Data for Conical Structures. Proc. OMAE Vol. 4 Arctic/Polar Technology, ASME, 1992.

Broms, B. 1964. The Lateral Resistance of Piles in Cohesionless Soils. JSMD, ASCE, Vol. 90, No. SM3, pp. 123-156.

Brown, T.G. and Bruce, J.R. 1995. Finite Element Analysis of First Year Ridge Interactions. Report by Bercha & Assoc. to Public Works and Government Services Canada, Calgary, AL, Canada.

Brown, T.G., Croasdale, K. R. and Wright, B. 1996. Ice Loads on the Northumberland Strait Bridge Piers – An Approach. Proc. of 6th ISOPE Conference, Los Angeles, 1996.

Case, P. C., 1991. A Model Scale Study of the Frictional and Cohesive Properties of Floating Ice Rubble. Institute of Marine Dynamics Report, LM 1991 03. St. John’s, Nfld., Canada.

Croasdale, K.R. 1980. Ice Forces on Fixed Rigid Structures, 1st IAHR State-of-the-Art Report on Ice Forces on Structures, pp 34-106, CRREL Special Report 80-26, Hanover, N.H., USA.

Croasdale, K.R. and Cammaert, A.B. 1993. An Improved Method for the Calculation of Ice Loads on Sloping Structures in First-Year Ice. First International Conference on Exploration of Russian Arctic Offshore, pp. 161-168, St. Petersburg, Russia.

Croasdale, K.R., Cammaert, A.B. and Metge, M. 1994. A Method for the Calculation of Sheet Ice Loads on Sloping Structures. Proceedings of the IAHR'94 Symposium on Ice, Vol. 2, pp 874-875, Trondheim, Norway.

Croasdale & Associates Ltd. 1995. Ice Load Models for First Year Pressure Ridges and Rubble Fields – Phase 1 Report. Joint Industry Government Project, Partly sponsored by the National Energy Board (PERD) and Public Works Canada.

Croasdale . K. R., Shkhinek, K. N. 1995. Ice Engineering Problems Related to Design & Construction of Arctic Offshore Structures. Transactions of Second International Conference. Development of Russian Arctic Offshore, St. Petersburg, Russia.

Croasdale & Associates Ltd., 1996. Ice Load Models for First Year Pressure Ridges and Rubble Fields. A Joint Industry-Government Project, Partly sponsored by PERD through the National Energy Board, Calgary, and supported by Mobil and Exxon.

Croasdale & Associates Ltd., 1996. Ice Load Consensus. A Joint Industry/Government Project. Calgary, Canada

Croasdale, K.R., Shkhinek, K.N. 1997. Ice Engineering Problems Related to Design & Construction of Arctic Offshore Structures. Proc. RAO 1995, St. Petersburg, Russia.

Croasdale, K. R. 1997. Ice Structure Interaction: Current State of Knowledge & Implications for Future Developments. ROA Conference, St. Petersburg, Russia.

Dolgopolov, Y.V., Afanasev, V.A., Korenkov, V.A. and Panfilov, D.F. 1975. Effect of Hummocked Ice on Piers of Marine Hydraulic Structures, Proceedings IAHR Symposium on Ice, pp. 469-478, Hanover, NH, U.S.A.

Edwards, R.Y. and Croasdale, K.R. 1976. Model Experiments to Determine Ice Forces on Conical Structures. Symp. of Applied Glaciology, International Glaciological Society.

Eranti, E., Lehmus, E. and Nortala-Hoikkanen, A. 1992. First-Year Ice Ridge Characteristics and Loads on Offshore Structures. Proceedings ISOPE'92, Vol. II, pp 681-687, San Francisco, USA.

Hirayama K. and Obara, I. 1986. Ice Forces on Inclined Structures. Proc. OMAE Conf. Vol. IV, pp 515-520, Tokyo, Japan.

Hoikkanen, J. 1984. Measurements and Analysis of Ice Pressure against a Structure in Level Ice and in Pressure Ridges. Proceedings of the 7th International IAHR Symposium on Ice, Vol. 3, pp.151-160, Hamburg, Germany.

Kato, K. 1986. Experimental Studies of Ice Forces on Conical Structures. Proc. IAHR Ice Symposium, Vol. I, pp. 185-196, Iowa City, U.S.A.

Kamesaki, K. and Yoshimura, N. 1987. Multiyear Ridge Load on a Conical Structrue. Proceedings POAC'87, pp 307-316, Fairbanks, Al., USA.

Korzhavin, K.N. 1971. Action of Ice on Engineering Structures. US Army CRREL Translation TL260, Hanover, N.H., USA.

Krankkala, T. and Määttänen, M. 1984. Methods for Determining Ice Forces Due to First- and Multi-Year Ridges. Proceedings IAHR Ice Symposium, Vol. IV, pp. 263-287, Hamburg, Germany.

Kry, R. 1981. Scale Effects in Continuous Crushing of Ice. Proceedings IAHR Symposium on Ice, pp 565-580, Quebec City, Canada.

Lepparanta, M. and Hakala, R. 1992. The Structure and Strength of First Year Ice Ridges in the Baltic Sea. Cold Regions Science and Technology, Vol. 20, pp. 295-311.

Lewis, J.W. and Croasdale, K.R. 1978. Modelling and Interaction Between Pressure Ridges and Conical-Shaped Structures. Proceedings IAHR Ice Symposium, Part 1, pp 165-196, Lulea, Sweden.

Maattanen, M. 1996. Cone First-Year Ice Force Models and Full Scale Data. NEB'96 Ice Load Workshop, Calgary, March 1996.

McKenna R.F., Bruneau S.E., Williams F.M., 1996. In-Situ Shear Strength Measurements of Model Ice Rubble Using a Punch Technique. Proceedings 49th Canadian Geotechnical Conference, St John's, Newfoundland.

Mellor, M. 1980. Ship Resistance in Thick Brash Ice. Cold Regions Science and Technology, Vol. 3, No. 4, pp. 305-321.

Nevel, D.E. 1992. Ice Forces on Cones from Floes. Proceedings 11th IAHR Ice Symposium, Vol. 3, pp 1391-1404, Banff, Alta., Canada.

Prodanovic, A. 1979. Model Tests of Ice Rubble Strength. Proceedings POAC'79, pp 89-105, Trondheim, Norway.

Prodanovic, A. 1981. Upper Bounds of Ridge Pressure on Structures. Proceedings POAC '81. Vol. III, pp. 1288-1302, Quebec City, P.Q., Canada.

Ralston, T.D. 1977. Ice Force Design Considerations for Conical Offshore Structures. Proceedings POAC'77, Vol. II, pp. 741-752, St. John's, Nfld., Canada.

Ralston, T.D. 1978. An Analysis of Sheet Ice Indentation. Proceedings IAHR Symposium on Ice, pp 13-31, Lulea, Sweden.

Sanderson, T. J. O. 1988. Ice Mechanics - Risks to Offshore Structures. Graham and Trotman, London, UK.

Sayed, M., Timco, G.W. and Sun, L. 1992. Testing Model Ice Rubble under Proportional Strains. Proceedings of the Offshore Mechanics and Arctic Engineering Symposium (OMAE 1992), Vol. IV Arctic/Polar Technology, pp.335-341.

Sayed, M, Neralla, V.R., and Savage, S.B. 1995. Yield Conditions of an Assembly of Discrete Ice Floes, Proceedings 5th Int. Offshore and Polar Eng. Conf., ISOPE, Vol.II, pp 330-335, The Hague.

Sayed, M. 1995. Numerical Simulation of the Interaction between Ice Ridges and Bridge Piers, Technical Report TR-1995-10, National Research Council, Ottawa, Ontario, Canada.

Sayed, M. 1997. Discrete and Lattice Models of Floating Ice Covers, Proceedings 7th International Offshore and Polar Engineering Conference, ISOPE, Vol IV, pp. 428-433, Honolulu, USA.

Shkhinek, K.N., Blanchet, D., Croasdale, K. R., Matskevitch, D. G., and Bhat, S. U. 1994. Comparisons of the Russian and Foreign codes and Methods for Global Load Estimations. Proc. OMAE, Houston, 1994.

Smirnov,V., Sheikin, I.B., Shushlebin, A., Kharitonov, V., Croasdale, K. R., Metge, M., Ritch, R., Polomoshnov, A., Surkov, G., Wang, A., Beketsky, S., and Weaver, J.S. 1999. Large Scale Strength Measurements of Ice Ridges: Sakhalin, 1998. RAO Conference, St. Petersburg, 1999.

Timco, G.W. 1984. Ice Forces on Structures: Physical Modelling Techniques. Proceedings 2nd IAHR State-of-the-Art Report on Ice Forces on Structures; published in the Proceedings IAHR Ice Symposium, Vol 4, pp 117-150, Hamburg, Germany.

Timco, G. W., Funke E.R., Sayed M. and Laurich P.H. 1992. A Laboratory Apparatus to Measure the Behaviour of Ice Rubble. Proc. OMAE 1992, Vol. IV, PP 369 – 375.

Timco, G.W. and Cornett, A.M. 1995. Model Tests of Ridge Interaction with a Bridge Pier for the Northumberland Strait Crossing. National Research Council Report TR-1995-02, Ottawa, Ont., Canada.

Vesic, A.S. 1973. Analysis of Ultimate Loads of Shallow Footings. JSMFD, ASCE, Vol. 99, No. SM1, pp. 45-73.

Wang, Y.S. 1984. Analysis and Model Tests of Pressure Ridges Failing against Conical Structures. Proceedings IAHR Symposium on Ice, Vol. 2, pp 67-76, Hamburg, Germany.

Weaver, J. 1994. Review of Ice Rubble Strengths and Failure Modes for the PEI Bridge Piers. Report to Canatec Consultants Ltd., Calgary, Alberta, Canada.